UNIVERSITÀ DEGLI STUDI DI PALERMO

Dottorato di Ricerca in Ingegneria Chimica, Gestionale, Informatica, Meccanica
Ingegneria Chimica e dei Materiali
Dipartimento di Ingegneria Chimica, Gestionale, Informatica, Meccanica
ING-IND 27

NOVEL PROCESSES FOR THE MODIFICATION AND THE STERILIZATION OF MACROMOLECULAR MATRICES

LA DOTTORESSA
Ing. Sonia Lanzalaco

IL COORDINATORE
Prof. Ing. Salvatore Gaglio

IL TUTOR
Prof. Ing. Alessandro Galia

IL CO TUTOR
Prof. Ing. Onofrio Scialdone

CICLO XXVI
ANNO CONSEGUIMENTO TITOLO 2016

To my angel in heaven

INDEX

.

INTRODUCTION

Living controlled radical polymerization (L/CRP) is among the most rapidly developing areas of polymer science, leading to the synthesis of new (co)polymers with desired architecture and materials for various advanced technologies and biomedicine. In this context, Atom Transfer Radical Polymerization (ATRP), which was developed in the second half of the nineties, has been one of the most successful varieties thanks to its versatility and easiness of application. ATRP is a metal-catalyzed method, being often catalyzed by a Cu(II)/Cu(I) redox couple. The reaction is based on a dynamic equilibrium between dormant species (bearing a C−halogen bond) and an activator (Cu^{I} complex). The halogen ion is reversibly transferred from the former to the latter species, which thus undergoes a one electron oxidation. Typically, this equilibrium is strongly shifted towards the dormant state and, as a result, it allows achieving a good control of the molecular weight and polydispersity of final polymers, tuning them by the halogen atom transfer and not by radical termination as in conventional processes.

In this Thesis, ATRP has been used to modify halogenated macromolecules such as poly(vinyl chloride) (PVC) and poly(vinylidene fluoride) (PVDF), which are widely used polymers at industrial scale for many applications. With a view to their biomedical applications, some of their drawbacks must be overcome. In particular, a modification procedure was carried out by grafting of hydroxyethyl methacrylate (HEMA), which allows obtaining more biocompatible and pH-sensitive copolymers. Poly(2-hydroxyethyl methacrylate) (PHEMA) is a widely used and investigated biocompatible polymer and, in this study, it was employed to enhance the biocompatibility of the hydrophobic surface of PVC and PVDF, responsible for unwanted protein adsorption and cell adhesion. Furthermore, the modification process allows a decrease of the release of additives like phthalates that are often used to give flexibility to PVC. Great attention was devoted to PVDF nanoparticles, taking into account the relevance of this fluoropolymer belonging to a very

interesting class of materials characterized by excellent properties, as it will be explained in subsequent chapters. Their modification was carried out by the "grafting from" method, with ATRP as radical polymerization technique. The same polymers were used as macroinitiators that allowed initiating the reaction from the C-halogen bond.

Recently, a research group from the MIT reported, for the first time, the grafting of fluorinated polymers in organic solvent by ATRP using fluoropolymers as macroinitiators and carrying out a "direct grafting". In fact, the modification occurs via the direct extraction of the halogen atom (fluorine) from the polymeric backbone, a challenging topic that seems very complicated due to the strong energy of the C-F bond (486 kJ/mol).

Based on these studies, the modification of PVDF was carried out in this work either in organic solvent or in supercritical medium, and electrochemical investigation was employed to better understand the mechanism of a Cu-catalyzed ATRP in the presence of a C-F bond. In organic medium, the study with PVC was also carried out to compare the particularities arising from a C-Cl bond, which was expected to be more active than the C-F one.

The first goal of this Ph.D. Thesis is to investigate the properties of catalysts, initiators and the rationalization of the activation mechanism by macroinitiators like PVC and PVDF by means of cyclic voltammetry and chronoamperometric measurements. Such electrochemical tools have been used since they allow: i) the analysis of important characteristics of catalyst employed in ATRP, and ii) the continuous reduction of metal in highest oxidation state by an electric field in the presence of very low concentrations of catalyst, thus making ATRP a “green method”.

A second important goal is to open a new way to modify fluorinated nanoparticles by a controlled technique, not only in the organic medium but also in supercritical carbon dioxide ($scCO_2$) aiming to perform the modification process in the absence of any toxic solvent and without dissolution of the polymer matrix, eventually preserving its original morphology.

The first section of this Thesis summarizes the existent literature on the L/CRPs, focusing the attention on the main characteristics and phenomena of an ATRP system. The state of the art regarding grafting techniques and the modification of the halogenated polymers is also discussed. Successively, the Thesis reports the experimental study of the redox behaviour of the ATRP catalysts in *N*-methylpyrrolidone (NMP) through electrochemical and spectrophotometric techniques, which allowed understanding the stability and the activity of the complexes. Two of the most used nitrogen ligands were considered, namely TPMA and Me_6TREN, and the dependence of the redox potentials on the nature of the copper salt, ligand, solvent and temperature was thoroughly analyzed. From this study, the most stable and active catalysts were employed to analyze the activation of the two macroinitiators (PVC and PVDF) by cyclic voltammetry and chronoamperometry and, finally, grafting reactions were carried out with the best catalysts. Worth mentioning, this first section also includes a fundamental study carried out during a period spent at the Chemistry Department of Carnegie Mellon University (Pittsburgh, PA, USA) under the supervision of professor Kristof Matyjaszewski related to the understanding of the mechanism of an ATRP system activated by a fluorinated initiator. This study comes from the need to solve the existing doubts among the scientific community about the activation of C-F bond by copper complex, and it was carried out by electroanalytical and polymerization techniques with a model fluorinated initiator in dimethylformamide (DMF).

The second section of the Thesis focus on the description of the literature on the use of supercritical CO_2 as polymerization medium, mainly on the modification and synthesis carried out by ATRP. This section reports the second goal of this study, namely the possibility to perform, for the first time, a graft copolymerization by ATRP in sc-CO_2. Different operation conditions including the effect of copper salts, ligands, initiation systems, temperature and CO_2 density were analyzed. It is interesting to note that ATRP alternative systems characterized by very low concentration of copper were used in order to make them more suitable for biomedical applications.

Finally, driven by the desire to assess the potentiality of sc-CO_2 as a green solvent in the biomedical field, its effect on the sterilization of a complex porous membrane composed by PLLA, which is widely used in tissue engineering, was evaluated. This last part of the Thesis was born from the increasing attention paid by the scientific community to the utilization of supercritical fluids as an alternative to the common sterilization processes such as steam autoclaving, gamma irradiation, and chemical treatments with ethylene oxide or hydrogen peroxide plasma. The bactericidal effect of sc-CO_2 is caused by specific interactions between the living cells and the fluid, involving for example the cell wall rupture/perforation, the inactivation of some key-enzymes, the intracellular electrolyte balance perturbation and the intra/extra cellular pH variation.

SECTION 1
UNDERSTANDING THE MECHANISM OF ATRP ACTIVATED BY HALOGENATED MACROINITIORS: FROM ELECTROCHEMICAL ANALYSES TO SYNTHESIS

CHAPTER 1.
RADICAL POLYMERIZATIONS

Radical polymerization (RP) is employed to produce annually ca. 100 million tons and half of this production is based on copolymers with thousands of different compositions (*1*). In this chapter, a brief overview of conventional free radical polymerization (FRP) is given. Then, the most important controlled radical polymerization techniques and their characteristics are exposed.

1.1 Free radical polymerization

Industrial application of RP is very important because more than 50% of commercial polymers are produced through this technique (polyethylene, polyvinylchloride, polystyrene and its copolymers, polyacrylates, polyacrylamides, polyviniylacetate, polyvinylalchol and fluorinated polymers) (*2*).

A radical polymerization occurs only in the presence of a free radical R•, an atomic or molecular specie with an unpaired electron linked to its structure (*3*). The R• could be created through different mechanisms: ultraviolet light exposition (molecule scission into two monoradicals I $\rightarrow$2R•, where I = initiator), ionizing radiation exposition, thermal activated decomposition (for species with labile covalent bounds ,as azo-compounds or peroxides, which decomposes allowing to the formation of two radical centers) and, under specific conditions, can react with a monomer leading to the formation of a macromolecular chain. Polymers created by RP exhibit high molecular weight (MW) and good regio-selectivity, as demonstrated by the high level of head-to-tail structures.

A typical chain polymerization is constituted by four fundamentals steps: initiation , propagation, chain transfer and termination.

The initiation step consists of two reactions, the generation of primary initiating radicals (In•), and the reaction of these radicals with a monomer (M).

$In - In \rightarrow 2In^{\bullet}$ k_d (1.1)

$In^{\bullet} + M \rightarrow P_1^{\bullet}$ k_i (1.2)

The first reaction is much slower than the second and is the rate determining step of the initiation process; representative values of the rate constants being $k_d \approx 10^{-5}$ s^{-1} and $k_i > 10^4$ $M^{-1}s^{-1}$. The primary radical so created during the initiation step can to add to the double bond of the monomer leading to the propagation step.

$P_1^{\bullet} + M \rightarrow P_{n+1}^{\bullet}$ k_p (1.3)

Rate constants of propagation have a weak chain length dependence on the degree of polymerization (DP = n_{In}/n_M, beyond ~10), with typical values of $k_p \approx 10^{3\pm1}$ $M^{-1}s^{-1}$. Teoretically, growing chains could be continue to propagate until monomer consumption, but free radicals can react with more reactive species leading to inert covalent bounds. The termination of chain can happen through:

- interaction between a growing chain and a radical created after initiator's decomposition;
- transfer of an active center to another active center as solvent, initiator or monomer;
- interaction with impurities;
- interaction between two growing chains.

Under pseudo-steady state conditions, the initiation rate is the same than the termination one (about 1000 times slower than the propagation rate) , thus, in order to realize a slow initiation phase, initiators with long half-life (for instance 10 h) have to be used. As before reported, propagation reactions are generally characterized by constant rate $k_p \approx 10^3$ $M^{-1}s^{-1}$, while for termination typical values are $k_t > 10^8$ $M^{-1}s^{-1}$; in order to obtain long chains termination reactions must be more slow than propagation. Taking into account that termination rate is characterized by a second order kinetic against radical concentration while the propagation by a first order kinetic, the termination becomes slower when radical concentration decreases;

for these reasons the radical concentrations have to be maintained very low (ppm or ppb values) (*2*).

The rate of monomer consumption of a homogeneous polymerization reaction can be described by the equation 1.4:

$$R_p = k_p[M]\left(\frac{f k_d[I]}{k_t}\right)^{1/2} \quad (1.4)$$

where polymerization rate R_p is a function of initiation efficiency (*f*), rate constant of initiator decomposition (k_d), rate constant of propagation (k_p), rate constant of termination (k_t) and concentrations of monomer and initiator (M and I).

Conventional RP can be carried out homogeneously in bulk monomer or in solution or heterogeneously in suitable suspendend media (precipitation, dispersion, suspension, emulsion, miniemulsion, microemulsion and reverse emulsion). The range of operative temperature is quite large (from -100°C to 200°C) and monomers become more active when the radical is stabilized by resonance or polar effects (styrene, methacrylates, methacrylamide, acrylonitrile, vinylacetate, vinylchloride and others halogenated alkenes). Most used initiators are peroxides, diazenes, redox systems and high energy source (*3*).

1.2 Ionic polymerization: the first step toward controlled polymers

In order to better understand the main features of the controlled radical polymerization that will be explained in the following paragraph, the characteristics and the advantages of ionic polymerization have to be reported. In 1950 and 1960 FRP became the most used method for the production of high molecular weight polymers for industrial applications. Some years after, some researchers have focused their attention on ionic polymerization that allowed to obtain a greater control of molecular structure than that obtained with radical polymerization. A very important innovation in this field was realized by Michael Szwarc (*4*, *5*) with the discovery of living anionic polymerization. Szwarc's work allowed the birth of well-

defined polymers and the synthesis of materials with controlled morphologies (*6*). For more than a decade, anionic polymerization has been the only example of living polymerization technique, based on kinetics different from that observed with conventional radical techniques. The elimination of transfer and termination reactions, the presence of fast initiations and relatively slow propagation lead to an effective control of block lengths, that it was not possible with the conventional radical processes (*7*). In anionic polymerization, the process is initiated by a suitable anion. There are a lot of possible different initiators used, but the most often used is butyl lithium that dissociates to form a positive lithium cation and a negative butyl anion (scheme 1.1). After reaction with the double bond of the monomer, a new carbanion was created and this first step is called *initiation*. The new carbanion reacts with another monomer molecule thus allowing the growing of the chain. This second step is called *propagation* (*7*).

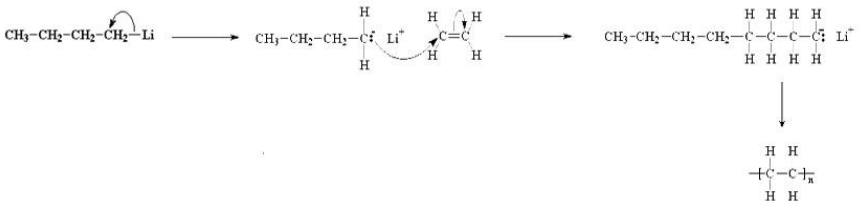

Scheme 1.1 Mechanism of an anionic polymerization

This type of polymerization is characterized by the resumption of propagation after addition of fresh monomer due to the absence of irreversible termination reaction. After full conversion of the monomer in the first solution, another portion of it could be added and polymerization be continued. Thus, Szwarc characterized this behavior of the polymerization as *living polymerization* and called these polymers *living polymers* (*4*). Here, the term *living* refers to the ability of the chain ends to retain their reactivity for a sufficient time enabling continued propagation without termination and transfer reactions. In order to stop them, something like water, which reacts irreversibly with the carbanions, has to be added to the polymer.

1.3 Controlled radical polymerization (CRP)

Driven by the developments in anionic polymerizations obtained by Michael Szwarc and in the attempt of achieving precise control over polymeric materials prepared by RP a specific category of radical polymerization called Controlled Radical Polymerization (CRP), based on a dynamic equilibrium between propagating radicals and various dormant species, was discovered (*8*, *9*). The most important features of living polymerization as the minimization of chain breaking reactions and the simultaneous growth of all chains were reproduced in this type of polymerization (*8*). As reported in scheme 1.2 radicals formed by initiation reaction may be:

a) reversibly trapped in a deactivation process (k_{deact}) by species X, which is typically a stable radical such as a nitroxide (*10*, *11*) or an organometallic species such a cobalt porphyrine (*12*) (Scheme 1.2 (a))
b) or involved in a "reversible transfer", degenerative exchange process (Scheme 1.2(b)).

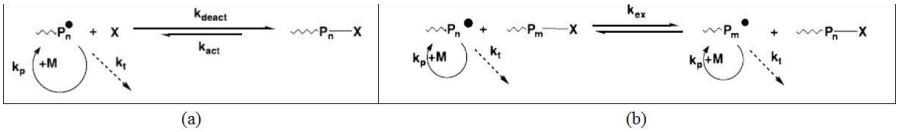

Scheme 1.2 Mechanism of radical trapped in reversible transfer in (a) a deactivation process or in (b) a degenerative exchange process.

In the first case (Scheme 1.2 (a)), the dormant species created can be activated (k_{act}) by different methods (thermally, with light, with appropriate catalyst) to reform radical species that can propagate (k_p), but also terminate (k_t). This mechanism is based on the persistent radical effect (PRE) which leads to a self regulating effect because the persistent radicals (X) can terminate only with the growing species in the deactivation step allowing an intermittent formation of active propagating species with chain length regulated by the equilibrium rate constant of the reaction (*2*).

In the second case (Scheme 1.2(b)), a chain transfer agent mediates the exchange between two growing radicals.

To better understand the systems based on PRE effect, the following division could be done:

- Stable free radical polymerization (SFRP) that includes nitroxide mediated radical polymerization (NMP) and cobalt mediated radical polymerization (CMRP) *based on the PRE effect*.
- Metal-catalyzed living radical polymerization and, especially, atom transfer radical polymerization (ATRP) that *operates via the PRE effect* and in the presence of a catalytic complex composed by transition metal
- Systems employing degenerative transfer *not based on PRE effect*; the most widely used methodology is reversible addition-fragmentation chain transfer (RAFT) polymerization

1.3.1. Stable free radical polymerization

One of the most important SFRP is the Nitroxide Mediated Polymerization (NMP) reported for the first time by Georges et al. in 1993 in a study related to the synthesis of polystyrene with a narrow molecular weight distributions by using a nitroxide stable free radical 2,2,6,6-Tetramethyl-1-piperidinyloxy (TEMPO,) as control agent and dibenzoyl peroxide as initiator (*11*).

By this technique, the control of polymeric structure is achieved with dynamic equilibrium between dormant alkoxyamines and actively propagating radicals. In particular, NMP is based on the reversible homolytic cleavage of a C−O bond to generate a growing radical and a less reactive species that cannot react (persistent radical) (*2*).

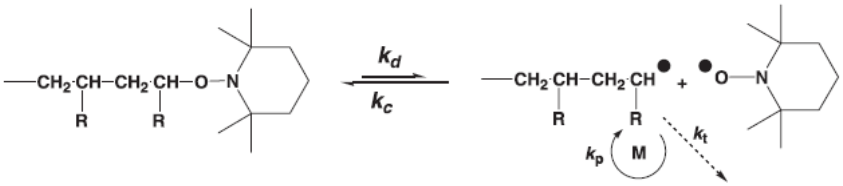

Scheme 1.3 Mechanism of NMP

Covalent bonds created by TEMPO and substituted TEMPO derivatives are relatively strong leading to an equilibrium shifted to the dormant species and reducing the polymerization rate. Typical values of equilibrium constant K_{NMP} that is the ratio between dissociation *(*k_d) and cross-coupling (k_c) rate constants are k_d/k_c = 2.0×10^{-11} at 120 °C for polystyrene (*9*). The lower the equilibrium constant, the harder the control of molecular weight; monomers forming less stable radicals such as vinyl acetate have not yet been successfully polymerized via NMP because of too low K_{NMP}. Also, alkenes such as methacrylates that form more sterically hindered tertiary radicals show difficulties in control by NMP owing to very slow deactivation and/or disproportionation (*13*). A possible solution is the utilization of several nitroxide mediators with different C−O bond strengths and better control over the side reactions. For instance, alkoxyamines derived from nitroxide radicals containing a H atom in the α-C such as DEPN and TIPNO (Scheme 1.4) are much less stable than those of TEMPO, undergoing fast decomposition to alkyl and nitroxide radicals; with K_{NMP} values much larger than those of TEMPO (K_{NMP} = 6×10^{-9} at 120 °C for PS) (*14*).

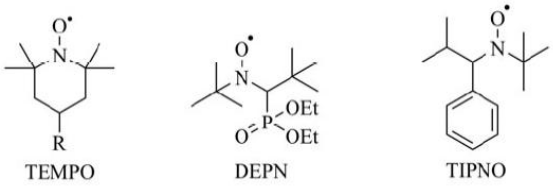

Scheme 1.4 Structures of nitroxide radicals.

1.3.2.Metal-catalyzed living radical polymerization

A large number of transition metal catalysts that can mediate radical polymerization have been investigated in M-LRP; examples include Ru, Cu, Fe, Ni, Mo, Mn, Os, Co. However, metal complexes based on copper, ruthenium, iron and nickel have recorded the highest success (*15*).

In the frame of CRP based on PRE and catalyzed by metal catalyst, ATRP is the most widely used and it will be better discussed later in the chapter. Right after first studies carried out in 1995 by Sawamoto et al. and corresponding to the controlled polymerization of MMA mediated by ruthenium(II) chloride with triphenylphosphine as ligand (*16*); the first example of ATRP carried out by copper catalyst (the most used until now) was reported by Matyjaszewski et al. in 1995 (*17*). In particular, the polymerization of styrene and MMA by using a catalytic system based on a copper(I)/copper(II) redox couple was reported (*17*).

The mechanism , that will be amply reported later, is presented in Scheme 1.5 where a metal complex in a low oxidation state reacts with a dormant species, either a macromolecular or an alkyl halide initiator, bearing a carbon-halogen bond (R-X)) to produce the propagating radicals and the oxidized metal complex coordinated by the halogen atom. Subsequently, the growing radical reacts with the double bond of the monomer (Y) until the deactivation that occurs through the abstraction of the halogen atom from the oxidized form of the catalyst (M_t^{n+1}) to produce the final product R-X-Y and the activator (M_t^n). As in NMP, the equilibrium between dormant and active states is shifted toward the dormant species (*18*).

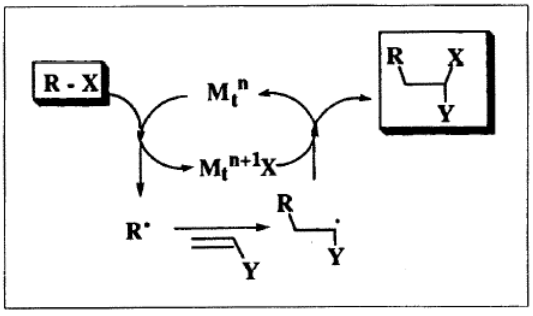

Scheme 1.5 ATRP mechanism

1.3.3.Reversible addition-fragmentation chain transfer polymerization (RAFT)

As regard CRPs not based on PRE, RAFT is surely the most important. This technique is based on a degenerative transfer (DT) and a steady state concentration of radicals is established via initiation and termination processes as in conventional RP (*2*). A simple example of DT occurs in the presence of conventional RP initiators and alkyl iodides process (Scheme 1.6) (*19*, *20*) characterized by rate constants over 3 times larger than propagation rate for most monomers and polydispersities lower than 1.3.

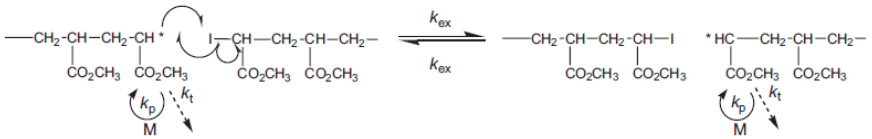

Scheme 1.6 DT Mechanism

In RAFT systems the selection of appropriate RAFT agent for each specific monomer has to be made. Various dithioesters, dithiocarbamates, trithiocarbonates and xanthates have been used as transfer agents to control molecular weights, molecular weight distributions and architecture (*21–23*). RAFT agent is an unsaturated compound that acts as a chain transfer agent (CTA) through a two-step addition-fragmentation mechanism. The general mechanism of RAFT polymerization is reported in Scheme 1.7 where it is possible to observe the typical structure of a RAFT agent. X and A, which are most often CH_2 or S, are groups capable of forming a double bond with a carbon atom C=X or C=A that is reactive toward radical addition, whereas the substituent Z is chosen to give the transfer agent an appropriate reactivity toward the propagating radicals and convey stability to the intermediate.

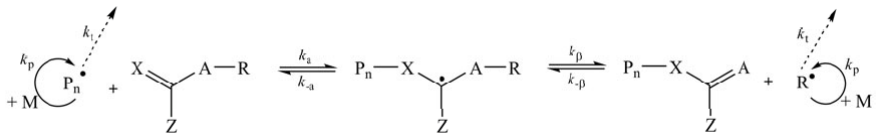

Scheme 1.7 Mechanism of reversible addition-fragmentation chain transfer polymerization (RAFT).

CTA is also bound to an alkyl group R attached to A, characterized by a labile bond able to undergo homolytic dissociation for fast re-initiation of the polymerization.
The selection of the R group should also take into account the stability of the dormant species and the rate of addition of R• to the monomer. The structure of group Z is equally important. For example, strongly stabilizing Z groups such as phenyl ring are efficient for the polymerization of styrene and methacrylate, whereas they retard polymerization of acrylates or inhibit that of vinyl esters. On the other hand, very weakly stabilizing groups, such as $–NR_2$ in dithiocarbamates or –OR in xanthates, are good for vinyl esters but less efficient for styrene. Thus, the proper choice of the Z substituent can dramatically enhance the reactivity of the CTA compounds (*2*).

1.4. Atom transfer radical polymerization

1.4.1.Mechanism

As before reported, ATRP is a controlled living polymerization based on PRE and catalyzed by complexes composed by transition metals. The metal most used until now is surely copper, even if ATRP has been successfully mediated by a variety of metals , including those from Group 4 (Ti (*24*)), 6 (Mo (*25–27*)), 7 (Re (*28*)), 8 (Fe (*29–32*), Ru (*33*, *34*), Os (*35*)), 9 (Rh, (*36*), Co (*37*)), 10 (Ni, (*38*, *39*), Pd (*40*)), and 11 (Cu (*41*, *42*)).

Scheme 1.8 reports the mechanism involved in an ATRP reaction. It is based on the activation (k_{act}) of an appropriate species P_n-X, in general an alkyl halide as molecule or macromolecule, by electron transfer from a catalytic complex in its lower state of oxidation, which is oxidized to its higher state after the halogen atom exchange. This exchange leads to the formation of a radical (P_n•) from initiating species, which can react with monomer (k_p) or terminate (k_t) as in a conventional free radical polymerization, or be reversibly deactivated (k_{deact}) in an equilibrium reaction with the catalytic complex.

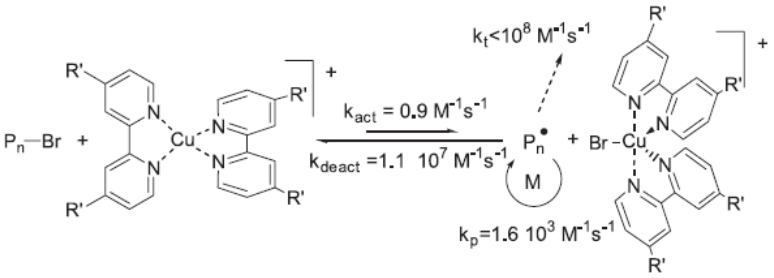

Scheme 1.8 ATRP mechanism

The most widely used halogen atom (X) that allows to make the most successful and well controlled ATRP is bromine, even if chlorine is also well studied; very poor is the literature about the utilization of iodine and fluorine atoms in ATRP processes.
The mechanism reported before can be divided in a series of sub equilibria that work together in defining the overall equilibrium constant K_{ATRP} ; the subequilibria are reported below :

1. Alkyl halides bond homolysis (K_{BH})
   $$RX \leftrightarrow R^{\bullet} + X^{\bullet} \quad (1.5)$$
2. Oxidation of the metal complex or *electron transfer* (K_{ET})
   $$Mt^{n}L \leftrightarrow Mt^{n+1}XL + e^{-} \quad (1.6)$$
3. Reduction of an halogen to halide ion or *electron affinity* (K_{EA})
   $$X^{\bullet} + e^{-} \leftrightarrow X^{-} \quad (1.7)$$

4. Association of the halide ion to the metal complex or *halogenophilicity* (K_X)

$$X^- + Mt^{n+1}L \leftrightarrow Mt^{n+1}XL \quad (1.8)$$

Various parameters affect the equilibrium constants of subequilibria which are strongly correlated with the overall equilibrium constant of reaction (K_{ATRP}) by equation 1.9:

$$K_{ATRP} = K_{BH}K_{ET}K_{EA}K_X = \frac{k_{act}}{k_{deact}} \quad (1.9)$$

First of all K_{ATRP} depends on the energetic of alkyl halides bond homolysis (equation 1.5) that strongly affects the activation step, but also the reactivation of the dormant species after monomer addition. To this purpose, alkyl halide bond dissociation energies (BDE) for a series of ATRP monomers/initiators were calculated and correlated with K_{ATRP} values (*43*).

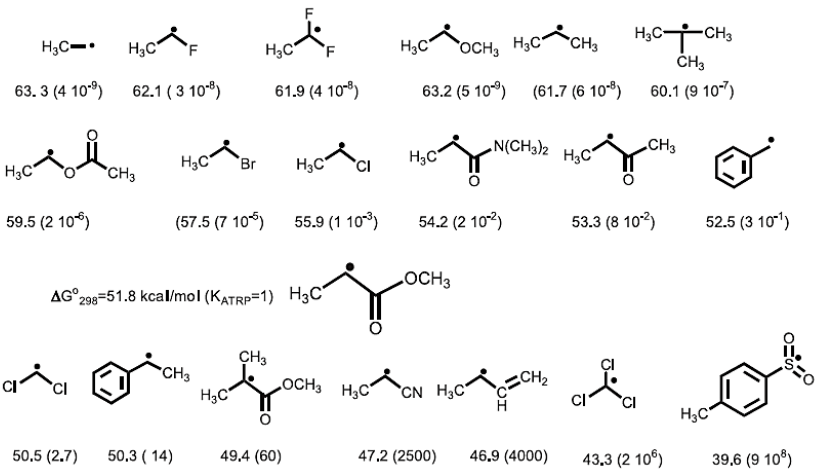

Scheme 1.9 Free energy change (ΔG^0_{298}) and relative values of K_{ATRP} for homolytic bond cleavage of several alkyl bromides .

By these studies it was possible to define the polymerization rates of less reactive monomers: for example, if the conversion of methyl acrylate is 90% in 1 h with a specific catalyst, for styrene 11 h are to be expected based on its BDE and 15 y for vinylacetate (*43*).

Another important parameter is the catalyst activity that depends on the redox potential of the complex, so as demonstrated by a linear correlation found between redox potential and equilibrium constant for a series of Cu(I) complexes (*44*, *45*), that will be explain better after in this chapter.

On the other hand, transition metals are characterized by different halogenophilicities that lead to variation of redox potentials in the presence of different halide ions. Furthermore, the catalytic activity depends on the stability constants of the complex in its two oxidation states (β^{n+1} e β^{n}) and, in particular, on the ratio between these constants. High value of β^{n+1}/β^{n} ratio corresponding to Cu(I) complex very reducing and catalytically active in ATRP (*46*). The equation that correlates redox potential with the stability constants of the complex in its two oxidation states is reported below:

$$E = E^0 + \frac{RT}{F}\ln\frac{[Cu^{II}]_{tot}}{[Cu^{I}]_{tot}} - \frac{RT}{F}\ln\frac{\beta^{II}}{\beta^{I}} \qquad (1.10)$$

where E^0 = standard redox potential .

As regard reactions involving the halide ion (eq. 1.7 and eq. 1.8), studies have showed that K_{EA} and K_X are strongly dependent on the nature of the solvent (*47*, *48*). Protic solvents better stabilize halide anions through solvation leading to high values of K_{EA} (*48*). Changes in solvent polarity influences K_X as reported by Tsarevsky et al. (*47*) in a study corresponding to the coordination of Br^- to copper (I) catalyst complexed by different ligand in CH_3CN and in aqueous medium. K_X values five orders of magnitude greater in organic medium than in water, in the presence of different ligands (bpy, PMDETA, Me_6TREN), are found showing that in aqueous media the majority of the halogen will be dissociated from the Cu deactivating species.

ATRP is a radical-based process where radicals can be formed from dormant species via several pathways. Mechanistically, halogen atom transfer from alkyl halide to Cu(I) complex can occur via either the outer-sphere electron transfer (**OSET**) or the inner-sphere electron transfer (**ISET**) as reported in Scheme 1.10. The ISET process proceeds through a transition state in which the halogen atom acts as a bridge for the electron transfer from the metal center to the C−X bond; the products of this step are R• and $[X{-}Cu^{II}L]^{+}$. OSET can proceed via a stepwise manner with radical anion intermediates (OSET-SW) or in a concerted process with simultaneous dissociation of alkyl halide to a radical and anion (OSET-C). Therefore, during the electron transfer (ET) , the possible interactions (in terms of bond breaking and formation) between the redox partners would sensibly decrease the activation barrier of the reaction. Conversely, Cu^{I} may behave as a simple outer sphere electron donor with negligible interaction with RX. As previously described, OSET pathways can occur through OSET-SW or OSET-C and in both cases, the halogen transfer follows the ET, and therefore the association of X^{-} to Cu morely affects the driving force of the reaction. According to Marcus analysis of electron transfer processes (*49*) OSET has an energy barrier ~15 kcal/mol higher than what is experimentally measured, i.e., OSET is $\sim 10^{10}$ times slower than ISET. The differences are much greater than any computational or experimental errors, and, consequently, it can be concluded that a copper-catalyzed ATRP occurs via concerted homolytic dissociation of the alkyl halide via ISET, i.e., an atom transfer process. In terms of energy, the two-step process via the radical anion intermediates is the least favorable [50].

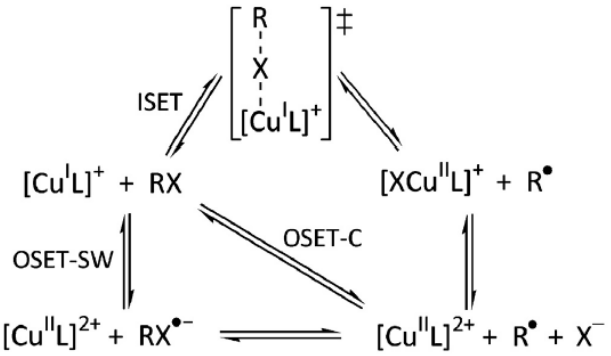

Scheme 1.10 Possible mechanisms of RX activation by Cu(I) complexes.

1.4.2. Components (Catalyst, Ligands, Initiators, Monomers and Solvents)

Catalyst. As before reported, copper is the most used metal catalyst in ATRP with four accessible oxidation states, Cu^0, Cu^I, Cu^{II} and Cu^{III}, but only Cu(I) and Cu(II) complexes are of relevance in ATRP catalysis. The +3 oxidation state has been postulated as an intermediate in Cu-catalyzed cross coupling reactions (*50*) and some complexes have been recently isolated. Most commonly, copper salt is introduced as cuprous halide (Cu^ICl or Cu^IBr) and the catalysis involves the Cu^I/Cu^{II} redox states even if alternative mechanism called Single Electron Transfer-Living Radical Polymerization (SET-LRP), based on disproportionation of Cu^I and exclusive activation by Cu^0 has been proposed by Percec et al in 2006 . Although there are evidences on the capability of Cu^0 to activate the C-X bond, this mechanism is subject of controversy (*51*).

The role of the catalytic system in ATRP is fundamental because it strongly influences the equilibrium constant K_{ATRP} and the activation rate constant k_{act}. By observing the following equation:

$$K_{ATRP} = \frac{k_{act}}{k_{deact}} = \frac{[Cu^{II}X_2L][P_n^\bullet]}{[Cu^IXL][P_nX]} \qquad (1.11)$$

it's possible to notice that best catalysts should have a low K_{ATRP} in order to provide a low concentration of propagating species, $P_n^{\bullet}$. In order to ensure a fast exchange between dormant and active species avoiding reactions between radicals, a reasonable polymerization rate has to be maintained and indeed a specific ratio of the redox catalytic couple as expressed by the following equation :

$$R_p = k_p[P_n^{\bullet}][M] = k_p \frac{k_{act}}{k_{deact}} \frac{[Cu^I XL]}{[Cu^{II} X_2 L]} [P_n X]_0 [M] \qquad (1.12)$$

A metal catalyst working in an ATRP process must have fundamental requisites . First of all the metal centre must have at least two accessible oxidation states separated by one electron, an expandable coordination sphere (to accommodate the halogen atom) and a significant affinity for the halogen atom; also, it should form stable Cu^I and Cu^{II} complexes, with high β^{n+1} and β^n, in the presence of ligand or halogen atoms. Thermodynamic studies revealed that both Cu^IX_n and $Cu^{II}X_n$ complexes are stable, with n = 1,2 for Cu^I and n = 1,2,3,4 for Cu^{II} (*52*, *53*). This difference in the coordination number denotes different capabilities of the coordination sphere for the two oxidation states. Indeed, Cu^I is basically tetracoordinated with tetrahedral or square planar configuration, whereas Cu^{II} is usually pentacoordinated with square pyramidal or trigonal bipyramidal structures (*54*). This is particularly important in ATRP since, during the atom transfer, the oxidation state of the metal increases by one unit.

Ligands. Doubtless nitrogen ligands are the most used in ATRP since they are superior than others in terms of performance. Different species as polydentate aromatic, aliphatic or cyclic amines have been mostly used (Scheme 1.11) and their employment which influences the solubility and the activity of the catalyst depends on several factors ; the most important are the topology of the ligand (cyclic bridged > branched > cyclic ~ linear), the number of N atoms (tetradentate > tridentate > bidentate), the nature of the N-ligand (pyridine ~ alkyl amine > alkyl imine >aryl imine > aryl amine) (*55*).

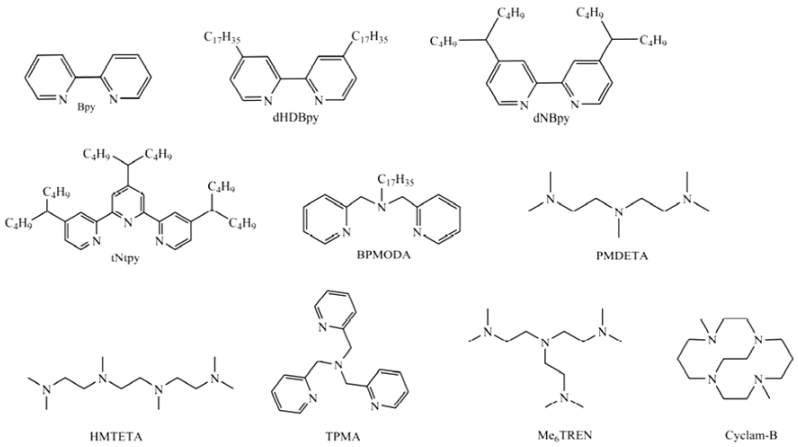

Scheme 1.11 Structures of ligands employed in ATRP

ATRP studies begun with the utilization of bipyridine (Bpy) or modified Bpy as ligands. The modified Bpy as DHBpy and dNBpy have electron donating aliphatic substituents which increase the electron donating properties of the metal centre allowing to easier C-X bond activation and k_{act} and K_{ATRP} are higher by a factor of up to 10 (*56*). Even if these systems allow a good control over the polymerization, their low activity (typically, $K_{ATRP} < 10^{-8}$) imposes high catalyst loadings (up to 1-2 mole percent with respect to the monomer), long reaction times and expensive purification procedures. To overcome these difficulties, new tri- and tetradentate ligands with ethylene linkages were developed; the most employed are PMDETA, TPMA and Me_6TREN which are characterized by an exceptional activity that allows to catalyze ATRP with only ppm amounts of copper (*57*). In particular, as regard tetradentate ligands, binary 1:1 complexes are expected to be formed due to the saturation of Cu^I coordination sphere. More recently, tetradentate cyclic ligands, which generate square planar Cu^I complexes, are used as copper(I) dimethyl crossbridged cyclam ([Cu^I/Cyclam-B), the most reducing and active catalyst ever studied until now (*44*).

ATRP rate constants of activation for various ligands with a specific initiator (ethyl-2-bromoisobutyrate) in the presence of Cu^IBr in MeCN were calculated, showing

that more than six orders of magnitude were accessible changing the ligand (*55*) as reported in figure 1.1.

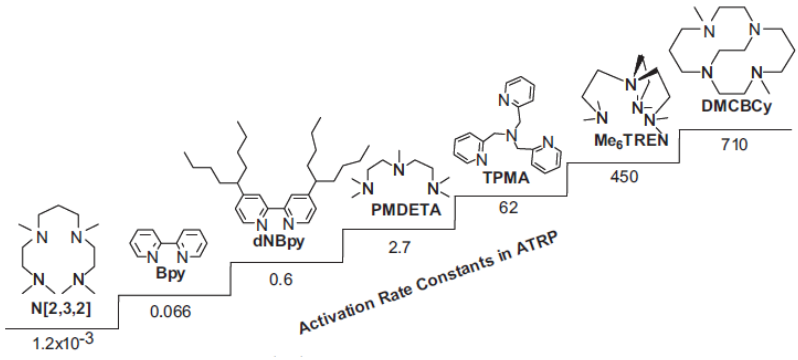

Figure 1.1 ATRP rate constants of activation (in M^{-1} s^{-1}) for various ligands with ethyl-2-bromoisobutyrate in the presence of $Cu^{I}Br$ in MeCN at 35°C.

Initiators. The broad availability of initiators provides ATRP with a significant advantage over other CRP techniques. Typically, alkyl halides (RX), in molecular or macromolecular structure, are used as initiators with the aim to initiate polymerization and to determine the number of growing polymer chains (*2*). In particular, from the degree of polymerization (DP), defined as the ratio between the concentration of monomer and that of initiator (DP = [M]/[I]), it's possible to calculate the molecular weight of polymer considering that all initiator's molecules are activated by the catalyst. This condition is verified only for polymerization systems in which termination events are negligible and the initiation efficiency is close to unity. By the reasons just mentioned it's possible to understand that the choice of initiator is very important and its reactivity depends on the alkyl halide BDE and on the catalyst employed (*43*). Figure 1.2 shows how the activation rate constants is strongly influenced by several rules pertaining to initiator structure; the activity depends on the degree of substitution (primary<secondary< tertiary), on the transferable atom (for methyl 2-halopropionates :Cl < Br < I) and on the radical stabilizing group (-Ph~-C(O)OR<<-CN) (*58*).

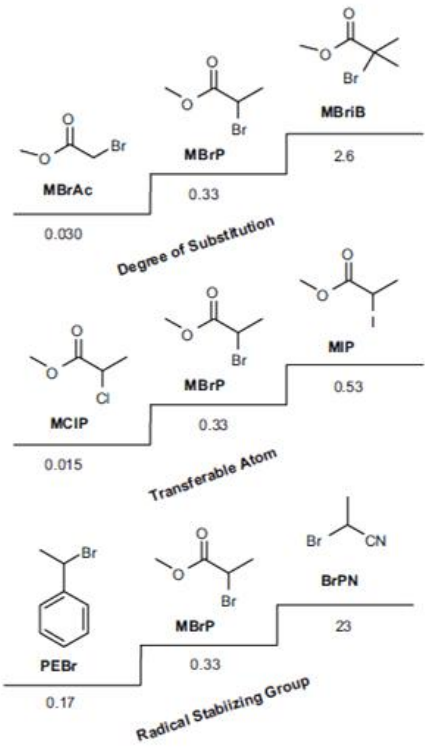

Figure 1.2 Values of k_{act} (in $M^{-1}s^{-1}$) in ATRP for various initiators with CuX/PMDETA in MeCN at 35°C

By observing the effect of bond strength in alkyl halides (and then the transferable atom), the order reported may suggest that alkyl iodides should be the most efficient initiating systems. However, for several drawbacks reported in literature (*59*), these systems are less stable than those based on chlorine or bromine atoms; for instance, iodides are light sensitive and the C−I bond may undergo heterolytic cleavage so that they are used in an alternative mechanism that leads to the polymerization through a degenerative transfer and called Iodine Transfer Polymerization (ITP).

Finally, very important is that the reactivity of R−X should be higher than that of P_n−X and, for this reason, the initiator structure should mimic that of the dormant macromolecular chain end so that the propagating radical Pn• is as reactive as the initiator radical R•. By this way, benzyl substituted halides are good initiators for the

polymerization of styrene due to their chemical structure resemblance, but they are inefficient for the polymerization of more reactive monomers such as methylmethacrylates. For similar reasons, α-halopropionates and α-halonitriles are good for the polymerization of acrylates and acrylonitrile, respectively.

Monomers. As reported about initiator, also for monomer the typology and the morphology of molecular structure could influence the evolution of an ATRP reaction. In the previous paragraph, the effect of initiator/monomer structure on activation was discussed and it is possible to deduce that the penultimate monomer unit can have a strong effect on k_{act} as evidenced in measurements of k_{act} from dimeric alkyl halides reported in the study carried out by Nanda et al. (*60*). So, in the presence of the same initiator, the type of the monomer used induces different kinetics and control of the final chains and then monomers containing substituents able to stabilize the propagating radicals have to be used in a successfull ATRP. Several monomers have been polymerized by ATRP allowing to well controlled final chains as styrenes, acrylates, methacrylates, acrylonitriles. Interestingly, the order of the equilibrium constants for a series of common monomers differs from SFRP and RAFT where steric effects are very important. In ATRP, that order is acrylonitrile >methacrylates>styrene~acrylates>acrylamides >>vinyl chloride>vinyl acetate (*2*).

Some monomers present drawbacks as (meth)acrylamides due to potential side reactions such as competitive complexation of the metal catalyst and displacement of the terminal halogen atom by reaction with the amide group. On the other hand, acidic monomers (e.g. acrylic acid) can protonate the nitrogen ligand and deactivate the metal catalyst, thus their ATRP polymerization requires protection of the acidic function.

Polymerization of less activated monomers, such as vinyl acetate, is still a challenge for ATRP: the dormant species is indeed a poorly reactive primary alkyl halide, 2-haloethylacetate, which requires highly reducing catalysts for the reductive cleavage of the C−X bond.

Solvents. Several factors affect the solvent choice such as the reduction of chain transfer to solvent and the evaluation of interactions between solvent and catalyst. Solvent-assisted side reactions as elimination of HX from polystyryl halides (*61*) and catalyst poisoning should be minimized (*62*). ATRP can be carried out either in bulk, in solution, or in a heterogeneous system (e.g., emulsion, miniemulsion, suspension) (*63*). Various solvents, such as acetonitrile, dimethylsulfoxide, dimethylformamide, acetone, benzene, toluene, anisole, ethylene carbonate, alcohols, water, supercritical carbon dioxide, and many others, have been used in the polymerization of different monomers. The role of this component is rather critical, especially for the catalytic system taking into account the possibility that its structure may change due to the action of the solvent as a solvating and coordinating medium.

For example, the ATRP of n-butyl acrylate with $CuBr(bpy)_3$ carried out in ethylene carbonate was found to proceed much faster than in bulk (*64*), while another very important study has predicted that K_{ATRP} should span over ca. 5 orders of magnitude going from the non polar toluene to water (*65*).

1.4.3. Typical Phenomenology: Kinetics, Molecular weight, Molecular weight distribution and Initiation systems

Kinetics. In the previous paragraph, in the discussion concerning the fundamental characteristic of catalysts employed in ATRP, the direct correlation between R_p and ratio between the concentrations of the two species of the redox couple was reported. Equation 1.12 was elaborated using the assumption that contribution of termination becomes insignificant due to the persistent radical effect and using a fast equilibrium approximation. By this way, a linear variation of conversion with time in semilogarithmic coordinates has to be observed due to the constant concentration of active species (*66*) as reported in figure 1.3.

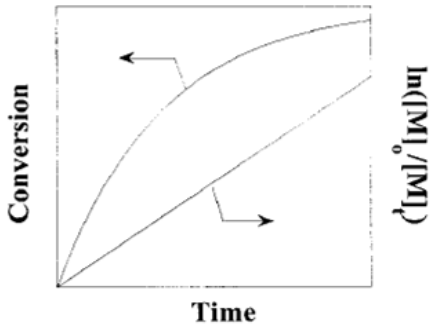

Figure 1.3 Schematic representation of the dependence of the conversion on time in linear and semilogarithmic coordinates.

However, since termination occurs continuously, the concentration of Cu(II) species increases and deviation from linearity may be observed. By kinetic studies carried out in the presence of different monomers as styrene (*62*), methylacrylate (*67*), methylmethacrylate (*68*, *69*) first-order kinetics with respect to monomer, initiator and Cu(I) complex concentrations were observed.

More difficult is the definition of the rate law for the deactivator due to the spontaneous generation of Cu(II) via PRE (*62*, *70*, *71*). When the initial concentration of Cu(II) is not sufficiently large to ensure a fast rate of deactivation, bimolecular termination of radicals occurs and the concentration of Cu(II) increases. With each radical termination event, 2 equiv of Cu(II) will form irreversibly. The objective is the definition of the conditions that ensure that the rate of radical combination is slower than the radical deactivation by Cu(II), so a controlled/living polymerization will proceed. Some studies analyzed the effect of a small amount (~10 mol %) of deactivator added initially to the polymerization in order to reduce the fraction of terminated chains (*72*).

Molecular weight and molecular weight distribution. The degree of polymerization allows to calculate the theoretical molecular weight of a polymer created by a well-controlled ATRP and is expressed by the following equation:

$$DP_n = \frac{\Delta[M]}{[I]_0} \qquad (1.13)$$

where $\Delta[M] = [M]_0$*conversion

$[M]_0$ = initial concentration of the monomer

$[I]_0$ = initial concentration of the initiator

while the theoretical molecular weight is

$$M_{n\,th} = DP_n * MW_0 \qquad (1.14)$$

with MW_0= molar mass of the monomer.

Even if the termination and other side reactions are also present in ATRP, well-defined polymers with molecular weights ranging from 1000 to 150000 have been successfully synthesized (*61*). Figure 1.3 reports a typical linear increase of the molecular weight with conversion in the ATRP of methyl acrylate (*67*) and the typical behavior of the molecular weight distribution that is the index of the polymer chain-lenght distribution. The drop of the polydispersity could be predicted by equation 1.15:

$$\frac{M_w}{M_n} = 1 + \left(\frac{[RX]_0 k_p}{k_{deact}[D]}\right)\left(\frac{2}{p} - 1\right) \qquad (1.15)$$

where if k_p and the concentrations of initiator $[RX]_0$ and deactivator [D] are known, the rate constant of deactivation can be calculated from the evolution of polydispersity with conversion p. Furthermore in the case reported, regarding acrylates, higher polydispersities were observed initially since the rate constants of propagation for this type of monomer are relatively large and several monomer units are added during each activation step but, with the progress of the reaction, chain become more uniform due to continuous exchange reactions (*67*). A well-controlled ATRP is characterized by a relatively narrow molecular weight distribution ($1.0 < M_w/M_n < 1.5$) and the equation 1.15 is correct only when the initiator is completely consumed and degrees of polymerization are sufficiently high.

1.4.4.Initiation Systems

Despite the extraordinary control of final polymeric structure and the potential commercial application of materials created by ATRP technique, their production on industrial scale is limited for different reason:

- high catalyst concentration that leads to expensive post-polymerization purifications;
- toxicity of many transition metal complexes employed with environmental repercussion after purification;
- utilization of special procedures in order to remove oxygen from systems.

Prompted by this limitation, many researchers developed several ATRP initiation systems addressed to make this technique more adapt for industrial production. The original **normal ATRP** starting with equivalent concentration of RX and catalyst was firstly modified in its initial state with the development of **Reverse ATRP**. Reverse ATRP starts by a catalyst in the higher state of oxidation that was converted to the activator by reaction with a conventional initiator as peroxides or azocompounds. The initial polymerization components are thus less sensitive to oxygen and can be easily prepared, stored and shipped for commercial use. This technique needs that the catalyst concentration must be comparable to the concentration of initiator because the transferable halogen atom or group is added as a part of the copper salt. Furthermore, the source of halogen atom must be the copper salt because in the presence of an ATRP initiator a dual initiation system is created and the technique is called **Simultaneous reverse and normal initiation (SR&NI)**. In this technique, radicals generated by AIBN are subsequently deactivated by an oxidatively stable Cu(II) salt forming Cu(I) and some halogenated chains (*73*). Cu(I) can then reactivate the ATRP initiator and concurrently mediate normal ATRP. The limitation of last techniques is in the inability to produce block copolymers due to the presence of the conventional radicals. To this purpose, a new initiation system called **AGET (Activators generated by electron transfer)** was created starting from reducing agents unable to initiate new chains as organic

derivatives of triethylamine (*74*) or ascorbic acid (*75*) and inorganic species as Sn^{II} (*76*) or Cu^0 (*77*, *78*). These chemical reactants react with Cu(II) complex to generate the Cu(I) activator followed by normal ATRP that proceeds in the presence of alkyl halides or macromonomers.

AGET was a precursor to **activator regenerated by electron transfer (ARGET)** ATRP in which small amount of catalyst is continuously regenerated by a reducing agent to account for unavoidable levels of radical termination. ARGET is a green procedure that uses ppm of the catalyst in the presence of appropriate reducing agents such as FDA-approved tin(II) 2-ethylhexanoate ($Sn(EH)_2$), glucose (*79*, *80*), ascorbic acid (*81*), hydrazine, phenylhydrazine (*82*, *83*), excess inexpensive ligands (*84*), nitrogen-containing monomers (*85*) or Cu^0. Another technique with low concentration of copper known as **initiators for continuous activator regeneration (ICAR)** was elaborated to both scavenge oxidants and decrease the amount of catalyst needed. This technique could be considered as a reverse ARGET in which a source of organic radicals is employed to continuously regenerate Cu(I), which would otherwise be consumed in termination reactions, when catalysts are used at very low concentrations (*83*). The rate of ICAR ATRP is governed by the rate of decomposition of the added free radical initiator, as in RAFT, while the degree of control, the rate of deactivation, and the molecular weight distribution are controlled by K_{ATRP} as in ATRP (*86*, *87*). A summary of typical ratios of all reagents employed in these techniques and principal mechanism are reported in figure 1.4.

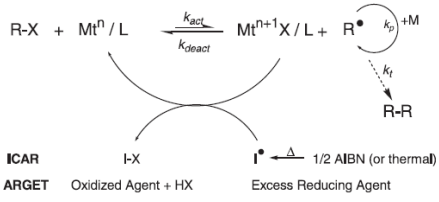

Typical ratios used in ATRP methods and RAFT

Method	M/*R*-*X*/Cu^I*X*/Cu^{II}*X*	*L*	RA	AIBN
Normal ATRP	200/1/1/—	1	—	—
Reverse ATRP	200/—/—/1	1	—	0.5
SR&NI ATRP	200/1/—/0.2	0.2	—	0.1
AGET ATRP	200/1/—/0.2	0.2	0.18	—
ARGET ATRP	200/1/—/<0.01	0.1	<0.1	—
ICAR ATRP	200/1/—/<0.01	0.01	—	<0.1
RAFT	200/1 dithioester/—/—	—	—	0.1

Figure 1.4 Mechanism of different ATRP techniques and typical ratios used .

Zerovalent metals such as Cu, Fe, Mg or Zn can also be used as reducing agent and, in addition, act as a supplemental activators by a direct reaction with alkyl halides. In particular, Cu^0 (**SARA ATRP**) and Fe^0 in form of powder, a turning, a wire, a mesh, a film and an electrode were used alone with ATRP ligands and also together with Cu^{II}/ligands and Fe^{III}/ligands to catalyze ATRP of acrylates, methacrylates and styrene (*88*, *89*). The role of Cu^0 and the effect of polar solvents on the kinetics of an ATRP were discussed in details in the studies carried out by Matyjaszewski et al. (*65*, *90*, *91*) where the disproportionation/comproportionation action of metallic copper is a relatively slow process rather than "instantaneous". In order to avoid the utilization of chemicals Matyjaszewski and Gennaro in 2011 (*92*) published for the first time a study in which chemical reducing agents were replaced by "electrons" fed to the system as electrical current and this technique namely **e-ATRP** (electrochemical ATRP) will be exposed in the details in the following paragraph.

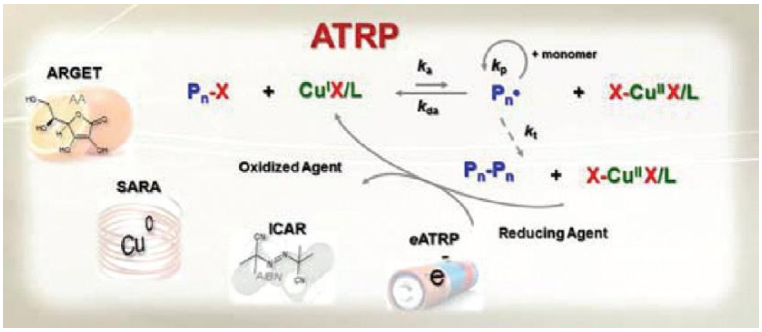

Figure 1.5 Low catalyst concentrations ATRP techniques

1.5 Electrochemical Investigation for ATRP

In the last years, it has been shown that electrochemical tools can be effectively used to collect very precious information on ATRP processes. In 2000, Amatore et al. studied several copper complexes successfully used as catalysts for ATRP by cyclic voltammetric experiments to relate their electrochemical properties with the kinetic features of ATRP (*44*). A general trend of the variation of redox potentials by

changing the ligand and the anion was observed and this trend is in agreement with the activities of the complexes in ATRP as demonstrated in the plot of log ($K_{eq\ app}$) versus $E^{1/2}$ (Fig. 1.6). The lower the redox potential, the larger the apparent equilibrium constant for the oxidation reaction of Cu(I) to Cu(II), and therefore the higher the activity in catalyzing the polymerization.

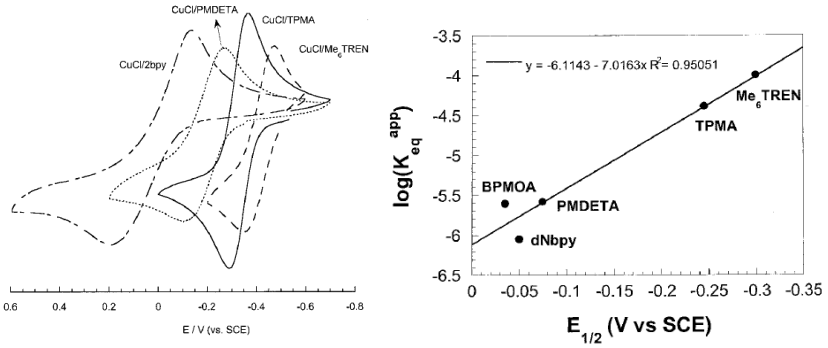

Figure 1.6 Cyclic voltammetry of CuCl/L (with L= bpy, PMDETA, TPMA or Me_6TREN) and variation of K_{eq} with $E^{1/2}$ for complexes composed by different ligands

Isse et al. studied the kinetics of the activation reaction between the RX initiator and the Cu(I) complex by chronoamperometric and cyclic voltammetric experiments (*93*). Investigation of the kinetics of activation of some alkyl halides by copper complexes used as ATRP catalysts and comparison with the kinetics of dissociative ET has unequivocally shown that the reaction between these complexes and alkyl halides is an inner-sphere ET, that is, a halogen atom abstraction. Considering the huge difference between the k_{act} values measured for the Cu complexes and the predictions of outer-sphere ET theory, the study concluded that the results obtained can be extended to the copper-catalyzed activation of alkyl halides in ATRP and related processes in general.

Cyclic voltammetry was also employed (often together with other measurements such as potentiometric and spectrophotometric ones) to study the main species that are present in the reaction medium during ATRP polymerization (*94*) , the effect of the ligand on the redox potentials of the transition metal redox couple, its stability and speciation, the role of the solvent and in general to gain better understanding of

the reaction mechanisms. By this work the standard reduction potentials of Cu^{II} and $Cu^{II}L$ as well as the global and step stability constants (β and K) of all complexes arising from the binary Cu-X or Cu-L and ternary Cu-L-X systems have been determined in CH_3CN. The binary Cu-X systems show only mononuclear CuX_x complexes, where x = 1, 2, 3, 4 for Cu^{II}, and x = 1, 2 for Cu^{I}. For both types of complex analyzed, Me_6TREN is a much better ligand than PMDETA, especially for Cu^{II}. This is most likely due to the presence of an additional nitrogen in Me^6TREN with respect to the tridentate PMDETA. The halidophilicity of both Cu^{II} and Cu^{I} significantly decreases upon complexation with the polyamine ligands.

Speciation diagrams of the ternary systems (Figure 1.7) show that while there is a wide range of conditions for the predominance of $Cu^{II}LX$, Cu^{I} is always present as a mixture of $Cu^{I}L^{+}$, $Cu^{I}L_2^{+}$, $Cu^{I}X_2^{-}$,$Cu^{I}LX$, $Cu^{I}X$, and $Cu^{I}_2LX_2$, with a distribution strongly depending on the concentration of the ligands. When $X = Br^{-}$, $Cu^{I}L$ remains the predominant species even at very high values of C^0_X/C^0_{CuI}..Thus, using bromides instead of chlorides appears to be more beneficial from the viewpoint of synthesis.

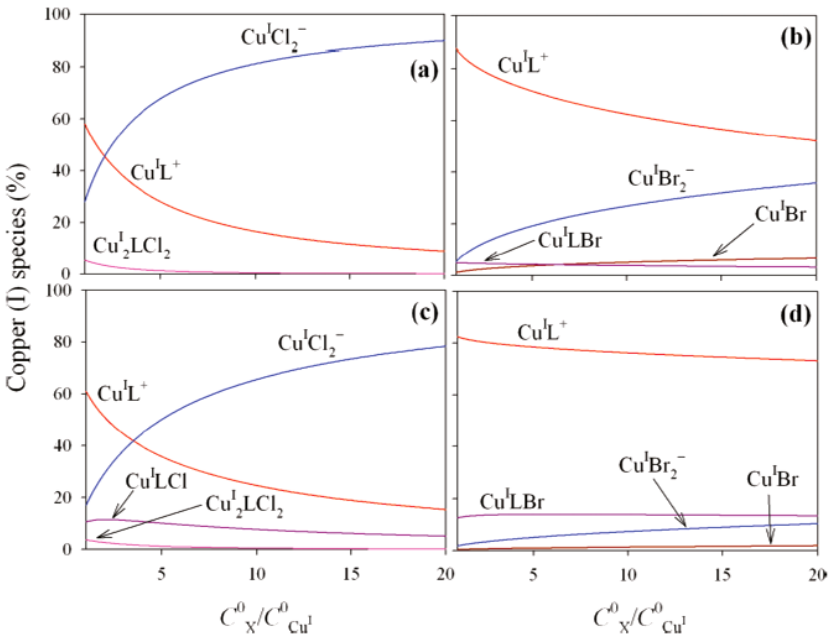

Figure 1.7 Speciation diagrams

It was recently shown that electrochemical tools can be also successfully used to have a better control of ATRP processes; Gennaro and co-authors showed both in organic (*92*) and aqueous media (*95*) that the utilization of an externally applied electric potential can reversibly activate the copper catalyst. This is the concept of electrochemically mediated ATRP (e-ATRP) in which the ratio of concentration of activator to deactivator is precisely controlled by electrochemistry. The mechanism of this type of ATRP is shown in scheme 1.12:

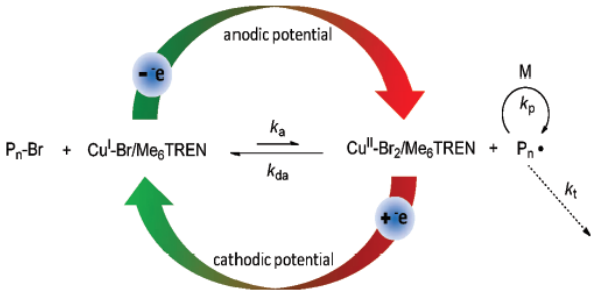

Scheme 1.8 Proposed mechanism for Electrochemical Control over an ATRP**.**

where it is possible to observe that a catalytic complex in its higher state of oxidation composed by $Cu^{II}Br_2/Me_6TREN$ is reduced to $Cu^{I}Br/Me_6TREN$ by the application of a cathodic potential. In the absence of mass transport limitations, the rate of reduction is dictated by the applied potential and the rate of an e-ATRP can be controlled by changing it. More negative the potential, more high is the ratio activator/deactivator and faster the polymerization rate. Figure 1.9 shows the effect of different values of the potential between -0.69 and -0.40 V vs Ag/Ag^+ standard electrode, respectively, in a polymerization of MA in MeCN at 25°C (MA =50 % v/v) and different conversions were achieved between on and off states (*92*).

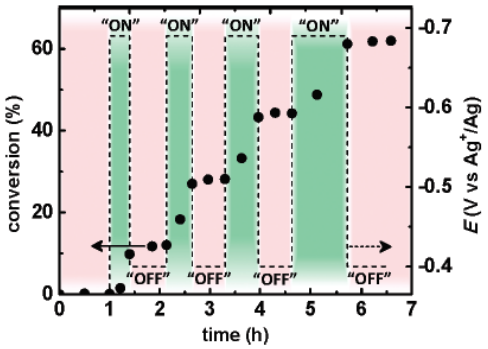

Figure 1.9 Conversion (solid circles) and applied potential (dashed line) with respect to time, in MA polymerization at two different applied potentials.

References

1. A. H. E. Müller, K. Matyjaszewski, *Controlled and Living Polymerizations, Wiley -VCH* (2009).
2. W. A. Braunecker, K. Matyjaszewski, *Prog. Polym. Sci.* **32**, 93–146 (2007).
3. C. Walling, *Free radicals in solution, New York: Wiley* (1957).
4. Szwarc M., *Nature*. **176**, 1168–9 (1956).
5. M. Szwarc, M. Levy, R. Milkovich, *J Am Chem Soc*. **78**, 2656–7 (1956).
6. Szwarc M., *Carbanions, living polymers and electron transfer processes. New York: Interscience Publishers;* (1968).
7. Szwarc M., (1972).
8. D. Greszta, D. Mardare, K. Matyjaszewski, *Macromolecules*. **27**, 638–44 (1994).
9. A. Goto, t Fukuda, *Prog Polym Sci*. **29**, 329–85 (2004).
10. C. Hawker, A. Bosman, E. Harth, *Chem Rev*. **101**, 3661–88 (2001).
11. M. Georges, R. Veregin, P. Kazmaier, G. Hamer, *Macromolecules*. **26**, 2987–8 (1993).
12. B. Wayland, G. Poszmik, S. Mukerjee, M. Fryd, *J Am Chem Soc*. **116**, 7943–4 (1994).
13. D. B. Guillaneuf, D. Gigmes, S.R.A. Marque, P. Astolfi, L. Greci, P. Tordo, *Macromolecules*. **40**, 3108–3114 (2007).
14. D. Benoit *et al.*, *J. Am. Chem. Soc.* **122**, 5929–5939 (2000).
15. M. Ouchi, T. Terashima, M. Sawamoto, *Chem. Rev.* **109**, 4963–5050 (2009).
16. M. Kato, M. Kamigaito, M. Sawamoto, T. Higashimura, *Macromolecules*. **28**, 1721–1723 (1995).
17. J.-S. Wang, K. Matyjaszewski, *J. Am. Chem. Soc.* **117**, 5614–5615 (1995).
18. K. Matyjaszewski, *Curr. Opin. Solid State Mater. Sci.* **1**, 769–776 (1996).
19. M. Iovu, K. Matyjaszewski, *Macromolecules*. **36**, 9346–54 (2003).
20. S. Gaynor, J.-S. Wang, K. Matyjaszewski, *Macromolecules*. **28**, 8051–6 (1995).
21. J. Chiefari *et al.*, *Macromolecules*. **31**, 5559–62 (1998).

22. G. Moad, E. Rizzardo, S. Thang, *Aust J Chem*. **58**, 379–410 (2005).
23. M. Destarac, D. Taton, S. Zard, T. Saleh, S. Yvan, *ACS Symp Ser*. **854**, 536–50 (2003).
24. Y. Kabachii, S. Kochev, L. Bronstein, I. Blagodatskikh, P. Valetsky, *Polym Bull*. **50** (2003).
25. E. Le Grognec, J. Claverie, R. Poli, *J Am Chem Soc*. **123**, 9513–24 (2001).
26. J. Brandts, P. van de Geijn, E. van Faassen, J. Boersma, G. Van Koten, *J Organomet Chem*. **584**, 246–53 (1999).
27. S. Maria *et al.*, *J Am Chem Soc*. **127**, 5946–56 (2005).
28. Y. Kotani, M. Kamigaito, M. Sawamoto, *Macromolecules*. **32**, 2420–4 (1999).
29. K. Matyjaszewski, M. Wei, J. Xia, N. McDermott, *Macromolecules*. **30**, 8161–4 (1997).
30. T. Ando, M. Kamigaito, M. Sawamoto, *Macromolecules*. **30**, 4507–10 (1997).
31. R. O'Reilly, V. Gibson, A. White, D. Williams, *Polyhedron*. **23**, 2921–8. (2004).
32. M. Teodorescu, S. Gaynor, K. Matyjaszewski, *Macromolecules*. **33**, 2335–9 (2000).
33. M. Kato, M. Kamigaito, M. Sawamoto, T. Higashimura, *Macromolecules*. **28**, 1721–3 (1995).
34. F. Simal, A. Demonceau, A. Noels, *Angew Chem Int Ed*. **38**, 538–40 (1999).
35. W. Braunecker, Y. Itami, K. Matyjaszewski, *Macromolecules*, 9402–4 (2005).
36. V. Percec, B. Barboiu, A. Neumann, J. Ronda, M. Zhao, *Macromolecules*. **29**, 3665–8 (1996).
37. B. Wang, Y. Zhuang, X. Luo, S. Xu, X. Zhou, *Macromolecules*. **36**, 9684–6 (2003).
38. C. Granel, P. Dubois, R. Jerome, P. Teyssie, *Macromolecules*. **29**, 8576–82 (1996).
39. H. Uegaki, Y. Kotani, M. Kamigaito, M. Sawamoto, *Macromolecules*. **30**,

2249–53 (1997).

40. P. Lecomte, I. Drapier, P. Dubois, P. Teyssie, R. Jerome, *Macromolecules*. **30**, 7631–3 (1997).
41. K. Matyjaszewski, J. Xia, *Chem Rev*. **101**, 2921–90 (2001).
42. J.-S. Wang, K. Matyjaszewski, *J Am Chem Soc*. **117:**, 5614–5 (1995).
43. M. Gillies *et al.*, *Macromolecules*. **36**, 8551–9 (2003).
44. J. Qiu, K. Matyjaszewski, L. Thouin, C. Amatore, *Macromol Chem Phys*. **201**, 1625–1631 (2000).
45. K. Matyjaszewski, B. Goebelt, H. Paik, C. Horwitz, *Macromolecules*. **34**, 430–40 (2001).
46. N. Tsarevsky, W. Tang, S. Brooks, K. Matyjaszewski, *ACS Symp Ser*. **944**, 56–70 (2006).
47. N. Tsarevsky, T. Pintauer, K. Matyjaszewski, *Macromolecules*. **37**, 9768–78 (2004).
48. T. Pintauer, B. McKenzie, K. Matyjaszewski, *Polym Prep (Am Chem Soc, Div Polym Chem)*. **43**, 217–8 (2002).
49. C. Y. Lin, M. L. Coote, A. Gennaro, K. Matyjaszewski, *J. Am. Chem. Soc.* **130**, 12762−12774 (2008).
50. F. Monnier, M. Taillefer, *Angew. Chem. Int. Ed.* **48**, 6954–6971 (2009).
51. L. M. Huffman, S. S. Stahl, *J. Am. Chem. Soc.* **130**, 9196–9197 (2008).
52. S. E. Manahan, R. T. Iwamoto, *Inorg. Chem.* **4**, 1409–1413 (1965).
53. S. Ahrland, K. Nilsson, B. Tagesson, *Acta Chem. Scand.* **37a**, 193–201 (1983).
54. T. Pintauer, K. Matyjaszewski, *Coord. Chem. Rev*. **249**, 1155–1184 (2005).
55. W. Tang, K. Matyjaszewski, *Macromolecules*. **39**, 4953–4959 (2006).
56. W. Tang *et al.*, *J. Am. Chem. Soc.* **130**, 10702–10713 (2008).
57. T. Pintauer, K. Matyjaszewski, *Chem.Soc.Rev.* **37**, 1087–1097 (2008).
58. W. Tang, K. Matyjaszewski, *Polym Prep (Am Chem Soc, Div Polym Chem)*. **46**, 211–2 (2005).
59. G. David *et al.*, *Chem. Rev.* **106**, 3936–3962 (2006).
60. A. Nanda, K. Matyjaszewski, *Macromolecules*. **36**, 8222–4 (2003).

61. K. Matyjaszewski, K. Davis, T. Patten, M. Wei, *Tetrahedron*. **53**, 15321 (1997).
62. K. Matyjaszewski, T. Patten, J. Xia, *J. Am. Chem. Soc.* **119**, 674 (1997).
63. M. F. Cunningham, *Prog. Polym. Sci*. **27**, 1039–1067.
64. K. Matyjaszewski, K. Nakagawa, C. G. Jasieczek, *Macromolcules*. **31**, 1535 (1998).
65. W. A. Braunecker, N. V. Tsarevsky, A. Gennaro, K. Matyjaszewski, *Macromolecules*. **42**, 6348–6360 (2009).
66. K. Matyjaszewski, J. Xia, *Chem Rev*. **101**, 2921–90 (2001).
67. K. Davis, H. Paik, K. Matyjaszewski, *Macromolecules*. **32**, 1767 (1999).
68. J. L. Wang, T. Grimaud, K. Matyjaszewski, *Macromolecules*. **30**, 6507 (1997).
69. V. Percec, B. Barboiu, H. J. Kim, *J. Am. Chem. Soc*. **120**, 305 (1998).
70. D. A. Shipp, K. Matyjaszewski, *Macromolecules*. **33**, 1553 (2000).
71. H. Fisher, *J. Polym. Sci. Part A Polym. Chem.* **37**, 1885 (1999).
72. K. Matyjaszewski *et al.*, *Pat. 9718247, U.S. Pat.5,* 807–937.
73. J. Gromada, K. Matyjaszewski, *Macromolecules*. **34**, 7664–71 (2001).
74. H. Tang, M. Radosz, Y. Shen, *Macromol Rapid Commun*. **27**, 1127–31 (2006).
75. K. Min, H. Gao, K. Matyjaszewski, *J Am Chem Soc*. **127**, 3825–30 (2005).
76. W. Jakubowski, Matyjaszewski K., *Macromolecules*. **38**, 4139–46 (2005).
77. K. Matyjaszewski, S. Coca, S. Gaynor, M. Wei, B. Woodworth, *Macromolecules*. **30**, 7348–50 (1997).
78. J. Queffelec, S. Gaynor, K. Matyjaszewski, *Macromolecules*. **33**, 8629–39 (2000).
79. W. Jakubowski, K. Matyjaszewski, *Angew. Chem., Int. Ed.* **45**, 4482−4486 (2006).
80. W. Jakubowski, K. Min, K. Matyjaszewski, *Macromolecules*. **39**, 39−45 (2006).
81. K. Min, H. Gao, K. Matyjaszewski, *Macromolecules*. **40**, 1789−1791 (2007).

82. S. Fleischmann, B. M. Rosen, V. Percec, *J. Polym. Sci., Part A Polym. Chem.* **48**, 1190−1196 (2010).
83. K. Matyjaszewski *et al.*, *Proc. Natl. Acad. Sci. U. S. A.* **103**, 15309−15314 (2006).
84. Y. Kwak, A. J. D. Magenau, K. Matyjaszewski, *Macromolecules*. **44**, 811−819 (2011).
85. K. Dong, H.; Matyjaszewski, *Macromolecules*. **41**, 6868−6870 (2008).
86. W. Tang, K. Matyjaszewski, *Macromol. Theory Simul.* **17**, 359−375 (2008).
87. K. D'Hooge, D. R. Konkolewicz, D. Reyniers, M.-F. Marin, G. B. Matyjaszewski, *Macromol. Theory Simul.* **21**, 52−69 (2012).
88. K. Matyjaszewski, S. G. Gaynor, S. Coca, *US 6, 541,580,* (2003).
89. K. Matyjaszewski, S. Coca, S. G. Gaynor, M. Wei, B. E. Woodworth, *Macromolecules*. **30**, 7348−7350 (1997).
90. Y. Zhang *et al.*, *Macromolecules*. **45**, 78−86 (2012).
91. T. Guliashvili, P. V Mendonca, A. C. Serra, A. V. Popov, J. F. Coelho, *J. Chem.--Eur. J.* **18**, 4607−4612 (2012).
92. A. J. D. Magenau, N. C. Strandwitz, A. Gennaro, K. Matyjaszewski, *Science (80-.).* **332**, 81−84 (2011).
93. A. A. Isse, N. Bortolamei, P. De Paoli, A. Gennaro, *Electrochim. Acta*. **110**, 655–662 (2013).
94. N. Bortolamei, A. A. Isse, V. B. Di Marco, A. Gennaro, *Macromolecules*. **43**, 9257–9267 (2010).
95. N. Bortolamei, A. A. Isse, A. J. D. Magenau, A. Gennaro, K. Matyjaszewski, *Angew. Chemie*. **123**, 11593–11596 (2011).

CHAPTER 2.
MODIFICATION OF POLYMERS BY GRAFTING

2.1 Graft Copolymerization

2.1.1 Radical grafting mechanism

One of the main important field in which the scientific community are addressed its interest is the modification of polymers with the aim to give them properties more suitable for specific field and also to effect a gradual replacement of natural materials with either all synthetic materials or modified natural ones. Several means to modify polymers properties such as blending, grafting, and curing are studied. In particular:

- Blending is the physical mixture of two (or more) polymers to obtain the requisite properties
- Grafting is a method that leads to the formation of covalent bonds onto the polymer chain
- Curing regards the polymerization of oligomer mixture in order to form a coating on a substrate by physical forces.

These methods are characterized by different time scales as minutes, hours or even days can be necessary for grafting , while curing is usually a more rapid process. The schematic reactions for the polymer modification are presented in Figure 2.1 (*1*).

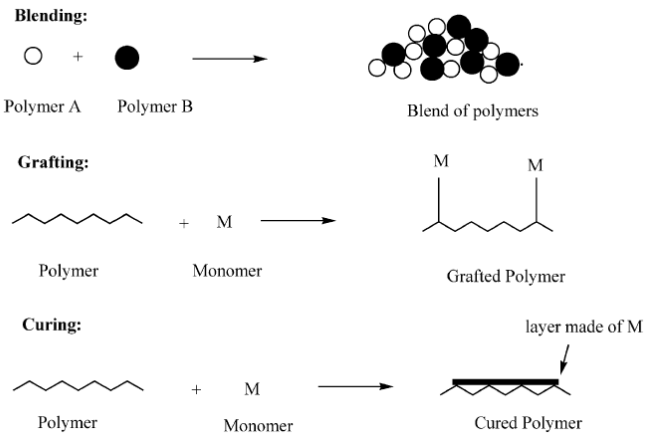

Figure 2.1 Schematic representation of the methods for polymer modification

In this thesis grafting method was used taking into account that it is an effective route and a stable type of modification that leads via covalent stable bonds formation to the tuning of the chemical-physical properties of polymers; for this reason grafting is also an important aspect of polymer science which continues to receive considerable attention (*2*).

A typical graft copolymer is characterized by a structure similar to that reported in scheme 2.1:

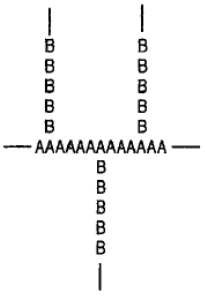

Scheme 2.1 General structure of a graft copolymer

where the main polymer backbone A, commonly referred to the trunk polymer, has branches of polymer chain B emanating from different points along its length and

that is usually indicated with the nomenclature A-*graft*-B, which can be further abbreviated as A-*g*-B.

The basic mechanism shown in Scheme 2.2 , commonly called "grafting from" mechanism (different from "grafting through" and "grafting onto" not used in this work and then not described here), begins by creating free radical sites on the trunk polymer chain which can react with double bond of vinyl monomers leading to the synthesis of a new polymer chain covalently bonded to the trunk polymer.

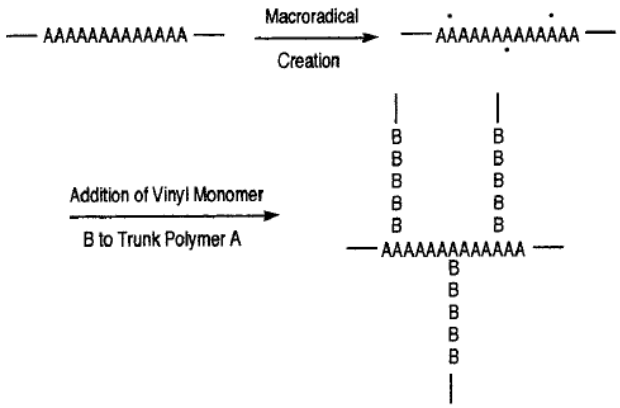

Scheme 2.2 General Mechanism of Graft Copolymerization of Trunk Polymer A with Vinyl Monomer B by Means of a Free Radical Mechanism

A drawback, not shown in scheme 2.2 is related to the formation of homopolymer when conventional radical initiator is used to synthesize a new chain (in the presence of vinyl monomer B). Moreover it is also possible that after a grafted chain has been initiated and begins to propagate, chain transfer from the growing grafted chain end can occur with some species in the medium to yield a free radical in solution that could initiate the growth of homopolymer B chains. This is a major problem encountered in graft copolymerization besides the difficulty of having a good control over the grafted chain molecular weight. In fact, homopolymer formation is the major reason for the lack of a widespread industrial development of graft copolymers Not only is the homopolymer a waste of monomer, but the separation of it from the grafted derivative is often difficult, and it thus creates

problems in characterizing the graft derivative. In fact, homopolymer formation is the major reason for the lack of a widespread industrial development of graft copolymers (*3*).

The main chemical intermediates which can initiate a grafting reaction are free radicals and ions and their role is critical in the determination of the evolution of the whole process. According to the nature of the intermediates involved it is possible to have free radical grafting or a ionic grafting . In this doctoral thesis radical grafting was carried out and for this reason the focus is on this particular type of methodology.

The generation of radicals could be achieved by direct or not direct methods. For example, a typical not direct method is based on redox reactions involving species as Mt^{n+}/H_2O_2 o Mt^{n+}/persulfates (*4*):

$$Fe^{2+} + H_2O_2 \rightarrow Fe^{3+} + OH^- + OH^{\bullet} \quad (2.1)$$

$$Fe^{2+} + O_3^-S - OO - SO_3^- \rightarrow Fe^{3+} + SO_4^{2-} + SO_4^{-\bullet} \quad (2.2)$$

$$SO_4^{-\bullet} + H_2O \rightarrow HSO_4^- + OH^{\bullet} \quad (2.3)$$

$$SO_4^{-\bullet} + R_{polymer} - OH \rightarrow HSO_4^- + R_{polymer} - O^{\bullet} \quad (2.4)$$

where OH· e $SO_4^{-\cdot}$ are the active species which can react with H_2O (equation 2.3) or directly with the polymeric chain (equation 2.4) showing that $SO_4^{-\cdot}$ species starts the copolymerization extracting an hydrogen from the polymer chain (*4*).

Another study carried out by Baijpai et al. (*5*) has focused its attention of the mechanism related to the formation of a macroradical (GO·) that occurs when the rate of vinyl polymerization is faster than the rate of H abstraction. The mechanism is reported in scheme 2.3 shown below:

$$R^{\cdot} + M \rightarrow RM^{\cdot}$$
$$RM^{\cdot} + M \rightarrow RMM^{\cdot}$$
$$RM^{\cdot}_{n-1} + M \rightarrow RM^{\cdot}_{n}$$
$$GOH + RM^{\cdot}_{n} \rightarrow GO^{\cdot} + R\text{-}M_n\text{-}H$$
$$GO^{\cdot} + M \rightarrow GOM^{\cdot}$$
$$GOM^{\cdot} + nM \rightarrow GOM^{\cdot}_{n}$$
$$GOM^{\cdot}_{n} + GOM^{\cdot}_{n} \rightarrow \text{graft co-polymer}$$

Scheme 2.3 Mechanism of radical graft copolymerization

The direct method leads to the formation of free radicals on the polymeric backbone through direct oxidation mediated by ions of transition metals (Ce^{4+}, Cr^{6+}, Co^{3+},…). In this case the redox potential of metallic ions is a crucial parameter in the evolution of degree of grafting that commonly improves when metals with low redox potentials are used. This mechanism leads to the formation of complexes between metallic ions and polymers , as below reported for Ce^{4+}:

$$Ce^{4+} + R_{polymer} - OH \rightarrow complex \rightarrow R_{polymer} - O^{\bullet} + Ce^{3+} + H^{+} \quad (2.5)$$
$$R_{polymer} - O^{\bullet} + M \rightarrow R_{polymer} - OM^{\bullet} \rightarrow R_{polymer} - OMM^{\bullet} \quad (2.6)$$

An alternative to the direct formation of radicals on polymers is the employment of compounds as azocompounds, peroxides, hydroperoxides which induce the formation of radicals by thermal decomposition. In this context the study carried out by Tsubokawa et al. (*6*) is very interesting and reports the utilization of organic pigments with azocompounds able to polymerize vinylic monomers by radical methods.

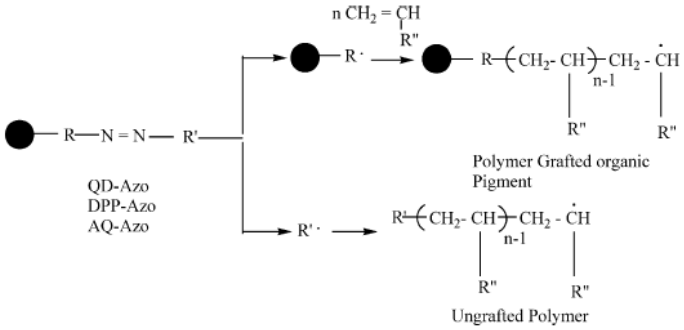

Scheme 2.4 Schematic illustration of a vynil polymerization carried out by azocompounds incorporated in organic species.

Among these species benzoyl peroxide (BPO) and azoysobutyrronitrile (AIBN) are surely the most used until now and typical mechanism involving them are reported below.

$$I_2 \rightarrow 2I^{\cdot}$$

$$I^{\cdot} + M \rightarrow IM^{\cdot} \rightarrow IMM^{\cdot}$$

$$I^{\cdot} + \text{Polymer} \rightarrow \text{Polymer}^{\cdot} + IH$$

$$IMM^{\cdot} + \text{Polymer} \rightarrow \text{Polymer}^{\cdot} + IMMH$$

$$\text{Polymer}^{\cdot} + M \rightarrow \text{Polymer-}M^{\cdot}\text{-}nM \rightarrow \text{Polymer}(M_n\text{-}M)^{\cdot}$$

$$IMM^{\cdot} + nM \rightarrow IM\text{-}(M)_nH$$

$$\text{Polymer-}(M_n)^{\cdot} + I^{\cdot} \rightarrow \text{Polymer}(M_n) - I$$

$$\text{Polymer-}(M_n)^{\cdot} + {}^{\cdot}MMI \rightarrow \text{Polymer-}(M)_{n+2}\text{-}I$$

Scheme 2.5 Mechanism of radical graft copolymerization in the presence of azocompounds

2.1.2. Applications of materials modified by grafting

Graft copolymers have a variety of potential applications resulting from the wide range of properties available when different polymer chains are connected to form a hybrid branched macromolecule. For instance, in the biomedical field a great variety

of studies were carried out regarding artificial heart valves where silicon rubber grafted with *N*-vinyl pyrrolidone and natural rubber grafted with 2-(*N*,*N*-dimethylaminoethyl) acrylate (both synthesized with radiation techniques) appear more biocompatible after treatment (*7–9*). Another interesting medical application relates to the synthesis of graft copolymers in order to reduce frictional forces between two dissimilar surfaces and is related to the tubular devices (catheters and cytoscopes) which are, as necessary for examination, inserted into various bodily orifices (*10*). For example, the surface grafting of a poly(urethane) film with dimethyl acrylamide resulted in a decrease of the coefficient of friction when the substrate was in the fully hydrated state(*11*).

Graft copolymerization has several important applications in the textile industry. For instance, improved soil release and fabric comfort can be obtained from grafting fibers with hydrophilic monomers. Moisture absorbency of cellulose fibers was greatly increased (as high as 3000% water uptake) by radiation- induced grafting of acrylic acid from the fiber followed by cellulose decrystallization upon exposure to $ZnCl_2$. (*12, 13*).

Leger et al. carried out grafting on composites materials with the aim to modify the mechanical properties and especially to improve the interfacial adhesion and friction (*14*). Since polymers of different chemical structure do not generally form intimate mixtures when blended together, the interfaces between dissimilar polymers (polyA and polyB) in a composite requires some type of compatibilizer for high-strength applications. Graft copolymers are ideal for this type of situation because when a hybrid branched macromolecule (polyA-*g*-polyB) is placed at the interface between polyA and polyB, the respective portions of the graft copolymer diffuse into the bulk portion of polyA and polyB. Although an overall bulk phase separation between polyA and polyB remains, the graft copolymer positioned at the interface provides a stronger bond between these two phases. Incorporating small amounts of poly(ethyl acrylate) (PEA)-*g*-poly(styrene) (PSt) into PEA/PSt blends increased compatibilization and results in tensile strength increases due to increased interfacial adhesion between PEA and PSt phases (*15*).

Examples just provided allow one to illustrate the impact of graft copolymers on improving the properties of various end-use materials. However further studies have to be conducted in order to better understand both intramolecular and intermolecular characteristics of this type of copolymers (*3*).

2.2 Grafting by atom transfer radical polymerization

Recently, an increasing attention was devoted to the grafting of polymers by atom transfer radical polymerization (ATRP) that can allow the synthesis of materials with controlled composition and molecular weight, narrow molecular weight distributions and specific molecular architecture. As discussed in the previous chapter living polymerizations allow to carry out controlled reactions using benefits of radical and ionic polymerization together. In ATRP the intermediates species used to create radical points on initiators are catalytic complexes composed by metal and ligand (Mt/L) . “Well-defined” grafted structures were obtained by this methodology using different techniques as “grafting through”, “grafting from” and “grafting to".

"Grafting through" or macromonomeric method is one of the most simple ATRP technique used to synthesized graft copolymers with well defined lateral chains. Scheme 2.6 reports the mechanism and shows that typically a monomer is copolymerized with a functionalized macromonomer (for example a methacrylate) which have been prepared by an other CRP (*16*).

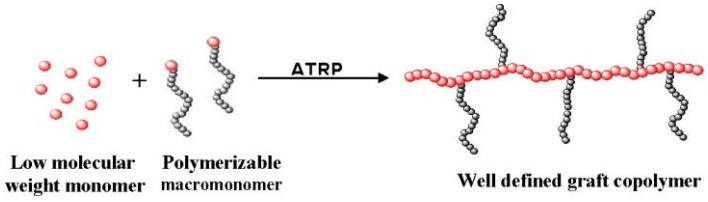

Scheme 2.6 Schematic illustration of "grafting through" by ATRP

Typically a low molecular weight monomer is radically copolymerized with a (meth)acrylate functionalized macromonomer. This method permits incorporation of macromonomers that have prepared by other controlled polymerization processes into a backbone prepared by a CRP. Functionalized macromonomers with halogenated pendant species (polyethylene, poly (ethylene oxide), polysiloxane, poly (lactic acid)) have been incorporated in a main chain of polystyrene or polymethyl methacrylate. The ramifications can be distributed homogeneously or heterogeneously based on the reactivity ratio of the terminal functional group on the macromonomer and of the low molecular weight monomer (*17*, *18*).

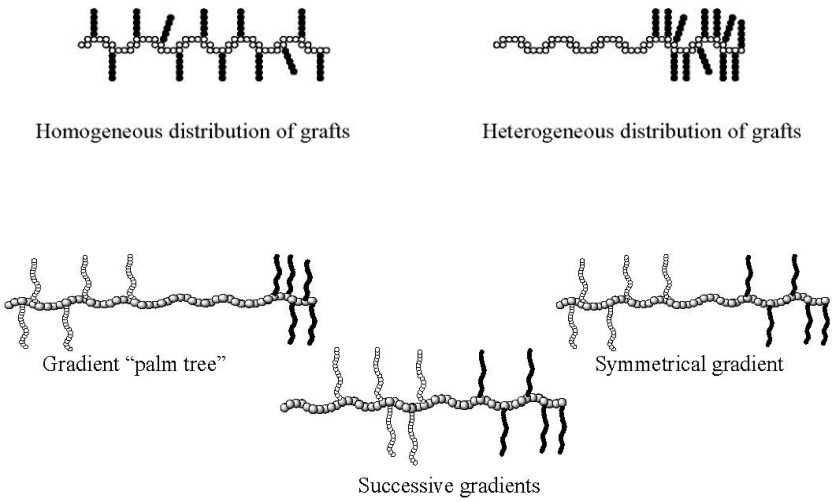

Scheme 2.7 Schematic illustration of different structures of grafted copolymers

Primary requisite for a **"grafting from"** reaction is the presence of a functionalized macromolecule as the one reported in scheme 2.8 that presents X moieties able to be abstracted by catalytic complex and then in this specific case, constituted by halogen atoms (*19–21*).

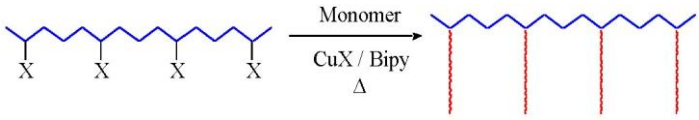

Scheme 2.8 Schematic illustration of "grafting from" by ATRP

Typically, this methodology is used to synthesize brushes macromolecules or polymeric structures similar to stars with very dense lateral chains among which steric repulsion is generated that will influence the conformation and the physical properties. The initiating sites can be incorporated by copolymerization (*19*, *22*) as an inherent part of the first polymer,(*23*) or incorporated in a post-polymerization reaction.

At the end only some general information about "grafting to" method that occurs by coupling reactions between linear chains with end functionalities and a precursor of the main chain. Compared to the others methodologies it has the advantage that the main chain and the side ones are prepared separately with a better controlled structure (*24, 25*).In fact, by this method ATRP of the single linear chain that will after coupled could be prepared by ATRP or other CRP to give them a good control of M_n and PDI.

2.3 Grafting of halogenated polymers (PVC and PVDF)

Grafting is surely one of the most widely used technique for modification and in particular "grafting from" method has been largely used to covalently immobilize new chains onto polymeric backbones (*26*).As exposed by literature, heterogenous graft copolymers show the properties of both (or more) polymeric backbone and new chain ends averaging the properties of both homopolymers (7). The grafting of halogenated polymers such as poly(vinylidenefluoride) (PVDF) and poly(vinylchloride) (PVC) is quite relevant for various applications (*27*) and, in recent years, the modification of these polymers has been extensively studied due to the technological and industrial relevance of these polymers. For instance, PVC is

well known for its compatibility with additives which improve its thermal and mechanical properties (*28*) and is used for the preparation of low cost ion exchange membranes, ion-selective electrode membranes or membrane sensors for ion-exchange columns for metal separation. For biomedical applications this polymer presents two main disadvantages: the utilization of phthalate ester plasticizers that have a potential carcinogenic effects and the poor biocompatibility of its hydrophobic surface that leads to unwanted protein adsorption and cell adhesion (*29*). To solve these problems many researchers have turned their efforts to its modification by suitable techniques (*30*, *31*). Figure 2.2 shows the results obtained by Lakshmi et al. about the modification of plasticized PVC that , although not a blood-compatible polymer, is the material most used for the manufacturing of blood bags and hemodialysis and, to this purpose, it is usually plasticized with di-(2-ethylhexyl phthalate) (DEHP) to impart flexibility . DEHP belongs to a class of agents called hypolipidemic hepatocarcinogens that could migrates in small quantities into the storage medium such as blood, plasma, or serum, resulting in a number of toxic effects. In this work the migration resistance and blood compatibility of flexible PVC could be significantly improved by grafting polyethylene glycol (PEG), the most blood-compatible polymer known today, onto the surface of flexible PVC. The method may also find use for preventing plasticizer migration from PVC cling films and polyvinylidene chloride films used extensively in food packaging (*31*).

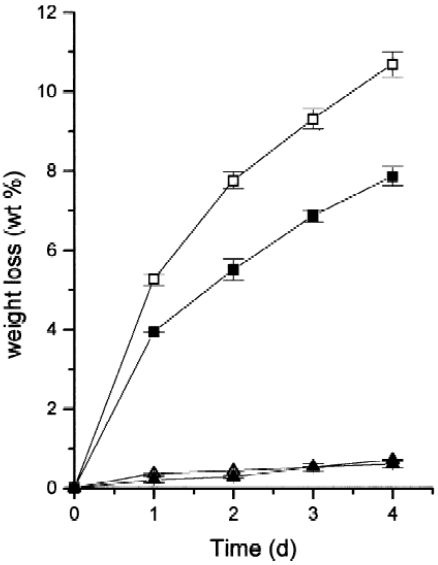

Figure 2.2 Effect of grafting on weight loss due to phtalates release from PVC tubes in different solvents (black and white signals) modified (Δ) and not (□) (*31*).

Because of high thermal and chemical stability, inertness to acids and solvents, low flammability and low dielectric constants, fluorinated materials play an important role in the development of new areas of material science, including fluoropolymers (2). These polymers are so-called “niche macromolecules" due to their applications in high tech field and modern technologies (3) and are attractive because of their versatility and employment in many applications (coatings, pipes, fluids for transmission, high-performance membranes) (4-6). Radical copolymerization of fluoropolymers have drawn great interest in the past decade and most commonly was realized by controlled radical technique (CRP). One of the most important fluoropolymers is surely poly(vinylidenefluoride) frequently used in bio-medical applications owing to its good biocompatibility; PVDF membranes, for example, are widely used in microfiltration and ultrafiltration system (*32*) and as carrier for drug delivery .

Due to the absence of functionalities on the fluoropolymer backbone or chain ends, introduction of an appropriate initiator or coupling agents is the first step toward copolymerization of these materials. Activation of fluoropolymers can be carried out

by several methods, including ozonization, γ-ray irradiation, electron beam exposure and controlled/living radical polymerization (CRP).

As an example of the effect of modification of PVDF a study carried out by ozonization is reported. Ozone-pretreated PVDF was modified by thermally induced graft copolymerization with N-isopropylacrylamide (NIPAM) and this modification was carried out in NMP solution (*33*) by Ying et al. The synthetic route is shown in scheme 2.9 where microporous membranes were fabricated from the PVDF-g-PNIPAM graft copolymers by phase inversion in aqueous media. After reaction the copolymer membranes exhibited reversible temperature-dependent permeability to calcein fluorescein isothiocyanate (FTIC)-dextran in phosphate buffer solution (*33*).

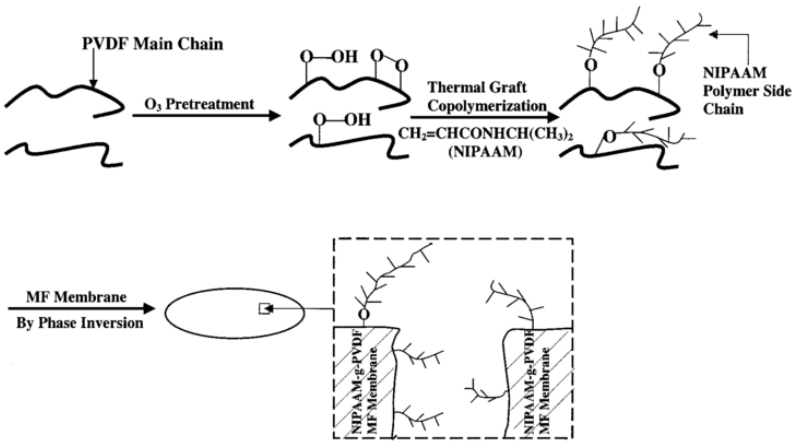

Figure 2.9 Schematic illustration of the processes of thermally induced graft copolymerization ofNIPAAMwith the ozone-preactivated PVDF backbone and the preparation of the NIPAAM-*g*-PVDF MF membrane by phase inversion.

2.4 Grafting of PVC and PVDF by ATRP

Both PVC and PVDF present the same hydrophobic nature, property sometimes not good for specific application. With the recent progress in polymerization methods, it

has become possible to design and obtain well-defined graft copolymers by CRP techniques, including NMRP, RAFT, ITP and ATRP.

Matyjaszewski et al. obtained graft copolymers of poly(vinylchloride) with styrene and methacrylates by ATRP method using a statistical copolymer of vinyl chloride with vinyl chloroacetate (99/1 cumulative molar composition) as macroinitiator (*34*). Other interesting studies were aimed to the modification of PVC by ATRP to create new materials for dye-sensitized solar cell (DSSC) applications (poly(vinyl chloride)-graft-poly(oxyethylene methacrylate) (*35*) (or to introduce 1,5-dihydroxynaphthalene (DHN) as a hydrogen bonding donor to form hydrogen-bonded macromolecules (poly(vinyl chloride-*graft*-4-vinyl pyridine) (*36*). The direct modification of the starting polymer was realized by direct activation of the halogen atom of its backbone so, or after functionalization with a more active pendant group (i.e. initiators containing bromine atoms are more active than those containing chlorine atoms). For instance some authors used the secondary chlorines of poly(vinylidenefluoride-co-chlorotrifluoroethylene) (PVDF-co-CTFE) as initiating site for the ATRP of different monomers (*37*).

But very interesting and of primary focus for this doctoral thesis is the possibility of a successful direct activation of PVDF and especially of the C-F bond that seems very challenging due to its strong energy (486 kJ/mol).

Very interesting the study carried out by a group of MIT related to the preparation of amphiphilic graft copolymers from commercial poly(vinylidenefluoride) by the extraction of the F atom directly from the polymeric backbone(*38*); in particular, graft-ATRP of methacrylates using polyvinylidene fluoride (PVDF) as macroinitiator was carried out (*38–40*) in order to create amphiphilic graft copolymers (poly(vinylidenefluoride)-g-poly(oxyethylene methacrylate)(PVDF-g-POEM) and poly(vinylidenefluoride)-g-poly(methacrylicacid)(PVDF-g-PMAA)) through direct initiation of the secondary fluorinated site of PVDF (*38*). As reported by Ameduri (*41*) the preparation of these copolymers is quite surprising for these main reasons: (i) it is possible that the grafting arises rather from the cleavage of the less stable C-H in the methylene and not of the more stable C-F bond, (ii) the chemical resistance of PVDF compared to others perfluoropolymers (PFTE, FEP) is

very poor,due to the presence of C-H bond, leading to the possible formation of byproducts as fluoride salt by reactions involving the acidic hydrogen atoms (*41*). Due to the strong energy of the carbon-fluorine bond and, of course, to the poor stabilization of the radical centers produced after C-F bond cleavage the results reported by the group of MIT seem quite surprising (*41, 42*). As explained by Kuila et al. (*42*) these disadvantages connected with C-F bond activation lead to rate of initiation slower than the propagation one and to a very poor control of molecular weight. Based on these considerations, these authors realized grafting of different monomers (methylmethacrylate (MMA), dimethylaminoethylmethacrylate (DMAEMA), tertiary butyl methacrylate (tBMA), diethylene glycol methyl ether methacrylate (MeO_2MA), n-butyl acrylate (nBA), t-butyl acrylate (tBA), diemthylacrylamide (DMA)) on PVDF after anchoring model ATRP-initiating sites , thus avoiding disadvantages previously reported connected with C-F bond activation. This work uses a combination between an initial ATRC (atom transfer radical coupling) and a final ATRP. In the first step, by replacing one fluorine atom from CF_2 of PVDF with pendant TEMPO moieties modified with alkyl halides, new model initiators were created; in the second step, these initiators react with monomers in the presence of copper catalyst by ATRP route(*42*). High conversion and good control of molecular weight were achieved through this new grafting strategy (*42*).

Very recently, the utilization of carbon fluorine bond as initiating site for ATRP was demonstrated by Peng et al. by a study carried out on perfluorosulfonic acid polymers (like Nafion) (*43*). By ^{19}F-NMR the authors showed that active sites are the tertiary C-F groups at both the main and side segments of Nafion and the CF_2 groups near to the tertiary ones(*43*). Figure 2.10 shows the (a) activation of Nafion chains for ATRA/ATRP reaction and,(b) Reaction of Nafion chains as ATRA of MWCNT bundles to result in MWCNT-Nafion hybrids followed by ATRP of NIPAAm to generate Nafion graft copolymer of Nafion-PNIPAAm and finally surface-initiated ATRP of styrene from Nafion 212 membrane (*43*).

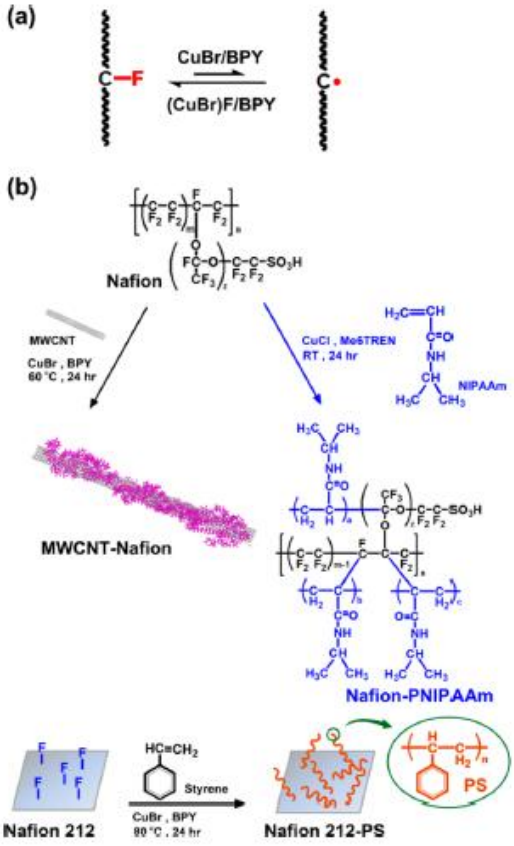

Figure 2.10 Schematic illustration of Atom Transfer Radical Addition/Polymerization of Perfluorosulfonic Acid Polymer with the C−F Bonds as Reactive Sites (*43*).

Surely, the reactivity of perfluorosulfonic acid and the incorporation of functional chemical groups in Nafion chains was demonstrated, but this study does not say anything about the mechanism involved and the control on molecular weight and molecular weight distributions of obtained final chains.

In this context the modification of polymers by ATRP become very interestingly when very strong carbon-halogen bond (as C-Cl or C-F) were employed, whereas the living nature of the process and therefore the control of the final chains are not insured.

2.5 Aim and organization of the Ph.D. thesis

The main objective of this work is to study the possibility of modifying halogenated polymers using them as ATRP macroinitiators realizing a DIRECT GRAFTING onto the polymeric backbone.

As reported by literature , ATRP was successfully used for "grafting-from" flat, convex, and concave surfaces, with the thickness of the polymer brushes precisely controlled by systematic variation of grafting density and DP_n of the tethered polymers.(*44*) Modification of surfaces with other polymer can be done to tailor surface properties such as hydrophilicity/hydrophobicity, (bio)compatibility, adhesion, adsorption, corrosion resistance, and friction. The surface properties can also be tuned by tethering block copolymers, with the composition and size of each polymer segment affecting the morphology and behavior of the polymer brushes. This study was carried out both in organic and in supercritical media The organic media, the most used until now, were used to investigate through electrochemical tools the livingness of an ATRP reaction activated by very strong bonds as C-Cl or C-F, while the potentiality as green solvent of supercritical carbon dioxide lead us to use it as an alternative solvent suitable for polymers used in biomedical field.To this purpose this thesis has been divided in two main sections (1 and 2) in order to separate the results obtained in the different solvents. The state of the art regarding supercritical solvent utilization will be reported at the begin of the section 2 in order to guide the reader to better understand of that specific part.

In the section 1 electrochemical methods for the study of various fundamental issues on Cu-catalyzed ATRP were used and mechanistic aspects, with particular regard to the main actors of ATRP, the copper catalyst and the macroinitiator/dormant species, were analyzed. Thus, a qualitative analysis of the kinetics of the activation process will be conducted as the study of the stability and the activity of the adopted Cu based catalytic systems and the evaluation of the effect on the performances of the process of various operating parameters such as the nature of the copper salt, the ligand, the reaction medium, the operating temperature and the reaction time. Besides these fundamental issues, another important goal of this project was pursued

during the period spent at Chemistry Department of Carnegie Mellon University (Pittsburgh, USA) under the supervision of prof. Krystof Matyjaszewski that allowed us to understand better the mechanism and the drawbacks of an ATRP reaction activated after C-F bond cleavage.

In the section 2 the studies on ATRP grafting carried out in supercritical carbon dioxide (sc-CO_2) will be reported taking into account the relevance of this chemical as reaction medium for polymers suitable for the biomedical field. The study of different initiation systems and parameters such as copper salts, ligands, temperature, carbon dioxide density and oxidation state of the metal on the grafting of hydroxyethylmethacrylate (HEMA) onto PVDF nanoparticles was carried out.

Given the biomedical character of the modified polymers we are interested to it was decided also to investigate the possibility of using sc-CO_2 as sterilizing agent of polymers contaminated by different microorganisms (bacteria and spores). This study was carried out to obtain information about the possibility of performing modification and sterilization of the polymer chains by a one step process.

References

1. A. Bhattacharya, B. N. Misra, *Prog. Polym. Sci.* **29**, 767–814 (2004).
2. Y. Gnanou, *J. Macromol. Sci., Rev. Macromol. Chem. Phys.* **C36 (1)**, 77 (1996).
3. H. A. J. Battaerd, G. W. Tregear, *Graft Copolymers, Interscience Publishers: A Division of John Wiley and Sons: New York* (1967).
4. M. Pepenzhik, A. Virnik, Z. Rogovin, *Vysok. Soedin Ser B*. **11**, 245–50. (1969).
5. U. Bajpai, A. Jain, S. Ray, *J Appl Polym Sci*. **39(11/12)**, 2187–204 (1990).
6. N. Tsubokawa, M. Kobayashi, T. Ogasawara, *Prog Org Coatings*. **36**, 39–4 (1999).
7. M. T. Razzak, K. Otsuhata, Y. Tabata, F. Onashi, A. Takeuchi, *J. Appl. Polym. Sci.* **38**, 829 (1989).
8. M. T. Razzak, K. Otsuhata, Y. Tabata, F. Onashi, A. Takeuchi, *Radiat. Phys. Chem.* **39**, 547.
9. A. Chapiro *et al.*, *Radiat. Phys. Chem.* **15**, 423 (1980).
10. Y. Uyama, K. Kato, Y. Ikada, *Adv. Polym. Sci.* **137**, 1 (1998).
11. K. Ikeuchi *et al.*, *Wear*. **161**, 179 (1993).
12. J. L. Williams, V. T. Stannett, *J. Appl. Polym. Sci.* **23**, 1265 (1979).
13. J. L. Williams, V. T. Stannett, *Text. Res. J.* **26**, 175 (1976).
14. L. Leger, E. Raphael, H. Hervet, *Adv. Polym. Sci.* **138**, 185 (1999).
15. D. G. Peiffer, M. Rabeony, *J. Appl. Polym. Sci.* **51**, 1283 (1994).
16. K. Matyjaszewski, *Curr. Opin. Solid State. Mater. Sci.*, 769–776 (1996).
17. C. Hawker *et al.*, *Makromol. Chem. Phys.* **198**, 155–166 (1997).
18. H. Shinoda, K. Matyjaszewski, *Macromolecules*. **34**, 6243–6248 (2001).
19. Y. Inoue, T. Matsugi, N. Kashiwa, K. Matyjaszewski, *Macromolecules*. **37**, 3651–3658 (2004).
20. L. Okrasa, T. Pakula, Y. Inoue, K. Matyjaszewski, *Colloid Polym. Sci.* **282**, 844–853 (2004).
21. H. Kaneyoshi, Y. Inoue, K. Matyjaszewski, *PMSE Prepr.* **91**, 41–42 (2004).

22. H. J. Paik, S. G. Gaynor, K. Matyjaszewski, *Macromol. Rapid Commun.* **19**, 47–52.
23. V. Percec, F. Asgarzadeh, *J. Polym. Sci., Part A Polym. Chem.* **39**, 1120–1135 (2001).
24. H. Gao, K. Matyjaszewski, *J. Am. Chem. Soc.* **129**, 6633–6639 (2007).
25. B. S. Sumerlin, N. V Tsarevsky, G. Louche, R. Y. Lee, K. Matyjaszewski, *Macromolecules*. **38**, 7540–7545 (2005).
26. Y. Inoue, T. Matsugi, N. Kashiwa, K. Matyjaszewski, *Macromolecules*. **37**, 3651–3658 (2004).
27. C. Gao, D. Yan, *Prog. Polym. Sci.* **29**, 183–275 (2004).
28. P. V. Smallwood, *Vinyl Chloride Polymers, Polymerization in: Encyclopedia of Polymer Science and Engineering, vol 17, 2nd edition*.
29. K. M. Mcginty, W. J. Brittain, *Polymer (Guildf).* **49**, 4350–4357 (2008).
30. V. K. Krishnan, A. Jayakrishnana, J. D. Francis, *J. Mater. Sci. Mater. Med.* **1**, 185–191 (1990).
31. S. Lakshmi, A. Jayakrishnan, *Artif. Organs*. **22**, 222–229 (1998).
32. D. Wang, K. Li, W. K. Teo, *J. Memb. Sci.* **163**, 211–220 (1999).
33. L. Ying, E. T. Kang, K. G. Neoh, 6416–6423 (2002).
34. H. Paik, S. G. Gaynor, K. Matyjaszewski, *Macromol Rapid Commun*. **52**, 47–52 (1998).
35. D. K. Roh *et al.*, *Electrochim. Acta*. **55**, 4976–4981 (2010).
36. J. H. Koh, J. A. Seo, J. K. Koh, J. H. Kim, *Nanotechnology*. **355604**, doi:10.1088/0957-4484/21/35/355604.
37. M. Zhang, T. P. Russell, *Macromolecules*. **39**, 3531–3539 (2006).
38. J. F. Hester *et al.*, *Macromolecules*. **35**, 7652–7661 (2002).
39. Inceoglu et al., *Des. Mon Pol.* **7**, 181–189 (2004).
40. A. et Al., *Adv. Mater.* **17**, 532–535 (2005).
41. B. Ameduri, *Macromolecules*. **43**, 10163–10184 (2010).
42. A. Kuila, D. P. Chatterjee, R. K. Layek, A. K. Nandi, *J. Polym. Sci. Part A Polym. Chem.* **52**, 995–1008.
43. K.-J. Peng, K.-H. Wang, K.-Y. Hsu, Y.-L. Liu, *ACS Macro Lett.* **4**,

197−201.

44. K. . Matyjaszewski *et al.*, *Macromolecules*. **32**, 8716−8724 (1999).

CHAPTER 3
UTILIZATION OF POLY(VINYLCHLORIDE) AND POLY(VINYLIDENEFLUORIDE) AS MACROINITIATORS FOR ATRP

3.1. Introduction

A great attention has been already devoted to the identification of the species really present in a typical reaction medium of ATRP reactions carried out in organic solvents in the work conducted by Bortolamei et al (*1*). These studies are crucial taking into account the fundamental role played by Cu in order to understand the reaction mechanism but also for further developments of ATRP as well as of its industrial applications.

In this chapter, the utilization of PVC and PVDF as macroinitiators for ATRP in NMP as solvent was studied using electroanalytical techniques as cyclicvoltammetry and chronoamperometry to investigate the effectiveness of the macroinitiators and to detect the relative population of the partners of the redox couple Cu(I)/Cu(II) during the copolymerization in organic solvent.

First of all, an overview of the materials, electrochemical techniques and grafting procedures used in this part of the research was reported.

Two catalysts commonly used in ATRP, CuX/TPMA and CuX/Me_6TREN were analyzed working with Cu species both in their first and second oxidation state , providing a detailed analysis of the several fundamental aspects of the activation process in ATRP. In particular, a considerable number of parameters and their effect on the stability and the activity of adopted Cu based catalytic systems was analyzed as the effect of the nature of copper salt, ligand, solvent and temperature of the reaction medium.

Cu catalysts and alkyl halide macroinitiators are characterized from kinetic standpoints, in order to obtain useful correlations between the structure and the reactivity of the catalytic system.

At the end, the grafting of HEMA on both PVC and PVDF was studied by carrying out some experiments at different operating conditions in terms of temperature, adopted catalysts and reaction time; these reactions were carried out using data collected in the first part of the chapter related to the choice of the optimal catalyst and the operative conditions that ensure the activation and then the grafting on halogenated polymers.

3.2 Experimental

3.2.1 Chemicals

1-Methyl-2-pyrrolidinone (extra dry with added Molecular Sieve, Acros Organics) and acetonitrile (99%, Sigma Aldrich) were stored under nitrogen atmosphere. Tetrabutylammonium hexafluorophosphate ($TBAPF_6$, 99%, Acros) and tetrabutylammonium bromide (TBABr, 99% Acros) were dried in an oven at 70°C prior their use. Cu(I)Br (98%), Cu(II)Br_2 (99%), Cu(I)Cl (98%) and Cu(II)Cl_2 (99%) were supplied from Sigma Aldrich and stored under nitrogen atmosphere. Tris(2-pyridylmethyl)amine (TPMA) (98%) and tris[2(dimethylamino)ethyl]amine (Me_6TREN) (97%) were both purchased from Aldrich and used as received (Scheme 2). PVDF used in this study was Hylar 461 (M_w = 440 kg/mol, M_w/M_n=4.1) obtained in powdery form (250 nm average particle size) from Solvay Specialty Polymers while PVC (high molecular weight, K-value (viscosity) 69-71, M_n=65 kg/mol) was purchased from Sigma Aldrich. Anhydrous 2-hydroxyethyl methacrylate (HEMA) (97%, stabilized with 250 ppm of monomethylether hydroquinone as inhibitor, reagent grade), ethanol (ACS, 99.8%) and 2,2,6,6-Tetramethylpiperidine 1-oxyl free radical (TEMPO, Acros Organics, 98%), KBr for FTIR analyses (99+%, FT-IR grade) were all purchased from Aldrich and used without further purification. Nitric acid (65% solution) for washing electrodes was purchased from Riedel-de Haën.

3.2.2 Experimental apparatus for electrochemical investigations and procedure

Cyclic voltammetry (CV) and chronoamperometric measurements were carried out in a jacketed three-electrode glass cell whose temperature was controlled by a thermostated bath (ULTRATEMP 2000, JULABO F30). An Autolab PGSTA30 potentiostat/galvanostat (EcoChemie, The Netherlands) run by a PC with GPES software was used to perform electroanalytical experiments. The working electrode was a 1 mm diameter Pt disk, whereas the counter and reference electrodes were a Pt coil and SCE respectively and they are inserted in the head of the cell as reported in Figure 3.1.

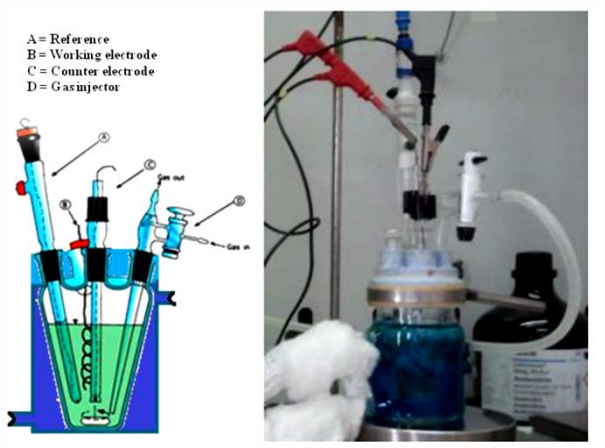

Figure 3.1 . Glass cell used for electrochemical investigations.

Prior to each experiment working and counter electrodes were cleaned by washing in a nitric acid solution (8 M) to remove copper followed by a washing in distilled water and ultrasonic rinsing in ethanol for 10 min.

The experiments were performed using the following sequence: the working solution composed by solvent and supporting electrolyte was first deareated with N_2 for 30 min, then the copper complex and, when used, the macroinitiator were added in two consecutive steps, each time recording cyclic voltammogramms of the system. The complex [Cu(I)XL] (X = Cl or Br, L = Me_6TREN or TPMA) was prepared in-situ by mixing stoichiometric amounts of the proper copper salt and

ligand. When used, TEMPO was always introduced in molar excess (15 times for chronoamperometry and 13 times for CV) with respect to copper ions to ensure quantitative scavenging of generated free radicals. For chronoamperometric measurements, the choice of the applied potential E_i was based on the voltammetric response of the system before the addition of the initiator P_nX. The potential was fixed to a value in the plateau region of the [Cu(I)XL] oxidation wave.

3.2.3. Electroanalytical techniques

Typical methods used until now to study ATRP systems based on gas chromatography, HPLC, NMR and UV−Vis are suitable only to the study of slow reactions with rate constants smaller than 1.0 $M^{-1}s^{-1}$. Most recently, detailed studies carried out by the group of professors Matyjaszewski and Gennaro utilized electrochemical methods to cover this deficiency and based on two different approaches: i) for relatively slow reactions, chronoamperometry to directly monitor the catalyst concentration during the activation reaction; ii) for fast reactions, with time scales in the range 1-10 seconds, kinetics was studied through voltammetric techniques, which exploit the transient electrogeneration of the active catalyst at the electrode surface (i.e. in the Nernst diffusion layer). In this work, these techniques were both carried out to investigate the activation of PVC and PVDF as macroinitiators.

Cyclic voltammetry. Cyclic voltammetry (CV) leads to achieve qualitative and quantitative information about electrochemical reactions. CVs offer a quick definition of the redox potential of the electroactive species and an assessment of the mediators effects on the redox process. During the scanning of the potential, the potentiostat measures the resulting current and, as the applied voltage increases for example in cathodic direction, the corresponding current increases until the

reduction potential of the test species is reached , thus generating a peak. The potential continues to grow until E_{final} is reached, but the cathodic current decreases because the even if the reduction potential is exceeded (figure 3.2) the relaxation of the diffusion layer decreases the limiting current that is the maximum recordable at the electrode surface. When the potential is inverted to complete the scan coming back to the $E_{initial}$, the species generated during the cathodic scan is re-oxidized at the electrode, giving origin to a curve I-V but with a resulting anodic peak (figure 3.2). This technique allows to study the system but not to change it (*2*).

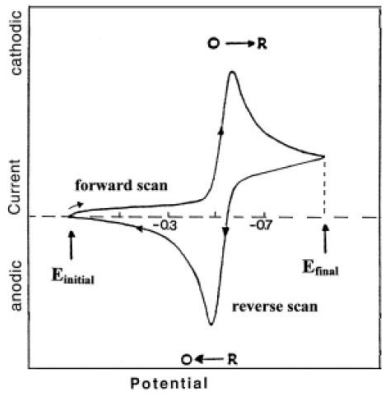

Figure 3.2 Typical cyclic voltammogram

By voltammogram it is possible to obtain four crucial information: the two current peaks and the two potential peaks which lead to determine the level of reversibility of the system. A reversible system is characterized by fast electron transfer kinetics, is governed by diffusion and it does not involve follow-up chemical reactions of electrogenerated species. For this reason the values of peak separation potential do not depend on the scan rate but only on the number of electrons involved in the redox reaction at the electrode. The variation of peak separation potential is expressed by equation 3.1 and the independence of scan rate is reported in figure 3.3 where CVs at different scan rates recorded in NMP solution with Cu(II)/L catalyst are presented.

$$\Delta E_p = E_{p,a} - E_{p,c} = \frac{59\ mV}{n} \quad (3.1)$$

where n is the number of exchanged electrons.

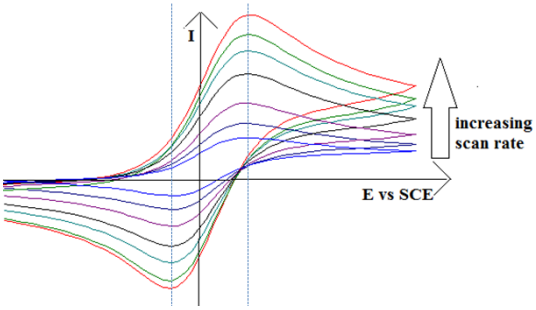

Figura 3.3. CVs of Cu(II)L complex at different scan rate

The redox potential can be estimated by equation 3.2 as a function of cathodic and anodic redox potentials are reported , $E_{p,c}$ and $E_{p,a}$ respectively.

$$E^0 = \frac{E_{p,a}+E_{p,c}}{2} \quad (3.2)$$

The ratio between peak currents is also an indication of the level of reversibility of the process. For a reversible electron transfer the following relation must be true simultaneously with aforementioned condition on peak separation potential:

$$\frac{i_{p,c}}{i_{p,a}} = 1 \quad (3.3)$$

Current peak intensity is directly proportional to the concentration of electroactive specie and increases with the square root of the scan rate as expressed by the Randles-Sevicik equation:

$$i_p = (2.69x10^5)n^{3/2}ACD^{1/2}Dv^{1/2} \quad (3.4)$$

where n = the number of electrons involved,

A = electrode area (cm^2),

D = diffusion coefficient (cm^2/s),

v = scan rate (V/s).

As reported in the literature (*3*) CVs were carried out in ATRP studies to investigate redox potentials of catalytic complex used and to analyze the activation step of the reaction. Figure 3.4 shows the electrochemical behavior of a solution of $Cu^{II}Br_2/Me_6TREN$ complex accomplished by application of a cathodic current (black curve). After addition of an alkyl halide initiator (ethyl 2-bromopropionate (EBP)), the CV changed and cathodic peak currents increased due to in situ regeneration of $Cu^{II}Br_2/Me_6TREN$ by reaction of the electro-generated $Cu^{I}Br/Me_6TREN$ complex with EBP (blue curve) according to chemical reaction:

$$Cu^{I}Br/Me_6TREN + EBP = EPB^{\circ} + Cu^{II}Br_2/Me_6TREN \quad (3.5)$$

The $Cu^{I}Br_2/Me_6TREN$ generated at the electrode reacts in solution to reduce EBP forming back $Cu^{II}Br_2/Me_6TREN$ that returns to the electrode surface to be reduced again. The cathodic current is thereby enhanced, because reduction involves apparently more than one-electron per copper ions, whereas the anodic current decreases, because $Cu^{I}Br_2/Me_6TREN$ is partially oxidized in solution.

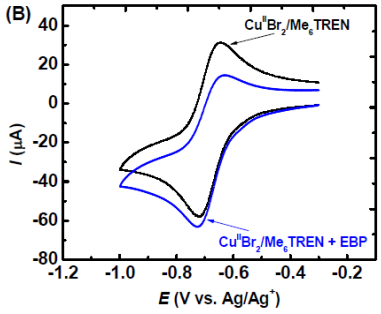

Figure 3.4 Voltammetric response after the addition of an alkyl halide initiator.

Utilization of poly(vinylchloride) and poly(vinylidene fluoride) as macroinitiators for ATRP

In this doctoral study cyclic voltammetries were recorded in most of cases at 0.1 V/s and 25 °C under magnetic stirring. $TBAPF_6$ (0.094 M) and TBABr (0.006 M) were used as supporting electrolyte if not differently stated. In some cases, experiments were performed at lower scan rates (up to 5 mV/s) and at different temperatures (in the range 25 – 60 °C) in order to evaluate the effect of these parameters.

Chronoamperometry. Activation kinetics was typically studied through chronoamperometry under steady state conditions (*4*). This consists in the polarization of the indicator electrode at a constant potential E_i, which may correspond to oxidation of Cu^I to Cu^{II} or vice versa, but always in the plateau region where the electrode process achieve at mass transfer controlled condition . The output of a typical chronoamperometry (*1*) is shown in Fig. 3.5 for the reaction between an alkyl halide (methyl 2-chloropropionate (MClP)) and the *in-situ* prepared Cu^I/Me_6TREN complex.

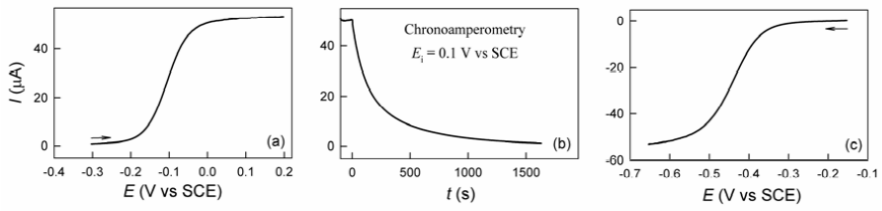

Figure 3.5 Activation kinetics of 0.460 mM methyl 2-chloroproprionate with 0.471 mM $[Cu^IMe_6TREN]^+$, in the presence of 9.73 mM TEMPO, in CH_3CN + 0.1 M $(C_2H_5)_4NBF_4$, T = 25 °C. **a)** LSV before addition of MClP; **b)** chronoamperometry at E_i = 0.1 V vs SCE during the activation reaction; **c)** LSV at the end of the activation reaction. WE = GC, v = 0.005 Vs-1(*1*)

In the absence of the initiator there is no homogeneous chemical reaction involving Cu^IL. Therefore, applying a potential E_i in the anodic plateau region, a constant oxidation limiting current I_L is produced (Fig. 3.5 a). The injecting of the initiator (Fig. 3.5 b) into the cell, with the electrode polarized at the same E_i value, causes a continuous decrease of I_L because now the bulk concentration of activator (Cu^I)

decreases owing to the ATRP reaction (Fig. 3.5 b). At the end of the reaction, the Cu^{I} oxidation current approaches zero because the activator was totally consumed by the initiator Fig. 3.5 b). Finally, a linear sweep voltammetry (LSV) was again recorded to detect the concentration of the deactivator ($X-Cu^{II}L$) and a new signal relative to the reduction of the generated $X-Cu^{II}L$ is detectable through LSV (Fig. 3.5 c).

In this work chronoamperometric measurement for the kinetic studies were carried out using the instrumentation described for the voltammetric experiments. The complex [Cu(I)L] (L = Me_6TREN, TPMA) was prepared in-situ by mixing stoichiometric amounts of copper salt and ligand. TEMPO (radical scavenger) was always introduced in a large excess with respect to the catalyst : [TEMPO]/[Cu(I)L] $\geq$ 10) in order to ensure the total capture of the macroradicals derived from the activation of the macroinitiators. The chronoamperometric experiment was started with a solution containing Cu(I)/TPMA and PVC or PVDF by stepping the working potential from a value in the region of stability of Cu(I) to a value in the plateau region where oxidation of Cu(I) to Cu(II) (Eq. 3.5) occurs under mass transport control, so that current (*I*) is given by Eq. 3.6. The presence of the macroinitiators stimulates the homogeneous redox initiation of ATRP, whereas the addition of the radical scavenger (TEMPO) favors to the formation of a stable product between the macroradical and the scavenger (Scheme 3.1).

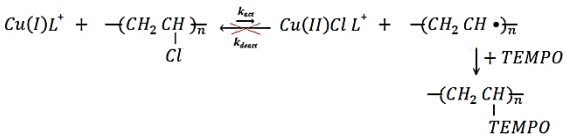

Scheme 3.1 ATRP mechanism in the presence of TEMPO

The reaction between the macroinitiator and the activator (Cu(I)) eventually leads to a decrease of the bulk concentration of Cu(I)L and, consequently, of *I*.

$$\mathrm{Cu(I)L} \rightarrow \mathrm{Cu(II)L} + \mathrm{e}^{-} \qquad (3.5)$$

$$I = F\, k_m C_{Cu(I)L} \tag{3.6}$$

where F is the Faraday constant, k_m is the mass transport coefficient and $C_{Cu(I)L}$ the concentration of the Cu(I) complex.

For slow reactions (k_{act} < 5 $M^{-1}s^{-1}$) pseudo-first-order kinetics is used to study the system that is characterized by $[RX]_0/[CuI]_0 > 20$ in order to neglect the variation in the RX concentration during the reaction. The reaction rate can be expressed as the rate of disappearance of a generic Cu^I activator (*4*). The kinetic rate law is:

$$v = -\frac{d[Cu^I]}{dt} = k_{act}[Cu^I][R-X] = k_{app}[Cu^I] \tag{3.7}$$

$$ln\frac{[Cu^I]}{[Cu^I]_0} = -k_{app}t \tag{3.8}$$

where $[Cu^I]^0$ is the initial concentration of Cu^I and k_{app} is the apparent rate constant, defined as $k_{app} = k_{act}\,[RX]_0$.

Substituting $[Cu^I]$ and $[Cu^I]^0$ in eq. 3.8 from eq. 3.6 gives:

$$ln\frac{I_L}{I_L^0} = -k_{app}t \tag{3.7}$$

3.2.4 Grafting procedure

The grafting reactions were carried out in a glass cell with a wall jacket; before each grafting reaction the reactor was loaded using the following sequence: PVDF or PVC powders and supporting electrolyte were dissolved in NMP (30 mL) at 50°C overnight under nitrogen, then the solution was cooled to room temperature and HEMA and the catalytic system (loaded under the form of copper salt and ligand) were added. At this point, the cell was sealed with a rubber septum and nitrogen gas was bubbled through the reaction mixture for 30 min while stirring. The reaction cell

was heated to the desired temperature for different times. At the end of the experiment the graft copolymer was precipitated into water to eliminate copper salts and supporting electrolytes and was purified twice by dissolution in NMP and reprecipitation with water. At this point the product was recovered and extracted with hot ethanol (150 mL) at 80°C in a sealed stainless steel vessel to recover any ungrafted PHEMA chains. The treated PVDF or PVC was again recovered by centrifugation, and then it was dried in an oven at 70°C overnight, to eliminate any residual ethanol.

3.2.5 Characterization of grafted polymers

The concentration of Cu(II) obtained by the ATRP reaction was monitored using an Agilent Cary 60 UV Spectrophotometer. Cu(II) complexed by the ligand was detected at λ = 960 nm after proper calibration with standard solution at known concentration using the Lambert Beer law.

The degree of grafting (DG) was estimated by liquid state ^{1}H-NMR. Spectra were obtained at room temperature using a Bruker Advance II 400 MHz (9.4 T) spectrometer employing deuterated dimethylsulfoxide (DMSO-d_6) or dimethylformamide (DMF-d_7) as solvents and setting the following parameters: 90° pulse on the 1H nucleus of 8 μs, repetition delay optimized to 2 s and 128 scans. Typical ^{1}H-NMR spectra for PVC-g-PHEMA and PVDF-g-PHEMA are depicted in Figure 1 together with the structure of repeating units constituting the copolymers. Peak assignment was done according to (*5–9*).

Gravimetric degrees of grafting have been calculated by the following equations:

$$\mathrm{DG_{PVC}}(\%) = \frac{S_e}{S_a} R_{PVC} 100 = \frac{S_d}{2S_b} R_{PVC} 100 \tag{3.8}$$

$$\mathrm{DG_{PVDF}}(\%) = \frac{S_e}{S_c} R_{PVDF} 100 = \frac{S_d}{S_c} R_{PVDF} 100 \tag{3.9}$$

where S_e and S_d denote the areas of NMR peaks at 3.8 and 4.1 ppm assigned to -C**H**$_2$OH and -COOC**H**$_2$- methylenic protons of HEMA repeat units respectively, S_a and S_b denote the areas of NMR peaks in the range 4.4-4.7 ppm and 2.1-2.7 ppm assigned to –C**H**Cl- and -C**H**$_2$- protons of VCM repeating units, respectively, and S_e is the sum of the area of peaks located at 2.9 and 2.4 ppm attributable to the -C**H**$_2$- methylenic protons of PVDF having, respectively, head-to-tail (ht) and head-to-head (hh) bonding arrangements. Values obtained using S_d and S_e differ by less than 10% and average values are reported in this study.

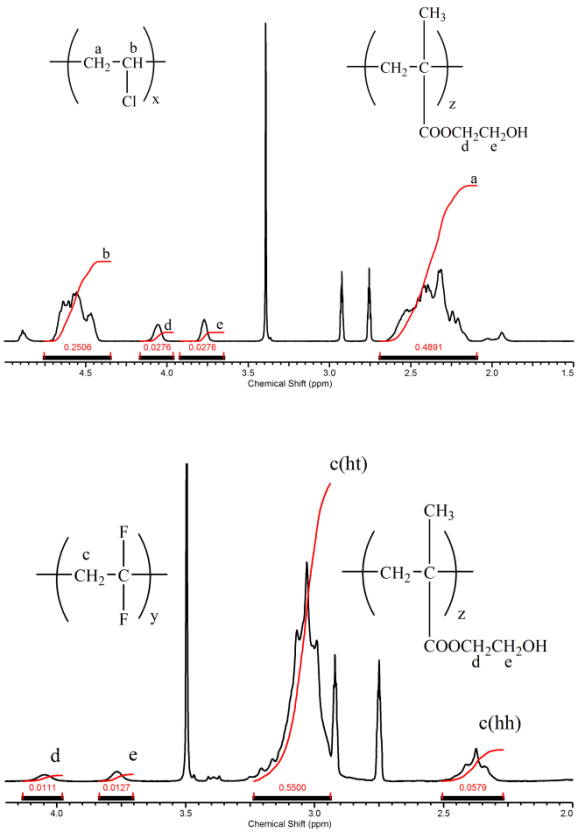

Figure 3.6. Typical 400 MHz ^{1}H-NMR spectra of PVC-g-PHEMA and PVDF-g-PHEMA copolymers in DMF-d_7

In eqs. 3.8 and 3.9, R_{PVC}=PM_{HEMA}/PM_{VCM} and R_{PVDF}=PM_{HEMA}/PM_{VDF} are the ratios between the molecular weight of HEMA and VCM repeating units and HEMA and VDF repeating units, respectively.

Number average molecular weight of the grafted copolymers $M_{n,graft}$ was calculated from ^{1}H-NMR data using the following equation:

$$M_{n,graft} = M_{n,Pol}\left[1 + \frac{DG(\%)}{100}\right] \quad (3.10)$$

where $M_{n,Pol}$ is the number average molecular weight of the macroinitiator ($M_{n,PVC}$ or $M_{n,PVDF}$) as obtained by their suppliers.

Calorimetric analyses of the copolymers were performed with a Perkin Elmer Jade differential scanning calorimeter (DSC). A pre-weighed amount of the copolymer (3–5 mg) was loaded into an aluminum pan sealed with an aluminum lid pressed slightly using a metal plunger and placed into the calorimeter holder under a N_2 flow of 20 mLmin^{-1}. The sample was heated twice from 18 °C up to 220 °C with a heating rate of 10 °Cmin^{-1}. The cooling rate between the two scans was 10 °C min^{-1} too.

In the case of PVDF-g-PHEMA copolymers melting temperatures, T_m, and enthalpies, ΔH_m, were determined at the maximum of the peaks and from the peak areas, respectively. The percent of crystallinity of these copolymers (X_c), was calculated from ΔH_m, by using:

$$X_c = \frac{\Delta H_m 100}{\Delta H_{100\%,cristallin\,e}} \quad (3.11)$$

where $\Delta H_{100\%,crystalline}$ is the heat of fusion of pure crystalline PVDF, which is reported to be 104.6 J/g.(39)

Grafted polymers were also characterized by infrared (IR) spectra recorded on a Perkin-Elmer Spectrum 2000 Explorer FTIR with an averaging of 16 scans at a resolution of 1 cm^{-1} using a near-IR fast recovery deuterated tryglicinesulfate

detector. Weighed amounts of grafted samples were mixed with KBr in a mortar and pressed into discs with a 10 ton pressure to obtain a film. Also in this case carbonyl resonance band identification was performed according to literature data (*10*).

3.3 Results and discussions

3.3.1 Determination of redox potentials of Cu(II) complexes

Aiming to assess the influence of various parameters like solvent, ligand, catalyst precursors and operating temperature, several electroanalytical experiments of catalysts composed by Cu^{II} species were performed. Two tetradentate amine ligands, namely tris(2-pyridylmethyl)amine (TPMA) and tris[2-(dimethylamino)ethyl]amine (Me_6TREN) (Scheme 3.1), were used as ligands since they allow the formation of very active catalytic complexes (*11*).

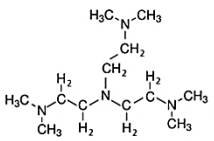

Tris [2-(dimethylamino)ethyl]amine
(Me_6TREN)

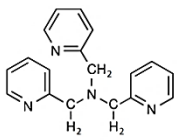

Tris (2-pyridylmethyl)amine
(TPMA)

Scheme 3.1 Structures of adopted ligands

NMP was the selected solvent owing to the high solubility of both, PVC and PVDF. Considering the scarce data available in literature on the role of this solvent for electroanalytical experiments, a thorough cyclic voltammetry investigation was first carried out. Some experiments were also repeated in MeCN for the sake of comparison, since this has been the prevailing solvent used in most studies reported so far (*4*, *6*, *12*). Moreover, different temperatures have also been used in order to

study the effect of this parameter on the activation of the C-F bond in ATRP "grafting from" reactions (*13*).

As exposed in Chapter 1, a comprehensive investigation of the redox behavior of the particular catalytic system can give precious preliminary information on the kinetics of the ATRP reaction. The analysis of the cyclic voltammograms recorded at 0.1 V/s with 2 mM $CuCl_2$ or $CuBr_2$ and TPMA or Me_6TREN as the ligand at different temperatures in the range 25 – 60 °C gave rise to data reported in Table 3.1, and can be associated to a one-electron peak.

Table 3.1 Redox potentials of adopted copper complexes in NMP at different temperatures measured by cyclic voltammetry[(a)]

Salt precursor and Ligand	T (°C)	$E_{1/2}$[(b)] (V)	ΔE_p (V)
$CuCl_2$ TPMA	25	-0.25	0.12
	45	-0.22	0.11
	60	-0.19	0.13
$CuBr_2$ TPMA	25	-0.22	0.10
	45	-0.16	0.12
	60	-0.15	0.12
$CuCl_2$ Me_6TREN	25	-0.40	0.22
	45	-0.38	0.19

	60	-0.38	0.19
	25	-0.35	0.12
$CuBr_2$ Me_6TREN	45	-0.31	0.13
	60	-0.29	0.13

[a] Potentials referred to SCE electrode at a scan rate of 0.1 V/s. Data obtained mixing CuX_2 (2 mM) with ligand. The ratio of Cu(II)/ligand is 1/1 for $CuBr_2$ (with TPMA and with Me_6TREN) and 1/3 for $CuCl_2$ (with TPMA and with Me_6TREN). $TBAPF_6$ (0.094 M) and TBABr (0.006 M) were used as supporting electrolyte.

[b] $E_{1/2}= (E_{p,c} + E_{p,a})/2$

Based on the results reported in Table 3.1, it can be concluded that the charge transfer was rather slow, since the peak-to-peak separation (ΔE_p) was higher than 60 mV expected for a Nerstian behavior. The half-sum of the oxidation and reduction peaks was calculated for each system as well, which allowed the estimation of the $E_{1/2}$ potential that is characteristic of the overall redox process, thus leading to a qualitative comparison between adopted systems (*6*). As shown in Table 3.1, the complexes formed using $CuCl_2$ yielded more negative potentials compared to those based on $CuBr_2$. As previously stated by Qiu et al. (*6*), the dependence of the redox potential on the nature of the halogen atom can arise from the involvement of the halide ion in the catalytic complex. This possibility was ascertained in acetonitrile also for Me_6TREN upon speciation studies performed by Bortolamei and co-authors (*12*). The difference in $E_{1/2}$ values obtained with $CuCl_2$ and $CuBr_2$ was in the range of 10 – 90 mV, depending on the nature of the ligand and the working temperature, thus ending in a higher equilibrium constant for the oxidation of CuCl complex. Both TPMA and Me_6TREN complexes presented quite negative redox potentials, thus making easier the oxidation of Cu(I) and the ATRP reactions. In particular, CuX/Me_6TREN yielded more negative $E_{1/2}$ values compared to CuX/TPMA. As shown in Table 3.1, higher temperature shifted the $E_{1/2}$ towards more positive potentials, which can be associated with a lower reduction ability of the complex.

3.3.2 Effect of monomer on redox potentials of Cu(II) complexes

The influence of HEMA was also studied since the grafting process has to be carried out in the presence of a high concentration of the monomer, which may affect the solvent power of the reaction medium. Furthermore, some researchers have been able to isolate many ATRP catalysts in the form $[Cu^{I}$ (PMDETA) $(\pi\text{-M})]^{+}$ where M=vinyl monomer, wherein the π-coordinated monomers as methyl acrylate, methyl methacrylate and styrene act as counter-ions (Figure 3.7). Under typical ATRP conditions ([M]/[Cu] = 100/1), about 10% of the methyl acrylate can move out Br^{-} ion and coordinate Cu^{I}/PMDETA at room temperature (*14*). More detailed studies have demonstrated that such kind of coordination of the monomer with Cu stabilizes the low oxidation state (I) and has great influence on the redox properties of the catalyst (*14*).

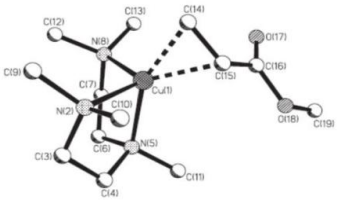

Figure 3.7 .Molecular structure of $[Cu^{I}(PMDETA)\ (\pi\text{-M})]^{+,}$ complex

Data collected from this study are reported in Table 3.2 and allow concluding that, in the presence of monomer, redox potentials of Cu(II) complexes change with ligands, copper salts and temperature as occurred in the absence of HEMA. However, if compared with data reported in Table 3.1, it can be deduced that redox potentials become more negative when using the monomer. Quite interestingly, the addition of HEMA strongly affected the $E_{1/2}$ values of all adopted catalytic systems, which may be due to coordination with Cu^{I}, as pointed out above.

Table 3.2 Redox potentials of adopted copper complexes in NMP + HEMA[(b)] at different temperatures measured by cyclic voltammetry[(a)]

Salt precursor and Ligand	T (°C)	$E_{1/2}$[(c)] (V)	ΔE_p (V)
$CuCl_2$ TPMA	25	-0.28	0.16
	45	-0.25	0.10
	60	-0.23	0.10
$CuBr_2$ TPMA	25	-0.24	0.10
	45	-0.17	0.12
	60	-0.19	0.13
$CuCl_2$ Me_6TREN	25	-0.45	0.11
	45	-0.42	0.14
	60	-0.39	0.14
$CuBr_2$ Me_6TREN	25	-0.39	0.09
	45	-0.35	0.10
	60	-0.31	0.14

[a] Potentials referred to SCE electrode at a scan rate of 0.1 V/s. Data obtained mixing CuX_2 (2 mM) with ligand. The ratio of Cu(II)/ligand is 1/1 for $CuBr_2$ (with TPMA and with Me_6TREN) and 1/3 for $CuCl_2$ (with TPMA and with Me_6TREN). $TBAPF_6$ (0.094 M) and TBABr (0.006 M) were used as supporting electrolyte.

[b] HEMA 16 % v/v

[c] $E_{1/2} = (E_{p,c} + E_{p,a})/2$

3.3.3 Effect of solvent on redox potentials of Cu(II) complexes

The effect of solvent on redox potentials of copper catalysts is summarized in Table 3.3. The solvent used for comparison was MeCN, the most employed until now for this type of studies. It can be seen that the redox potentials of both, $CuCl_2$/TPMA

and $CuBr_2$/TPMA, were more negative in MeCN compared to NMP. Moreover, in MeCN, the addition of HEMA shifted the $E_{1/2}$ towards more positive values, thus giving rise to less reducing complexes (see Fig. 3.8a and Table 3.3), whereas in NMP, the opposite effect was observed (Fig. 3.8b and Table 3.3). Hence, the values of $E_{1/2}$ obtained in NMP and MeCN tended to be more similar in the presence of HEMA.

Table 3.3. Study of Cu(II)/TPMA by cyclic voltammetry in various solvents at 25 °C[(a)]

Catalytic system	$E_{1/2}$ (V) NMP	$E_{1/2}$ (V) NMP+HEMA[(b)]	$E_{1/2}$ (V) MeCN	$E_{1/2}$ (V) MeCN+HEMA[(b)]
$CuCl_2$/TPMA	-0.25	-0.28	-0.37	-0.31
$CuBr_2$/TPMA	-0.22	-0.24	-0.30	-0.27

[a] Potentials referred to SCE electrode at a scan rate of 0.1 V/s. The ratio of Cu(II)/ligand is 1/1 for $CuBr_2$ complexes and 1/3 for $CuCl_2$. [CuX_2/L] = 2 mM. $E_{1/2}$= ($E_{p,c}$ + $E_{p,a}$)/2. $TBAPF_6$ (0.094 M) and TBABr (0.006 M) were used as supporting electrolyte.

[b] HEMA 16 % v/v

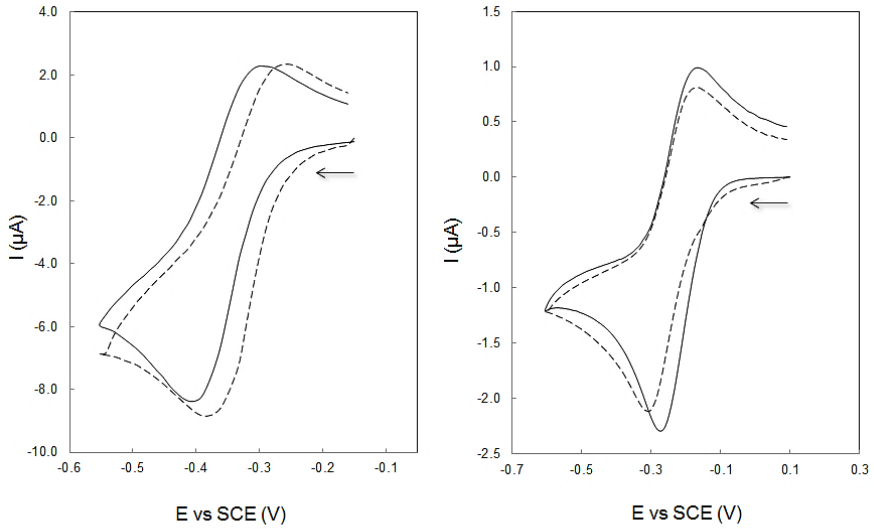

Figure 3.8 Cyclic voltammograms of $CuBr_2$/TPMA in MeCN (-) and MeCN+HEMA (- -) (a) and NMP (-) and NMP+HEMA (- -) (b). Experiments carried out with 2 mM $CuBr_2$/TPMA, 0.094 M $TBAPF_6$, 0.006 M TBABr, 16 % v/v of HEMA at 0.1 V/s and T = 25 °C.

3.3.4 Stability study of the catalytic system composed by Cu^I

In order to evaluate the stability of the catalytic system, cyclic voltammetry and spectrophotometric analyses were carried out with Cu(I) complexes. In NMP at 25 °C, voltammetric behavior of the CuBr/TPMA system was quite stable with time (Fig. 3.9a). When such experiments were performed with the same system in the presence of HEMA (20 % v/v), different phenomena were observed: first, the anodic peak decreased with time, probably as a result of the disproportionation of Cu(I); second, an additional cathodic peak at about -0.5 V vs. SCE appeared after several hours (Fig. 3.9b), which can be related to the formation of a catalytic complex involving HEMA. Some authors showed that Cu(I) can form complexes with a tridentate ligand, such as N,N,N^I,N^{II},N^{III}, pentamethyldiethylenetriamine

(PMDETA), methyl acrylate or methyl methacrylate (*15*). These authors explained that PMDETA acted as a tridentate ligand, while the tetrahedral coordinaton geometry was completed by π-complex with the monomer. In our experiments, the behavior could be even more complicated due to the presence of tetradentate ligands.

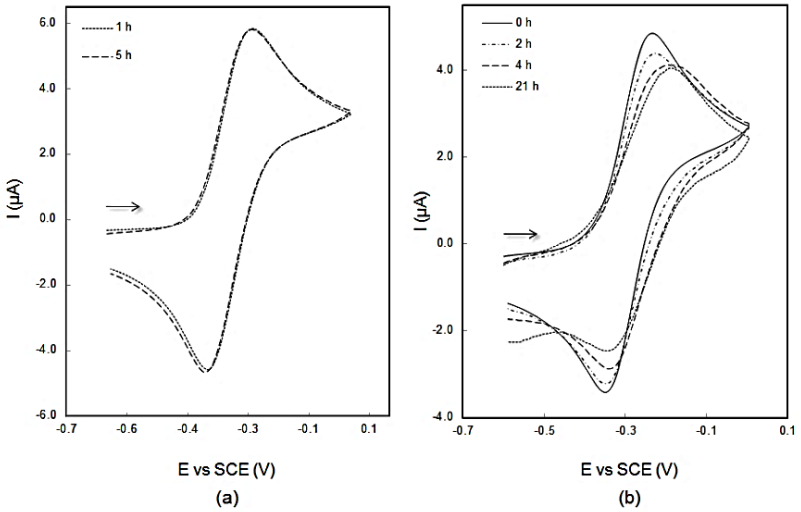

Figure 3.9. Cyclic voltammograms at 25 °C and 0.1 V/s of CuBr/TPMA in NMP (a) and NMP+HEMA (20 % v/v) (b). Experiments performed with 0.094 M $TBAPF_6$ and 0.006 M TBABr as supporting electrolytes

In addition to cyclic voltammetric analysis, UV/VIS spectra of Cu^{I} solutions were recorded to study the effect of temperature, ligand and HEMA, aiming to monitor the formation of Cu^{II}. In Fig. 3.10, the curve in blue corresponds to the spectrum of CuBr, which displayed two peaks at 540 and 640 nm, whereas in the presence of the ligand a shift of the peaks to higher wavelengths (about 930 nm) was observed. This led to the conclusion that this shifted peak can be related to the species complexed by the ligand.

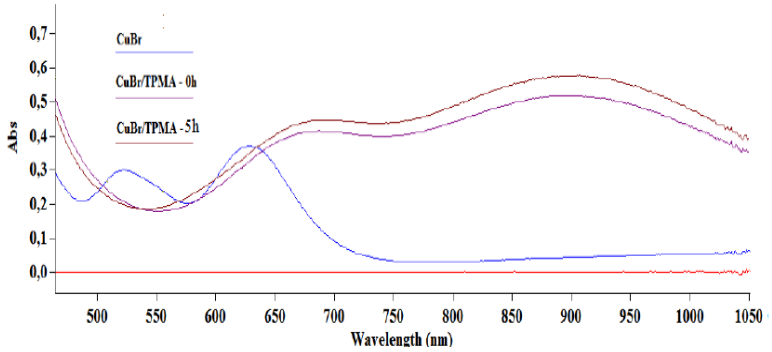

Figure 3.10 UV-VIS spectra of 5 mM CuBr/TPMA in NMP+HEMA (20 % v/v) at 25 °C.

Experiments performed with 0.094 M $TBAPF_6$ and 0.006 M TBABr as supporting electrolytes

The spectrophotometric analyses confirmed that no significant concentrations of Cu(II) were formed after 5 h at 25°C. However, an increase of temperature up to 45 °C and 60 °C gave rise to the formation of increasing amounts of Cu(II), always lower than 5% of the total copper concentration (Fig. 3.11a). Conversely, when the experiments were repeated at 45 °C with Me_6TREN, a significant formation of Cu(II) was observed (Fig. 3.11b). Thus, the presence of Me_6TREN favors the Cu(I) disproportionation reaction, in agreement with findings reported in literature (*16*).

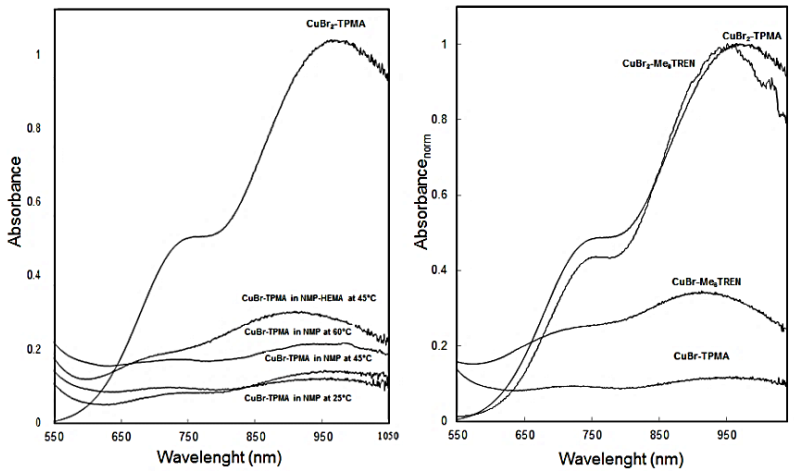

(a) **(b)**

Figure 3.11 (a) UV-VIS-NIR spectra of 5 mM CuBr/TPMA (1:1) after 5 h at different temperatures (25, 45 and 60°C) in NMP or NMP/HEMA (20 % v/v). The spectrum of 5 mM $CuBr_2$/TPMA in NMP is reported for comparison. (b) UV-VIS-NIR spectra of 5 mM CuBr/TPMA (1:1) after 5 h in NMP in the presence of different ligands (TPMA and Me_6TREN) at 25 °C. The spectra of 5 mM $CuBr_2$/TPMA and $CuBr_2$/Me_6TREN in NMP are reported for comparison. Experiments performed with 0.094 M $TBAPF_6$ and 0.006 M TBABr as supporting electrolytes.

Indeed, a higher amount of Cu(II) was detected by spectrophotometric analyses after 5 h in NMP/HEMA (Fig. 3.11a) compared to that observed in NMP, thus suggesting that the presence of HEMA favors the disproportionation reaction. When experiments were repeated in NMP/HEMA with CuBr/Me_6TREN, a higher amount of Cu(II) was also observed compared to that formed with CuBr/TPMA, thus confirming that this ligand is less effective in stabilizing the metal in its reduced state.

3.3.5 Study of the interaction between the catalytic system and the macroinitiator

As mentioned above, cyclic voltammetry and chronoamperometry allow obtaining information on the activation reaction. In particular, a specific voltammetric response is expected when activation of halogenated initiators occurs after C-halogen bond cleavage. The behavior is reported in paragraph 3.2.2 and is characterized by an increase of Cu^{II} and a decrease of Cu^{I} peak currents due to ATRP reaction. Considering a fast ATRP reaction, the addition of the initiator to a solution containing the Cu(II) complex should enhance the cathodic peak arising from the direct electroreduction of Cu(II) to Cu(I) on the electrode surface (*3*, *17*). This is due to the regeneration of Cu(II) in the close vicinity of the electrode as a result of the ATRP initiation coupled with a reduction of the anodic peak of the catalyst related to the oxidation of Cu(I) to Cu(II). The studies exposed below aim to analyze the activation of PVC and PVDF and, particularly their C-Cl and C-F bonds, by the selected catalyst.

For this, a series of cyclic voltammograms were obtained in NMP solutions of CuBr/TPMA and $CuBr_2$/TPMA in the absence and presence of increasing amounts of macroinitiators (PVC or PVDF) at 45 °C to achieve some preliminary information on the ATRP reaction. The $CuBr_2$/TPMA system in NMP was chosen because of the high stability of the redox couple. Moreover, some chronoamperometric measurements were performed in NMP solutions with CuBr/TPMA and, in some cases, with CuBr/Me_6TREN, in the presence of PVC or PVDF and of the radical scavenger 2,2,6,6-tetramethylpiperidine 1-oxyl (TEMPO) to study the kinetics of the reaction between Cu(I) and the macroinitiator in a larger timescale.

3.3.5.1 Activation of PVC

Utilization of poly(vinylchloride) and poly(vinylidene fluoride) as macroinitiators for ATRP

Preliminary cyclic voltammetries were recorded with the $CuBr_2$/TPMA system in the absence and presence of PVC at 45 °C at various scan rates (5-100 mV/s). The experiments were carried out with and without TEMPO as radical scavenger, since it traps radicals and then increases the amount of Cu^{II} in the reaction medium.

This radical scavenger shifts the ATRP equilibrium to the right (Scheme 3.2) and, consequently, causes a more significant decay of the Cu(I) concentration.

For comparison, a very active initiator containing a bromine atom as the halogen to be extracted by catalyst was employed in some cases. Ethyl 2-bromopropionate (EBP) was chosen as a model compound, and two tests were conducted in NMP at 25 °C with the CuBr catalyst (5 mM) complexed with TPMA or Me_6TREN as ligands(Fig. 3.12).

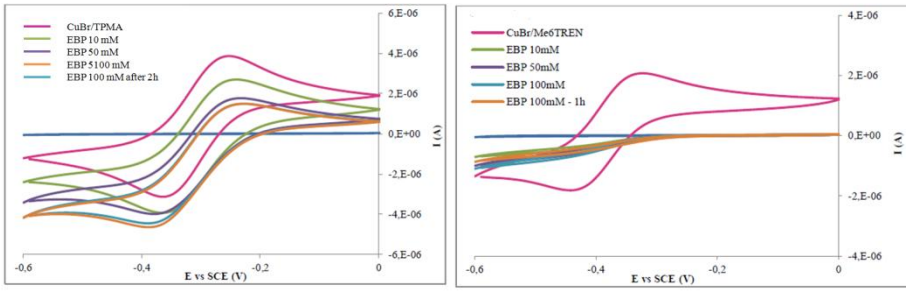

(a) (b)

Figure 3.12 Cyclic voltammograms of 5 mM CuBr as (a) CuBr/TPMA and (b) CuBr/Me_6TREN in the absence and presence of different amounts of EBP at scan rate of 100 mV/s. Experiments performed in NMP (0.094 M $TBAPF_6$; 0.006 M TBABr) at 25 °C

First, the system containing only the catalytic complex was analyzed. Afterwards, several additions of EBP were carried out, to reach a cumulative concentration of 10 mM, 50 mM and 100 mM. An increase and decrease of the cathodic and anodic peak currents, respectively, can be observed due to ATRP reaction. From Figs 3.12, it is evident that the activation of EBP is more greatly enhanced in the presence of

CuBr/Me_6TREN compared to CuBr/TPMA, which is due to the more negative and then reducing power of catalyst composed by this ligand.

As previously mentioned our main interest was focused on studying the activation of PVC. As shown in Fig. 3.13a, at 100 mV/s, the addition of 100 mM of PVC to a solution of 5 mM $CuBr_2$/TPMA (1:1) led to a slight decrease of the anodic peak, with no significant modifications of the cathodic one. This behavior could be accounted for by the slow rate of the reaction between the macroinitiator and the catalytic complex. To test the validity of this hypothesis, cyclic voltammetry experiments were repeated at slower scan rates (5-40 mV/s) in order to increase the time scale for the accumulation of products arising from the homogeneous redox reaction. As a result, when PVC was added to the solution, an increase of the cathodic peak and a decrease of the anodic one were clearly observed (Fig. 3.13b), thus confirming the occurrence of a redox reaction between PVC and the Cu(I) complex. This reaction was also studied using the CuBr/TPMA system and recording a set of cyclic voltammograms at different times. As shown in Fig. 3.13c, when PVC and TEMPO were simultaneously present in solution, a strong decrease of the anodic peak was observed after 7 h due to the consumption of the Cu(I) complex by the ATRP reaction. Also, a decrease of the initial current density at -0.6 V/SCE was observed, probably due to the cathodic reduction of the Cu(II)/TPMA complex formed by the ATRP reaction.

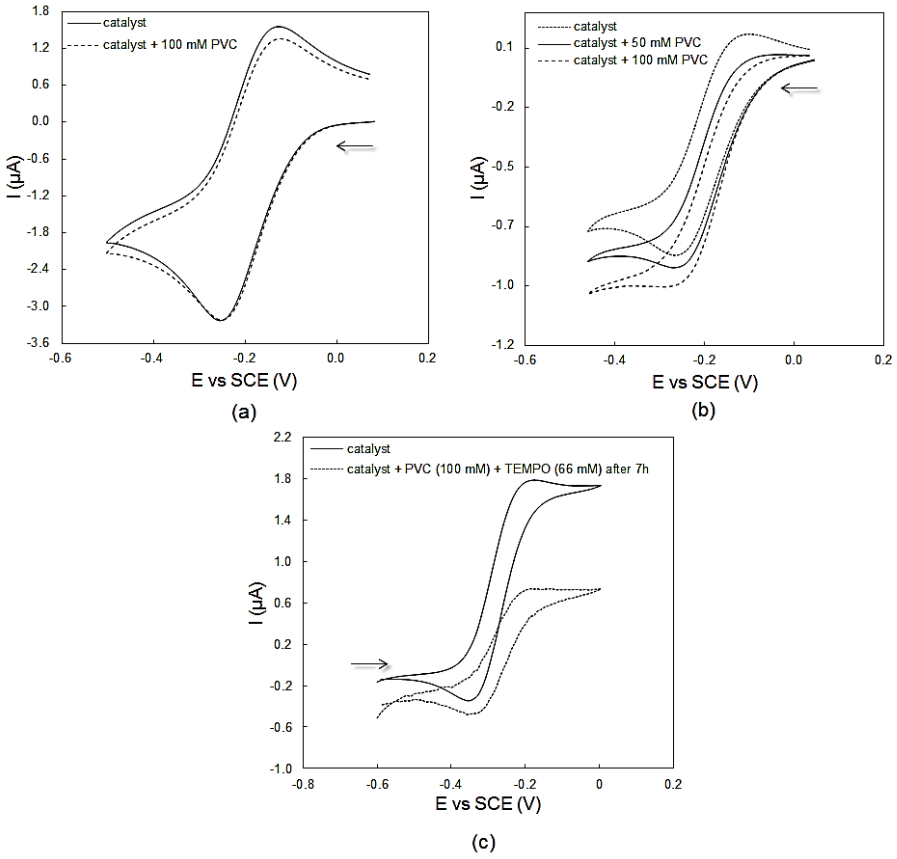

Figure 3.13 Cyclic voltammograms of 5 mM $CuBr_2$/TPMA (1:1) in the absence and presence of different amounts of PVC at a scan rate of 100 mV/s (a) and 5 mV/s (b). In (c), voltammograms of 5 mM CuBr/TPMA (1:1) at time zero (-) and after 7 h in the presence (•••) of TEMPO (66 mM) and PVC (100 mM), at 0.01 V/s. Experiments performed in NMP (0.094 M $TBAPF_6$; 0.006 M TBABr) at 45 °C.

Based on the approach proposed by Isse et al. for relatively slow reactions (*4*), the reaction between the Cu(I) complex and PVC was also studied by a series of chronoamperometric measurements at 45 °C. The reaction kinetics was examined under pseudo-first-order conditions using a ratio between the concentration of the macroinitiator and that of the catalyst ≥ 10.

It is important to note that, in our system, this approach does not allow a precise estimation of *k*' since the experiments were performed in the absence of stirring, in order to minimize the signal disturbance, thus causing a limited variation of the thickness of the diffusion layer and, consequently, of the k_m value during the measurements. Nevertheless, the scope of this analysis was not to reach a precise estimation of *k*' and thus, the proposed approach has allowed obtaining precious information on the kinetics of ATRP reaction activation.

Fig. 3.14 reports the natural logarithm of the ratio between the observed current I_L and the initial one I_L^0 as a function of time *t* for experiments performed in the absence and in the presence of different concentrations of PVC. In the absence of chlorinated polymer, no significant decrease of the current was observed, as expected from the high stability of the Cu(I)/TPMA catalytic complexes. In contrast, in the presence of the chlorinated polymer, a marked decrease of the current value occurred because of the ATRP reaction. As shown in Fig. 3.14, in the presence of increasing amounts of C_{RX}^0, a faster decrease of I_L was observed. As a result, a very rough estimation of k_{act} of about 3 10^{-4} mol^{-1} dm^3 s^{-1} was achieved.

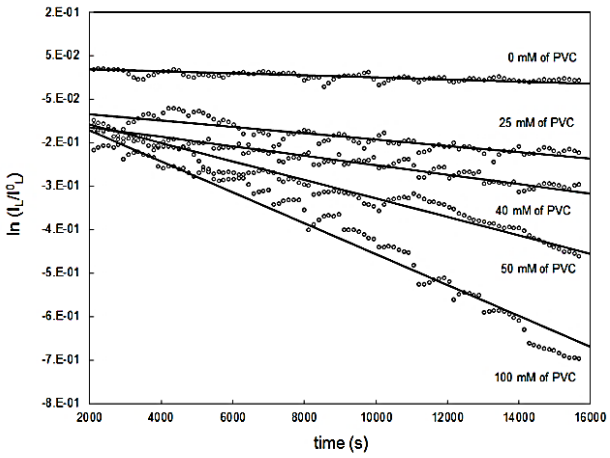

Figure 3.14 Ln($I_L/I_L°$) vs. time obtained from chronoamperograms in solutions of 2.5 mM of CuBr/TPMA complex in NMP (0.094 M $TBAPF_6$; 0.006 M TBABr)

without and with PVC (25, 40, 50 and 100 mM) in the presence of 32.5 mM of TEMPO at 45°C

3.3.5.2 Activation of PVDF

After the study with PVC, cyclic voltammograms were recorded with the $CuBr_2$/TPMA system in the absence and in the presence of PVDF (up to 100 mM) at 45 °C and various scan rates (5 - 100 mV/s). No evidence of ATRP reaction appeared in those trials. Therefore, the expected reduction of the anodic peak and the enhancement of the cathodic one were not observed at any adopted scan rate. This result can probably be associated to the high strength of the C-F bond. However, cyclic voltammetry is not really well adapted to detect follow-up homogeneous reactions whose rate is too low to affect the concentration of electroactive species within the time window necessary to scan the potential interval. For this reason, in order to elucidate the existence of the ATRP reaction also with this macroinitiator even if presenting a slow kinetics, a series of chronoamperometric measurements were carried out with the same approach above described for the case of PVC. As shown in Fig. 3.15, in the presence of PVDF, a very slow decrease of the limiting current was observed. From these data, a very low value of k_{act} of about one order of magnitude lower than that estimated for PVC was obtained, in agreement with the higher strength of the C-F bond compared to the C-Cl one.

Trying to favor the reaction between Cu(I) and PVDF, some chronoamperometric measurements were repeated using the more reducing Cu(I)Br/ME_6TREN catalyst, both in the absence and presence of PVDF. As shown in Fig. 3.15, in the absence of the macromolecule, a quite significant decrease of the current value occurred as a result of the lower stability of this complex, which probably results in the formation of both Cu(II) and Cu(0) via disproportionation reaction. Then, in the presence of PVDF, a significant increase of the slope of the $\ln(I_L/I_L°)$ vs. time plot was observed, thus suggesting that this catalytic complex can activate the PVDF.

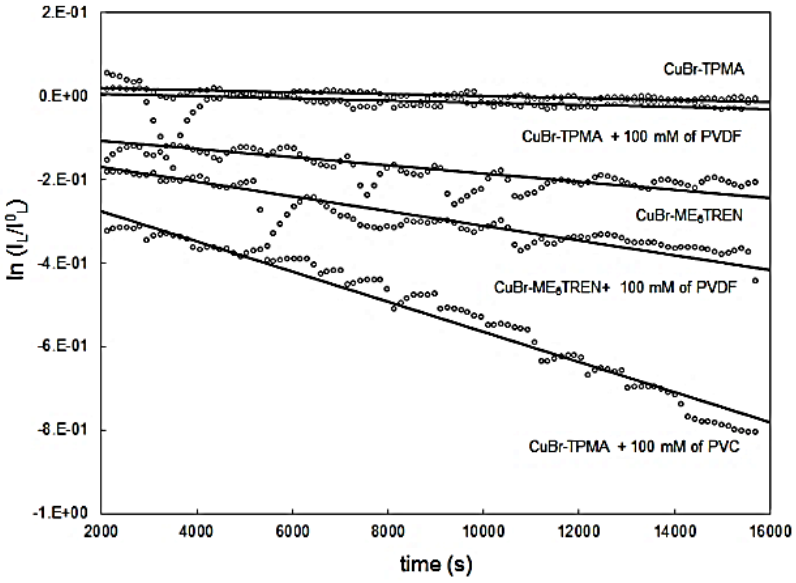

Figure 3.15 Chronoamperometric measurements of 2.5 mM of CuBr/L (L= TPMA or Me_6TREN) complex in NMP (0.094 M $TBAPF_6$; 0.006 M TBABr) without and with macroinitiator (PVC and PVDF) in the presence of 32.5 mM of TEMPO at 45°C.

3.3.6 Grafting experiments

Eventually, the grafting of HEMA on both PVC and PVDF was studied by carrying out some experiments at different operating conditions including temperature, adopted catalysts and reaction time. First experiments were carried out with CuBr/TPMA in NMP with HEMA (7% v/v) and PVC for 20 h at different temperatures (25, 45, 60 and 90 °C). As shown in Table 3.4 (entries 1-4), a quite high degree of grafting (DG) and number average molecular weight of the graft copolymer ($M_{n,graft}$) was obtained at the lowest adopted temperature. The DG and $M_{n,graft}$ decreased when the reaction temperature was increased. This result can be explained by the lower stability of the redox catalyst at higher temperature. It was

previously shown that the nature of the salt can affect the reducing power of the complex. In order to verify if the nature of the salt can affect the grafting process, a grafting experiment was repeated at 45 °C using CuCl instead of CuBr.

Table 3.4 Effect of operating parameters on the grafting of HEMA on PVC or PVDF

Entry	Macroinitiator	Catalyst precursor	Ligand	T (°C)	DG (%)	$M_{n,graft}$ (kg/mol)
1	PVC	CuBr	TPMA	25	42	92.3
2	PVC	CuBr	TPMA	45	28	83.1
3	PVC	CuBr	TPMA	60	19	77.6
4	PVC	CuBr	TPMA	90	12	72.8
5	PVC	CuCl	TPMA	45	35	87.5
6	PVDF	CuBr	TPMA	45	< 0.5	<107.9
7	PVDF	CuCl	TPMA	45	< 0.5	<107.9
8	PVDF	CuCl	Me_6TREN	45	2	108.9
9	PVDF	CuCl	Me_6TREN	90	5	112.5

Reactions carried out in a solution of NMP/HEMA (HEMA 7% v/v), the ratio of Cu(I)/ligand is 1/1, the concentration of copper catalyst is 5 mM, the supporting electrolyte for cyclic voltammetry measurement is $TEAPF_6$ (0.1 M), and reaction time is 20 h.

As shown in Table 3.4 (entries 2 and 5), in the presence of CuCl, which exhibits a higher reduction power compared to CuBr (see Table 3.1), a higher DG was obtained. The kinetics of the grafting was evaluated by carrying out a series of experiments at different times with CuCl/TPMA as catalyst at 45 °C. As shown in Fig. 3.16, at this temperature the grafting was characterized by a quite high initial rate as DG reached a value of 10%, corresponding to a $M_{n,graft}$ of 71.6 kg/mol, after just 0.5 h. The grafting rate decreased with time and a stable DG value close to 40% with $M_{n,graft}$ of 90.4 kg/mol was approached after 16 h.

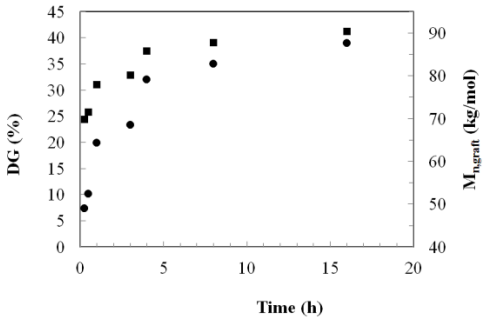

Figure 3.16 Effect of reaction time on the grafting of HEMA on PVC powders in NMP+HEMA (HEMA 7% v/v) in the presence of 5 mM CuCl/TPMA (1:1) at 45 °C. Supporting electrolyte: 0.1 M $TBAPF_6$. (●) DG(%), (■) $M_{n,graft}$ (kg/mol).

For the evaluation of the grafting of HEMA on PVDF, some experiments were first carried out with CuCl/TPMA or CuBr/TPMA at 45 °C for 20 h. For both experiments, a DG lower than 0.5 % was achieved (Table 3.4, entries 6-7) as a result of the high strength of the C-F bond and the corresponding very slow kinetics of the reaction between Cu(I) and PVDF. In order to shift the reaction between PVDF and Cu(I) to the right, some experiments were repeated with the Cu(I)/Me_6TREN. Quite interestingly, as shown in Table 3.4 (entries 7 and 8), the utilization of Cu(I)/Me_6TREN allowed achieving a significant enhancement of the DG which reached a value of 2%. Note that, since a disproportionation reaction occurs, the system contains both Cu(I) and Cu(0). Hence, it is not possible to exclude a potential participation of Cu(0) in the activation of PVDF.

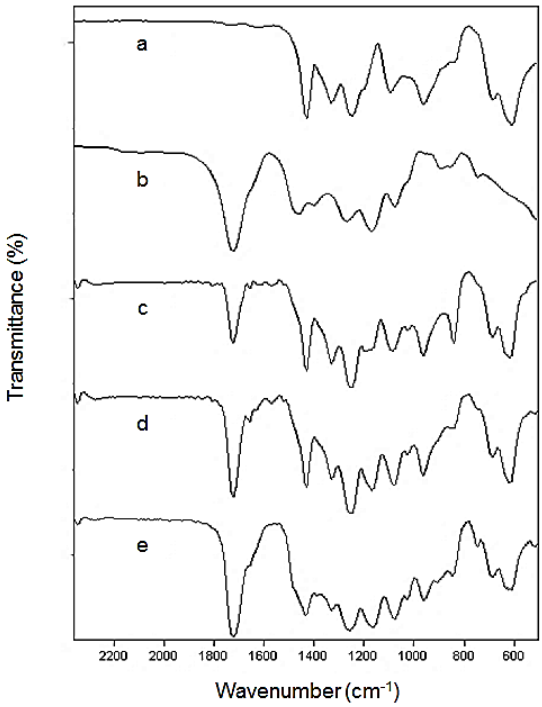

Figure 3.17 FT-IR spectra of PVC-g-PHEMA powders treated at different reaction time under operative conditions reported in the legend of Fig. 6: (a) pristine PVC , (b) PHEMA, PVC-g-PHEMA after a reaction time of (c) 15 min , (d) 3 h and (e) 8 h.

According to the literature, the grafting of methacrylate on PVDF can be successfully achieved at temperature of 90 °C (*13*). Thus, the grafting was repeated at 90 °C with the Cu(I)/Me_6TREN. The increase from 45 to 90 °C allowed a further enhancement of the DG from 2% to 5%.

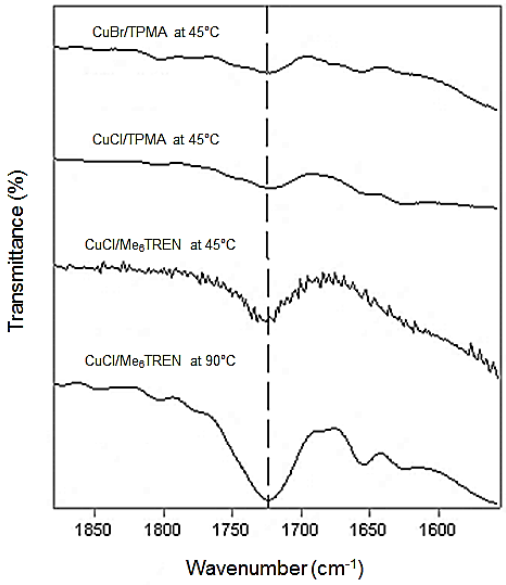

Figure 3.18 FT-IR spectra of PVDF-g-PHEMA powders treated with different catalytic complexes CuBr/TPMA at 45 °C (DG < 0.5%), CuCl/TPMA (1:1) at 45 °C (DG < 0.5%), CuCl/Me_6TREN at 45 °C (DG = 2%), CuCl/Me_6TREN at 90 °C (DG = 5%). Reactions carried out in a solution of NMP/HEMA (HEMA 7% v/v), 5 mM CuX/L (1:1) and 0.1 M $TBAPF_6$ as supporting electrolyte.

Grafted polymers were also analyzed by FT-IR. In Figures 3.17 and 3.18, spectra of selected samples of PVC-g-PHEMA and PVDF-g-PHEMA copolymers are reported. The resonance band of the carbonyl group of HEMA repeat units can be clearly detected at 1730 cm^{-1} in all grafted polymers. Absorption bands measured with modified PVDF have much lower intensity with respect to those obtained with modified PVC, in agreement with results of ^{1}H-NMR characterizations.

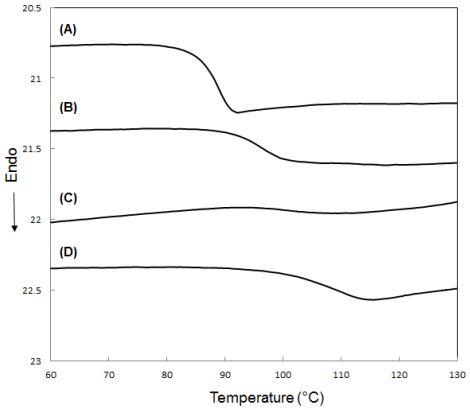

Figure 3.19 DSC data for (A) PVC, (B) PVC-g-PHEMA DG=12%, (C) PVC-g-PHEMA DG=28%, (D) PHEMA. Calorimetric scans correspond to the second heating of the polymer samples.

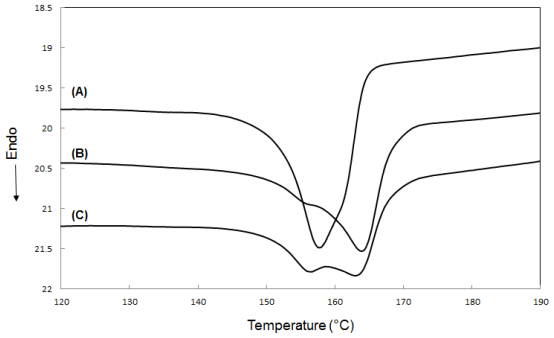

Figure 3.20 DSC data for (A) PVDF, (B) PVDF-g-PHEMA DG=2%, (C) PVDF-g-PHEMA DG=5%. Calorimetric scans correspond to the second heating of the polymer samples.

Grafted copolymers were also analyzed by differential scanning calorimetry (DSC). In the case of modified PVC polymers, second heating traces exhibited glass transition temperatures that are intermediate between those of PVC and PHEMA and that increased with the grafting degree (Fig. 3.19). Modified PVDF polymer samples were characterized by second heating calorimetric crystallinity of 44-45% independently of the DG. These values were slightly higher than that of virgin

PVDF, which was measured to be 40%. Furthermore, in grafted PVDF samples, the melting peak at 162-164°C, which is just a shoulder in pure PVDF, became more evident. This suggests that grafted PHEMA chains can modify the crystallization behavior of PVDF chains (Fig. 3.20). Collected calorimetric results can be considered a further indication of successful grafting reactions as well as interactions between grafted chains and the main polymer chains, both in the case of PVC and PVDF.

3.3.7 Conclusions

The grafting of hydroxyethylmethacrylate (HEMA) on PVC and PVDF by copper catalysts was studied by both, electroanalytical techniques and simple grafting experiments. The use of cyclic voltammetry and spectrophotometric analyses has shown that that Cu(I)/TPMA presents a very good stability in NMP. The addition of the monomer, the increase of temperature or the utilization of Me_6TREN ligand led to a decrease of the stability of the catalytic complex. Cyclic voltammograms and chronoamperograms have revealed that PVC can be activated also at moderate temperature with both, Cu(I)/TPMA and Cu(I)/Me_6TREN, whereas PVDF activation requires the utilization of a more reducing catalyst such as Cu/Me_6TREN due to the higher bond energy of the C-F bond. Grafting experiments confirmed the indication of electroanalytical experiments. Indeed, HEMA was successfully grafted to PVC with short reaction times in a wide range of temperatures using Cu(I)/TPMA as catalyst, whereas in the case of PVDF significant but drastically lower degrees of grafting were achieved only in the presence of Cu/Me_6TREN and high temperature. The results confirmed that an electrochemical approach can serve to achieve precious information on complex ATRP processes.

References

1. N. Bortolamei, *Ph.D. thesis*.
2. G. A. Mabbott, *J. Chem. Educ.* **60**, 697–702 (1983).
3. A. J. D. Magenau, N. C. Strandwitz, A. Gennaro, K. Matyjaszewski, *Science (80-.).* **332**, 81−84 (2011).
4. A. A. Isse, N. Bortolamei, P. De Paoli, A. Gennaro, *Electrochim. Acta*. **110**, 655–662 (2013).
5. K. L. Beers, S. Boo, S. G. Gaynor, K. Matyjaszewski, *Macromolecules*. **32**, 5772–5776.
6. J. Qiu, K. Matyjaszewski, L. Thouin, C. Amatore, *Macromol Chem Phys*. **201**, 1625–1631 (2000).
7. M. Hidalgo, H. Reinecke, C. Mijangos, *Polymer,*. **40**, 3525–3534 (1999).
8. H. Paik, S. G. Gaynor, K. Matyjaszewski, *Macromol Rapid Commun*. **52**, 47–52 (1998).
9. X.-K. Lin, X. Feng, L. Chen, Y.-P. Zhao, *Front. Mater. Sci. China*. **4**, 345–352 (2010).
10. L. Ferreira, M. M. Vidal, M. H. Gil, *Int. J. Pharm.* **194**, 169–180.\ (2000).
11. W. Tang *et al.*, *J. Am. Chem. Soc.* **130**, 10702–10713 (2008).
12. N. Bortolamei, A. A. Isse, V. B. Di Marco, A. Gennaro, *Macromolecules*. **43**, 9257–9267 (2010).
13. J. F. Hester *et al.*, *Macromolecules*. **35**, 7652–7661 (2002).
14. W. A. Braunecker, K. Matyjaszewski, *Prog. Polym. Sci.* **32**, 93–146 (2007).
15. W. A. Braunecker, T. Pintauer, N. V. Tsarevsky, G. Kickelbick, K. Matyjaszewski, *J. Organomet. Chem.* **690**, 916–924 (2005).
16. B. M. Rosen *et al.*, *J. Pol. Sci. Part A Pol. Chem.* **47**, 5606–5628 (2009).
17. N. Bortolamei, A. A. Isse, A. J. D. Magenau, A. Gennaro, K. Matyjaszewski, *Angew. Chemie*. **123**, 11593–11596 (2011).

Utilization of poly(vinylchloride) and poly(vinylidene fluoride) as macroinitiators for ATRP

CHAPTER 4
UNDERSTANDING THE MECHANISM OF ATRP ACTIVATED BY A FLUORINATED INITIATOR : IS IT "LIVING" OR NOT?

4.1 Introduction

The grafting reactions reported in chapter 3 have confirmed the hypothesis that it is possible to achieve the direct grafting of halogenated polymers by using Cu(I) complexes with suitable reducing power. It was also confirmed that the grafting on PVDF is feasible even if with drastically lower DG with respect to that obtained with PVC as a result of the higher strength of the C-F bond with respect to the C-Cl one. As discussed in chapter 2 , grating of fluorinated polymers is not so clear and Ameduri recently observed that no significant spectroscopic evidences were provided to confirm it (*1*). In this context, the study that is reported in this chapter is aimed to better understand the mechanism of an ATRP reaction carried out after the activation of the C-F bond. To reach this goal, a study of a model fluorinated initiator was carried out during a research period spent at Carnegie Mellon University. Very important results were achieved and four points could be used to summarize the activities carried out:

1. Electrochemical investigations of the redox behavior of the catalytic complexes Cu^{II}/ligand (ligand= TPMA or Me_6TREN) and different halogen (F, Cl, Br and I) in dimethylformamide.
2. Electrochemical study of activation of the selected fluorinated initiator (diethylfluoromalonate, DFM).
3. Study of the deactivation reaction by reverse ATRP technique.
4. Study of normal ATRP activated by a fluorinated initiator in order to define the livingness of the specific process.

4.2 Experimental

4.2.1 Materials

Methyl methacrylate (MMA), methyl acrylate (MA) and styrene (Sty) were purchased from Aldrich. Monomers were stored at 4°C and passed through basic alumina to remove inhibitors/antioxidant before use. N,N-Dimethylformamide (DMF) (anhydrous 99.8%) was purchased from ACROS and drawn under N_2 atmosphere before each experiment. Tris(2-pyridylmethyl)amine (TPMA) and tris[2 (dimethylamino)ethyl]amine (Me_6TREN) were synthesized according to literature (*2*) tetrabutylammoniumperchlorate (TBAClO4, 98%, Alfa Aesar), tetrabutylammoniumchloride (TBACl, >97%, Aldrich), tetrabutylammoniumbromide (TBABr, >99%, Aldrich), tetrabutylammoniumiodide (TBAI, puriss., Aldrich), potassium fluoride (KF, Aldrich), copper(II) trifluoromethane-sulfonate ($CuII(OTf)_2$, 98%, Aldrich), copper(I) bromide (99.999%, Aldrich), copper(I) chloride (Anhydrous, Aldrich) and diethylfluoromalonate (DFM, 97%, Aldrich) were used as received.

4.2.2.Electroanalytical measurements

Cyclic voltammetries (CV) were carried out in a three-electrode cell with a wall jacket through which ethylene glycol from a thermostated bath was circulated. A PARC 263A potentiostat/galvanostat was used to perform electroanalytical experiments. Pt or glassy carbon (GC) disks (each with 3 mm diameter) were used as working electrodes (WE) whereas the counter (CE) and reference (RE) electrodes were a Pt coil and $Ag/AgI/I^-$ respectively. Prior to each experiment working and counter electrodes were cleaned. The WE was initially polished by diamond paste (0.25- μm particle size). After each polishing step, it was cleaned in bidistillated water in an ultrasonic bath for 5 min. The reference electrode was separated from the

working solution by a glass frit and a salt bridge synthesized from methyl cellulose gel saturated with $(C_2H_5)_4NBF_4$. The experiments were performed using the following sequence: the solvent-supporting electrolyte solution (DMF + 0.1 M of $TBAClO_4$) was first bubbled with N_2 for 30 min, then the copper complex(composed by copper salts and ligand) and the initiator (DFM) were added in two consecutive steps, each time recording cyclic voltammograms of the solution.

4.2.3. General Polymerization Procedures

All reactions were carried out under an inert atmosphere of dry N_2. In a typical polymerization carried out under normal ATRP technique ,a 10-mL Schlenk flask was charged with DMF (9 mL) and the amount of Cu^IX (X= Br or Cl) and ligand (TPMA, PMDETA or ME_6TREN) necessary to reach a nominal concentration of 0.011 mol/L for each of the components (molar ratio Cu^I/Ligand=1). The solution was purged with nitrogen flow for 20 min to eliminate oxygen. MA or Sty (1 mL) was degassed by purging with nitrogen for 15 min prior to add the initiator. The initiator/monomer solution was further degassed for 15 minutes and then added to the liquid phase in the Schlenk flask. The polymerization was started by heating the reaction mixture at the desired temperature in an oil bath. At regular timed intervals during the polymerization, 0.2 mL of the solution was withdrawn under nitrogen atmosphere to be analysed by NMR or GPC.

A similar procedure was used for polymerization carried out under reverse ATRP technique using AIBN at 1 mmol/L concentration as free radical source and a catalyst composed by $Cu^{II}(OTf)_3$ (1mmol/L) complexed by TPMA (Cu^{II}/ligand molar ratio 1) and halogen ions derived from different salt precursors added in equimolar amount with respect to the transition metal (TBAX, where X=I, Br, Cl or F).

4.2.4. Characterization

Monomer conversion was evaluated from the concentration of the residual monomer by H NMR (300 MHz) spectra taken on a Bruker Avance 300 MHz spectrometer using $CDCl_3$ and DMF as deuterated solvent and internal standard respectively. Number-average molecular weight (M_n) and molecular weight distribution were determined by gel permeation chromatography (GPC) using a Water 515 HPLC pump and a Waters 2414 refractive index detector equipped with two PSS columns in series . Analyses were performed using THF as an eluent with a flowrate of 1 mL/min at 35°C against PMMA or PS standards and with diphenyl ether as an internal standard. GPC instrument was . Each sample was filtered over neutral alumina to remove catalyst prior to analysis.

4.3 Results and discussions

4.3.1 Effect of halides ions and temperature on copper complexes redox potentials

The dynamic equilibrium of an ATRP process regulates the control over polymerization and it is dominated by different factors as the carbon-halogen bond (P_m-X) homolysis, the redox reaction involving the two oxidation states of the transition metal complexes, the association of halogen atom to the oxidized form of the copper catalyst (X-Cu(II)L). Kinetics of elemental reactions characterizing an ATRP process could be strongly affected also by the nature of the halogen atom bound to the dormant chain end/or to the ternary catalytic complex. In order to understand the effect of F^-, Cl^-, Br^- and I^- anions on the redox behaviour of the catalytic system some preliminary electroanalytical experiments were performed. DMF was selected as solvent owing to the good solubility of fluorinated compounds

and $TBAClO_4$ at concentration of 0.1 mol/L was used as supporting electrolyte. The effect of temperature on the electrochemical behavior of the catalytic system was also studied since the polymerization reaction had to be performed at different values of this parameter. Cyclic voltammetric curves were recorded at 0.1 V/s with 1 mM Cu(II)trifluoromethanesulfonate ($Cu(II)(OTf)_3$) and TPMA as ligand at different temperatures in the range 25-70°C. Electrochemical data giving rise to data reported in Table 4.1, correspond to one-electron peak. The half-sum of the oxidation and reduction peaks was computed for each system, to achieve an estimation of the $E_{1/2}$ potential characterizing the overall redox process, thus allowing a qualitative comparison between adopted systems

Table 4.1. Peak current ratio (i_b/i_f), half wave potential($E_{1/2}$) and peak potential separation (ΔE) measured by cyclic voltammetry of ternary complexes composed by different halides at different temperatures in DMF[a]

Halide	*T (°C)*	i_b/i_f[b]	$E_{1/2}$[c] *(mV)*	ΔE[d] *(mV)*
None	25	0.77	287	86
	40	0.76	309	84
	55	0.78	335	88
	70	1.00	362	95
I^-	25	0.76	328	84
	40	0.75	337	87
	55	0.87	354	95
	70	0.89	368	99
Br^-	25	0.77	206	90
	40	0.84	229	108

	55	0.97	251	114
	70	0.93	266	122
Cl^-	25	0.60	134	129
	40	0.70	157	146
	55	0.79	177	150
	70	0.91	207	150
F^-	25	0.80	77	334
	40	0.85	94	292
	55	0.86	113	264
	70	0.97	136	232

[a] Potentials referred to Ag/AgI at a scan rate of 0.1 V/s. Data obtained mixing CuX_2 (X =$(OTf)_3$, I^-, Br^-, Cl^- or F^-) with TPMA. The ratio of Cu(II)/X/L is 1:1:1 for I^-, Br^-, Cl^- and 1:1:2 for F^-. $TBAClO_4$ (0.1 M) was used as supporting electrolyte.

[b] i_b/i_f is the ratio of backward to forward peak current

[c] $E_{1/2} = (E_{p,c} + E_{p,a})/2$

[d] $\Delta E = E_{p,a} - E_{p,c}$

The redox reaction underlying the reversible peak couple observed in CV is:

$$Cu^{II}L^{2+} + e^- \leftrightarrow Cu^{I}L \quad (4.1)$$

corresponding to the species composed by copper and ligand; but in the presence of halides ions other reactions have to be considered as reported below (equation 4.2 and 4.3)

$$[X - Cu^{II}L]^+ + e^- \leftrightarrow [X - Cu^{I}L] \quad (4.2)$$

$$[X - Cu^{I}L]^{+} \leftrightarrow [Cu^{I}L] + X^{-} \quad (4.3)$$

The association of halides ions (X) to the binary complex (Cu-L) leads to the formation of ternary species (Cu-L-X) which are involved in equilibrium with the binary one as reported by equation 4.3. Studies reported in the literature (*3*) have shown that when X = Br^-, $Cu^{I}L$ remains the predominant species as before reported (chapter 1).Ternary complexes have been observed by CVs at redox potentials different from that of the binary species.

As shown in Table 4.1, the complexes formed using bromine, chlorine and fluorine ions displayed more negative $E_{1/2}$ potentials, that is a good approximation of the standard redox potential E^0, than those measured in the absence of halides ions. In particular, redox potentials follow the order $Br^- > Cl^- > F^-$ and, quite interestingly, in the presence of iodine ions the ternary complex showed a redox potential more positive than that observed with the halogen free binary one. It looks like iodine ions stabilizes Cu^{I}, rather than the others halides (Br^-, Cl^- and F^-) that stabilize Cu^{II}. Higher temperature displayed the $E_{1/2}$ towards more positive potentials, thus giving rise to a less reducing complex.

The difference between the standard potentials of the $[Cu^{II}L]^{2+}/[Cu^{I}L]^{+}$ and $[Cu^{II}LX]^{+}/[Cu^{I}LX]$ couples (where X = I^-, Br^-, Cl^- or F^-) previously estimated by cyclic voltammetry can be used to estimate also the relative halidophilicities of $[Cu^{II}L]^{2+}$ and $[Cu^{I}L]^{+}$. Taking into account the association equilibria for $[Cu^{II}L]^{2+}$ and $[Cu^{I}L]^{+}$ with halide ions (X^-) :

$$[Cu^{II}L]^{2+} + X^{-} \leftrightarrow [Cu^{II}L(X)]^{+} \qquad K^{II}_{X} \quad (4.4)$$

$$[Cu^{I}L]^{+} + X^{-} \leftrightarrow [Cu^{I}L(X)] \qquad K^{I}_{X} \quad (4.5)$$

where K^{II}_X and K^{I}_X are the association constants defined by the following equations

$$K^{II}_X = \frac{[Cu^{II}L(X)]^{+}}{[Cu^{II}L]^{2+}[X^-]} \qquad K^{I}_X = \frac{[Cu^{I}L(X)]}{[Cu^{I}L]^{+}[X^-]}$$

And the redox equilibria involving binary and ternary redox couples:

$$[Cu^{II}L]^{2+} + e^{-} \leftrightarrow [Cu^{I}L]^{+} \tag{4.6}$$

$$[Cu^{II}LX]^{+} + e^{-} \leftrightarrow [Cu^{I}L(X)] \tag{4.7}$$

the ratio between halidophilicity constants for different ternary complexes can be expressed as a function of standard redox potentials using the Nerst equations

$$E^{0}_{[Cu^{II}L(X)]^{+}/[Cu^{I}LX]} = E^{0}_{[Cu^{II}L]^{2+}/[Cu^{I}L]^{+}} + \frac{RT}{F} ln \frac{K_X^I}{K_X^{II}} \tag{4.8}$$

Figure 4.1 shows the ratios estimated from cyclic voltammetries as a function of temperature and it is possible to observe that, increasing the temperature, the ratio between halidophilicity constants slightly increases for ternary complexes composed by chlorine and fluorine ions, while it is stable in the presence of bromine ions. Quite interestingly is the effect of iodine ions on ternary complexes, because in this case the ratio between the halidophilicity constants decrease enough, reaching the value corresponding to the binary complex at the highest adopted temperature (70°C).

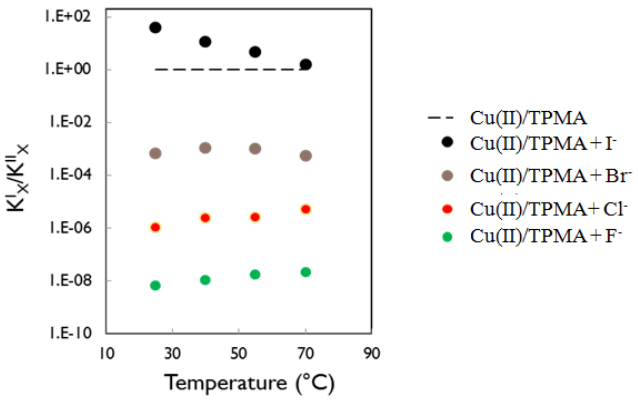

Figure 4.1 Ratio between K^I_X and K^{II}_X estimated from eq. 4.3 using cyclic voltammetric data of 1 mM solution of $Cu(II)(OTf)_3$/TPMA in DMF in the presence of 1 mM of TBAI, TBABr, TBACl and TBAF as salt precursors for the halides.

The results reported in figure 4.1 suggest variation of halidophilicity ratio with the temperature with the different ternary complexes, but individual constants values are necessary to understand better the evolution of concentration of the deactivator (ternary complex) in solution. Quite interestingly for this study is to understand that the temperature could influence the rate constant of the ATRP reaction because, as before reported, it is connected to the halidophilicity and calculated as the products between all rate constants of sub-equilibria.

4.3.2 Electrochemical analysis of the activation of the fluorinated initiator

Diethylfluoromalonate (DFM) was used as fluorinated initiator and its behavior was analyzed by a series of cyclic voltammetries performed in DMF solutions at 2 mM concentration of $Cu^{II}(OTf)_3$/TPMA and $Cu^{II}(OTf)_3$/Me_6TREN in the absence and in the presence of increasing amounts of DFM. Both TPMA and Me_6TREN complexes presented quite negative redox potentials, thus making easier the oxidation of Cu(I)

and the ATRP reactions. In particular, $Cu^{II}(OTf)_3/Me_6TREN$ displayed more negative redox potential than $Cu^{II}(OTf)_3$/TPMA, as described in the literature (*4*). The reaction of the alkyl halide (DFM) with $[Cu^{I}L]^+$ (L = TPMA, Me_6TREN) was investigated through CV measurements performed in the presence of the radical scavenger 2,2,6,6-tetramethylpiperidine 1 oxyl (TEMPO) that traps radicals obtained by ATRP reaction making it irreversible as previously explained (see chapter 3).

In the absence of the fluorinated initiator (Figure 4.2, [DFM]=0mM), the voltammetric response of $Cu^{II}Me_6TREN$ recorded with a scan rate of 0.1 V/s shows a redox potential $E_{1/2}$ =32.5 mV vs Ag/AgI with a peak separation ΔE_p = 273 mV, and a i_b/i_f = 0.82 which underlines the *quasi* reversible character of the electron transfer involving the $[Cu^{II}L]^{2+}/[Cu^{I}L]^+$ couple ($[Cu^{II}L]^{2+} + e^- \rightarrow [Cu^{I}L]^+$. After addition of TEMPO and DFM with a ratio $\gamma = C_{RX}/C_{Cu^{II}L}$ = 0.5 (Figure 4.2, [DFM]=1 mM), the pattern changes, showing a new peak at a more negative potential, $E_{1/2}$ = -173.5 mV vs Ag/AgI, which was attributed to the heterogeneous reduction at the working electrode surface of the deactivator $[FCu^{II}L]^+$ produced by the following homogeneous chemical reaction (equation 4.9):

$$[Cu^{I}L]^+ + R{-}F \rightarrow [FCu^{II}L]^+ + R^{\bullet} \qquad (4.9)$$

Also, the $[Cu^{II}L]^{2+}$ reduction peak is slightly increased as a consequence of the equilibrium previously reported in the equation (1). Further addition of DFM up to reach a 2 and 5mM concentration (corresponding to $\gamma = 1$ and $\gamma = 2.5$ respectively) led to a marked increase of the $[FCu^{II}L]^+$ reduction peak due to faster rate of reaction 4.4 and a decrease of the $[Cu^{I}L]^+$ oxidation peak.

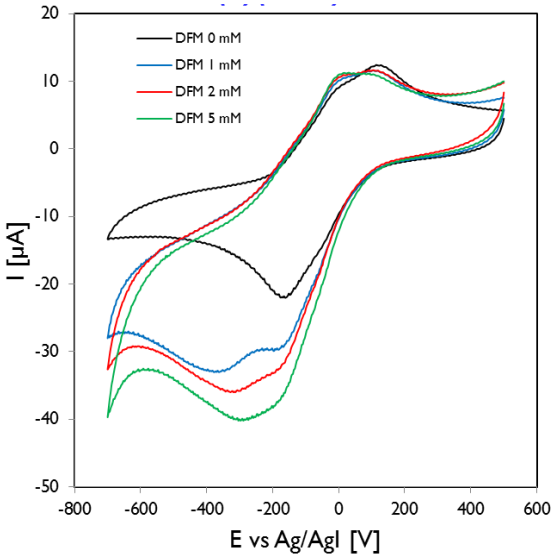

Figure 4.2 Cyclic voltammograms of 2 mM $Cu^{II}Me_6TREN$ in DMF the presence of 1, 2 and 5 mM of DFM . The analyses were carried out at 0.1 Vs^{-1} and 25°C.

The same experiments carried out with TPMA as ligand (Figure 4.3) shows a similar cyclic voltammetric response, but, as expected, a smaller increase of cathodic peak corresponding to electrochemical reduction of the ternary complex $[FCu^{II}L]^+$ was obsverved. Both set of experiments confirmed the possibility of activating the selected fluorinated initiator, when catalyst composed by $Cu^{II}Me_6TREN$ was employed the activation was found to be faster.

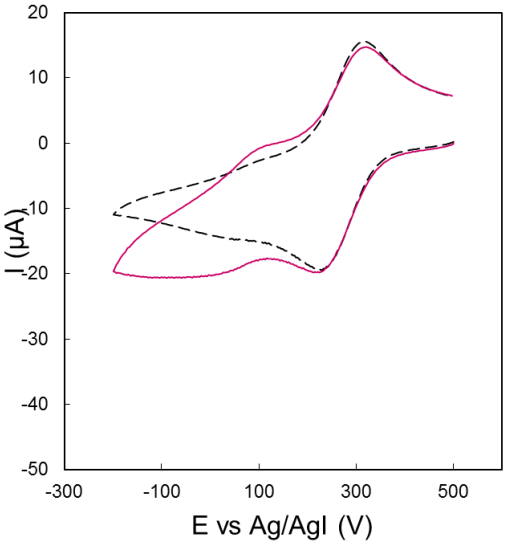

Figure 4.3. Cyclic voltammograms of 2 mM Cu^{II}TPMA in DMF in the presence of 5 mM of DFM . The analyses were carried out at 0.1 Vs^{-1} and 25°C.

4.3.3.Deactivation of growing chains in the presence of different ternary complexes

Electroanalytical investigations reported in the previous paragraph showed that activation of the fluorinated initiator DFM by very reducing catalytic complexes with Me_6TREN as ligand effectively occurs. At this point the main objective is to understand how an ATRP reaction involving fluorine atoms proceeds.

To this purpose, a series of polymerization reactions started with ternary complexes composed by different halides ions were carried out using $Cu^{II}(OTf)_3$ as copper salt precursor and TPMA as ligand. Reactions were performed by reverse ATRP technique in order to better understand the kinetics of deactivation reactions for experiments involving fluorine atoms and to compare it with others halides (I^-, Br^- and Cl^-). Reverse ATRP differs from normal ATRP in its initiation process, where a conventional radical initiator, such as AIBN, is used in order to extract the halogen atom X from the oxidized transition-metal species (XMt^{n+1}), after its thermal

decomposition at a specific temperature, and to create reduced transition-metal species (Mt^n) and the dormant species, I-X or I-P_1-X. Instead of first activation of a dormant species, reverse ATRP originates from the deactivation reaction between radicals (*5*).

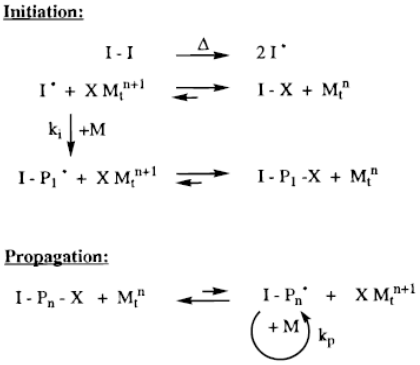

Scheme 4.1. Reverse ATRP mechanism.

Reverse ATRP of methyl methacrylate (MMA) and methyl acrylate (MA) were performed at 65°C in the presence of 2,2′-Azobis(2-methylpropionitrile) (AIBN) as radical source. Polymerizations with or without $Cu^{II}(OTf)_3$ (as a free radical polymerization) complexed by TPMA were carried out and molecular weight and polydispersity of the obtained final chains were compared.

In particular, free radical polymerization of MMA carried out in DMF (0.1 M of $TBAClO_4$ as supporting electrolyte) in the presence of catalytic complexes composed by $Cu^{II}(OTf)_3$ as copper precursor, TBAX salts as halides ions precursors fotr I^-, $Br^-$and Cl^- and KF for F^-(in the ratio of Cu(II)/X/L is 1:1:1 for I^-, $Br^-$and Cl^- and 1:1:2 for F^-.) and TPMA as ligand. The reactions leads to the formation of chains with M_n of $3.64*10^5$ g/mol at a monomer conversion of 34%. The same experiments were repeated in the presence of ternary complexes composed by iodine, bromine, chlorine and fluorine anions leading to very different products. Table 4.2 shows the results obtained and it can be noticed that with F anions higher conversion and molecular weight than with other halides were obtained; in particular, values of the molecular weight ($1.91*10^5$ g/mol for a monomer conversion of 33.4%) more similar to that obtained in the free radical

polymerization were achieved. Furthermore, it is possible to observe greater monomer conversion at the same reaction time (3h) changing catalyst $Conv_{(F)}$ > $Conv_{(Cl)}$ > $Conv_{(Br)}$ > $Conv_{(I)}$. It seems as the deactivation reaction become more slow leading to a larger addition of monomer units.

Table 4.2. Monomer conversion and M_n of syntehsized PMMA for Reverse ATRP of MMA with ternary complexes composed by different halides.

Entry	***Halides***	***t(h)***	***Conversion (%)***	***M_n (g/mol)***
1	F	3	33.4	$1.91*10^5$
2	Cl	3	28.6	$7.22*10^4$
3	Br	3	20.8	$1.25*10^5$
4	I	3	8.5	$9.84*10^4$

Slightly different results were obtained with polydispersity as shown in Figure 4.4 (polydispersity indexes behavior), where it can be noticed that more controlled chains were obtained only when catalyst composed by bromine ions was used and polydispersity decreased from 2.1 to 1.3. On the other hand, the utilization of chlorine and even more of fluorine atoms led to loss of control with higher polydispersities. It seems that Cl^- and F^- decrease the rate of the deactivation step promoting the formation of less controlled chains; on the other hand, it is known that (*6*) fast deactivation of active species to dormant polymer chains is necessary to minimize the contribution of chain termination and leads to a narrow molecular weight distribution thus indicating that, in this case, the loss of the control is due to slow kinetics of deactivation.

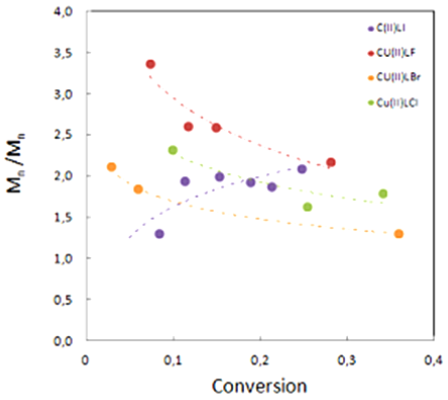

Figure 4.4 Polydispersity indexes for reaction carried out with reverse ATRP technique and different ternary complexes (Cu^{II} LX, where X = F, Cl, Br and I). T = 65° C [MMA]=1.105 M, [Cu(II)LX] (1:1:1) =1 mM, [AIBN]=2 mM, T=65°C.

A similar series of experiments were carried out using MA rather than MMA because radical of MMA is more active and can be better abstractor of X from Cu(II)-L-X; also MMA can work at very low concentration of Cu(I), while MA would need more Cu(I) so that an induction period is expected whose duration depends on the specific halide. In fact, an induction time corresponding to time necessary for copper (II) reduction was observed in all cases except for ternary complex composed by fluorine atoms. Figure 4.5b shows the enlargement of the initial zone of the Figure 4.5a where the plot of the monomer conversion with the time is reported. In particular, larger induction period was observed in the presence of chlorine anions, followed by bromine and iodine, respectively. Only in the presence of fluorine this induction period was not observed and the initial slope is similar to that obtained without halides.

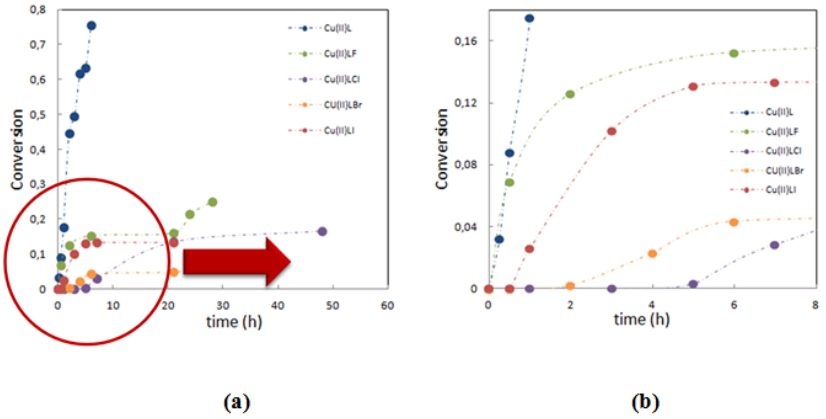

Figure 4.5. Effect of the presence of different initial ternary complex on the conversion of MA polymerization with reverse ATRP technique. Experimental conditions: [MA]=1.105 M, [Cu(II)LX] (1:1:1) =1 mM, [AIBN]=1 mM, T=65°C

This order seems correlated to the binding energy between the metal and the halo-anions; the stronger the bond between copper and halide, the larger the induction period. The absence of initial induction time in the presence of fluorine atoms allows to think that deactivation reaction is too slow and the radical formed by AIBN adds monomer as in a free radical polymerization reaching rapidly the maximum of conversion.

For the sake of comparison, the reaction carried out in the absence of halides was carried out leading very fast to high conversions and molecular weight (Table 4.3, entry 1). The reverse ATRP reaction carried out with fluorine led to M_n similar to that of FRP (Table 4.3, entry 2) but lower polydispersity, thus indicating a better control even if in the first hour of the reaction the conversion is similar to that of FRP. Other reactions carried out in the presence of Cl, Br and I ions allowed to lower conversion and molecular weight, as more controlled final chains as indicated by polydispersity indexes (Table 4.3, entry 3,4 and 5).

Table 4.3. Conversion ,M_n and polydispersity ($Đ$) for reverse ATRP of MA with ternary complexes composed by different halides.

Entry	*Halides*	*t (h)*	*Conversion (%)*	*M_n (g/mol)*	*Đ*
1	None	6	75	$3.2*10^4$	1.98
2	F	28	25	$3.78*10^4$	1.43
3	Cl	28	16.5	$2.38*10^4$	1.46
4	Br	28	8.5	$1.16*10^4$	1.30
5	I	20	13.4	$1.89*10^3$	1.23

Reverse ATRP reactions carried out in the presence of different ternary complexes ($Cu^{II}LX$, where X = F, Cl, Br and I). T = 65° C [MA]=1.105 M, [Cu(II)LX] (1:1:1) =1 mM, [AIBN]=1 mM, T=65°C.

4.3.4 Defining the limit of ATRP activated by C-F group

Once defined the behavior of catalyst composed by fluorine atoms and evaluated the effect of a ternary complex as Cu^{II}TPMAF on the deactivation reaction, a series of experiments using the selected fluorinated initiator (diethylfluoromalonate, DFM) were conducted; the activation of this initiator, as previously reported, was before evaluated by electrochemical investigations. Then the normal ATRP of MA in the presence of this initiator was conducted in order to study the "livingness" of an ATRP reaction activated from a C-F bond with different catalyst and operating conditions.

As a starting point, polymerization of methyl acrylate (MA) with normal ATRP technique was carried out in the presence of DFM as initiator and Cu^{I}Br/TPMA as catalyst; the same temperature employed for reverse ATRP was used (65°C); higher

conversion than with the reverse technique during the first hours of the reaction was achieved with molecular weight closer to the theoretical values (before calculated by the product of the degree of polymerization and the molecular mass of the monomer). Direct activation by normal technique of fluorinated initiator by Cu^{I}TPMA complex allowed a faster monomer conversion and confirmed the activation of diethylfluoromalonate by this catalyst. However, the control of the molecular weight was not good and M_n values about 3.5 times greater than those theoretically predicted were achieved. One possible explanation for this behavior could be the very slow deactivation rate of Cu^{II} complex in reverse technique that leads to species with higher molecular weight after radical addition of great amount of monomer or radical coupling reactions.

Effect of temperature was observed by performing reactions in the range from 25 to 80°C. Gratifyingly, the increase of temperature increased the initiation efficiency that reached a value f = 0.73 at the highest investigated temperature (entry 4, Table 4.4),while f = 0.13, 0.16 and 0.29 were observed at 25°C, 45°C and 65°C, respectively. Molecular weight very close to theoretical values were achieved and this improvement could be due to a growing amount of initiator molecules activated at high temperature. Faster activation leads to more radicals present in the reaction medium and to a DP ([M]/[I], ratio between monomer and initiator concentrations) more close to the predicted one. Furthermore, cyclic voltammetric analyses (Figure 4.6a) carried_out with Cu^{II}TPMA as catalyst and 20 mM of DFM as initiators showed that increasing temperature from 25 to 55°C an enhancement of the cathodic peak, arising from the electroreduction of Cu^{II} to Cu^{I}, coupled with a reduction of the anodic one, was observed, thus confirming improvement of the activation of fluorinated initiator. GPC traces reported in Figure 4.6b ,corresponding to the same reaction time (3h), shows that, at high temperature, species with higher M_n were obtained except at 80°C; this temperature led to the formation of chains similar to those obtained at 25°C.

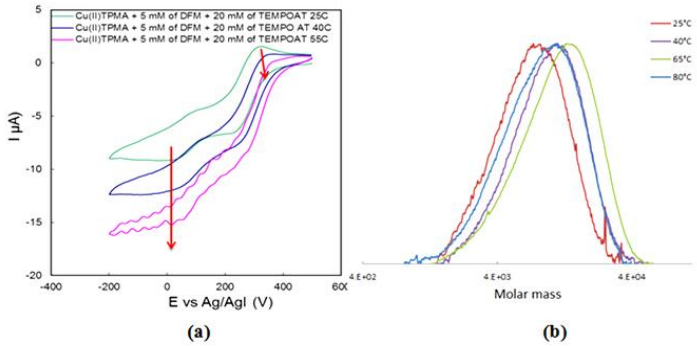

Figure 4.6 (a) Cyclic voltammetry of Cu(II)TPMA catalyst in the presence of 5 mM of DFM and 20 mM of TEMPO at different temperatures.(b) GPC traces of normal ATRP of MA at different temperatures.

In order to improve the deactivation reaction, a different catalyst composed by PMDETA as ligand was employed taking into account that this ligand is characterized by a greater k_{deact} as described in the literature (*3*). Linear evolution of M_n with conversion was obtained but, unfortunately, smaller initiation efficiency was detected. This behavior could be due to less active catalyst created with PMDETA that leads to the activation of a smaller fraction of initiator molecules.

Table 4.4. Reaction Conditions for the Polymerization of Methyl Acrylate (MA) under Normal ATRP activated by fluorinated initiator (DFM)

entry	*Ligand*	*temp (°C)*	*conv (%)*	$M_{n,obs}$ *(g/mol)*	$M_{n,th}$ *(g/mol)*	*Đ*	*Initiation efficiency*
1	TPMA[a]	25	7.8	5260	678	1.37	0.13
2	TPMA	40	12.5	6860	1080	1.42	0.16
3	TPMA	65	26.1	7891	2260	1.48	0.29
4	TPMA	80	41.4	4930	3580	1.76	0.73
5	DETA[b]	65	24.1	15090	2070	1.43	0.14

[a]TPMA = tris(2-pyridylmethyl)amine, [b]PMDETA = *N*,*N*,N^{I},N^{II},N^{II}-pentanethyldiethylenetriamine, DFM = Diethyl fluoromalonate. Reaction conditions : [MA]:[DFM]:[CuBr]:[TPMA]=100:1:1:1 (11.1 mM of DFM).

Driven by the consideration that an ATRP process involving an equilibrium based on the exchange of fluorine ions is characterized by very slow kinetics, it was decided to use a monomer with a different propagation rate constant and in particular with a different ratio between k_d and k_p (k_d/k_p). In particular, a monomer with a propagation rate slower than methyl acrylate was employed, in order to decrease the characteristic time available to add monomer units to growing chains; the selected monomer was styrene; in fact, it was estimated for this monomer (*7*) an higher value of the ratio k_d/k_p with respect to acrylates (k_d/k_p = 20 for styrene against k_d/k_p = 6.2 for acrylates at 90°C). Very pertinent to this case, the explanation about the reasons that led to these different values, corresponding to different reactivity and stability of radicals; in particular, the more nucleophilic styril radical shows the highest affinity for halogen abstraction, whereas the most electrophilic acrylate radical has the lowest, allowing to a possible improvement of deactivation reaction and livingness of process when styrene is used. For the sake of comparison, a reaction was carried out with styrene at the same conditions of entry 3 in Table 4.4 related to methyl acrylate. Surprisingly, final chains with observed molecular weight very close to theoretical value was achieved and initiation efficiency very high , *f* = 0.95 as showed in Fig.4.7.

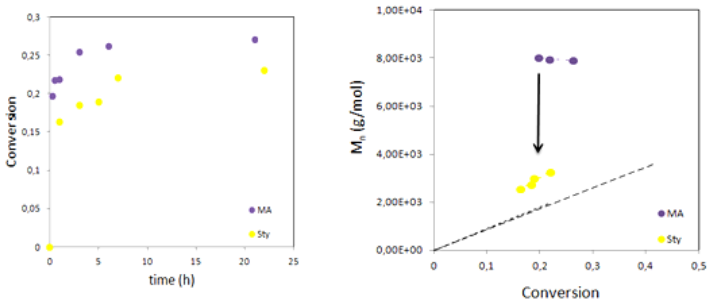

Figure 4.7 Comparison between monomer conversion and M_n obtained by normal ATRP of MA or Styrene activated by a fluorinated initiator. [M]=1.105 M, [Cu(I)Br] (1:1) =11 mM, [DFM]=11 mM, T=65°C.

Table 4.5. Reaction Conditions for the Polymerization of Styrene (Sty) under Normal ATRP activated by fluorinated initiator (DFM)

entry	*Ligand*	*Monome*	*Temp (°C)*	*Conv (%)*	*Copper salt*	*Cu(I)/RF*	$M_{n,obs}$ *(g/mol)*	$M_{n,th}$ *(g/mol)*	*Đ*	*Initiation efficiency*
1	TPMA	MA	65	26.1	CuBr	1/1	7891	2260	1.48	0.29
2	TPMA[a]	Sty	65	22.1	CuBr	1/1	2430	2300	1.57	0.95
3	TPMA	Sty	65	32.7	CuCl	1/1	213000	3400	2.35	0.016
4	Me_6TREN[b]	Sty	65	32.9	CuBr	1/1	22500	3420	2.44	0.15
5	TPMA	Sty	110	39.5	CuBr	1/1	27670	4120	2.64	0.15
6	TPMA	Sty	110	49.8	CuBr	2/1	34660	5190	2.71	0.15

[a]TPMA = tris(2-pyridylmethyl)amine, [b]Me_6TREN = Tris[2(dimethylamino)ethyl]amine, DFM = Diethyl fluoromalonate. Reaction conditions : [Sty]:[DFM]:[CuX]:[TPMA]=100:1:1:1 (11.1 mM of DFM).

Entry 3 and 4 in Table 4.5 reports the same experiment carried out with CuCl (entry 3) as salt precursor or Me_6TREN (entry 4) as ligand. Both experiments led to molecular weight higher than the theoretical value and polydispersity index greater than 2.3 thus suggesting limited control of the polymerization. In particular, the utilization of CuCl instead of CuBr led to a very bad control of molecular weight suggesting that Cl- coming from copper salt precursor works in the deactivation reaction. The Cu^{II}-Br bond is weaker than the Cu^{II}-Cl resulting in faster deactivation of the propagating radical and low polydispersity (*6*).

As regard the utilization of Me_6TREN (Table 4.5, entry 4), although monomer consumption increased, evolution of molecular weight as a function of conversion was not linear and values higher than the theoretical ones were obtained. As observed by cyclic voltammetric analyses (Figure 4.8), obtained after background current subtraction and current normalization with respect to the scan rate *v*, at 65°C the complex is not stable , most probably due to the disproportionation reaction (eq. 4.10) (*8*):

$$2Cu^{I} = Cu^{0} + Cu^{II} \qquad (4.10)$$

Even if the activation of fluorinated initiator by $Cu^{I}Me_6$TREN complex is faster than with Cu^{I}TPMA, the disproportionation reaction leads to a significant loss of catalyst and then a decrease of the fraction of activated initiator. On the other hand, a too fast activation against a slow deactivation further damages the control.

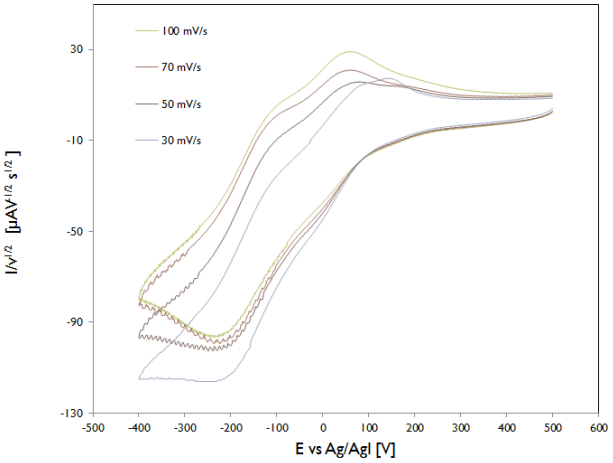

Figure 4.8 Effect of the scan rate on cyclic voltammetry of 2 mM of $[FCu^{II}L]+$ (L = Me6TREN) in DMF + 0.1 M TBAClO4, *T* = 65°C.

Finally, the effect of temperature was evaluated carrying out reactions at 110°C. Doubled monomer conversion and linear increase of molecular weight were achieved, but, as observed by GPC traces, greater polydispersity indexes were obtain as a consequence of the formation of chains with higher molecular weight during the polymerization; from reaction carried out without catalyst it was noticed that a thermal activation of styrene at 110°C was realized leading to high molecular weight and polydispersity indexes.

4.3.5 Conclusions

In this work experiments on a model fluorinated initiator were designed and performed to collect information on the evolution of an ATRP reaction activated after cleavage of a C-fluorine bond. Cyclic voltammetric analyses of copper complexes composed by bromine, chlorine and fluorine anions displayed more negative potentials than those calculated in the absence of halide ions, while in the

presence of iodine anions the ternary complex showed a redox potential more positive than that observed with the binary one. Higher temperature displayed the $E_{1/2}$ towards more positive potentials, thus giving rise to a less reducing complex.

Reverse ATRP of methyl methacrylate (MMA) and methyl acrylate (MA) in the presence of different catalysts composed by I, Br, Cl and F were performed at 65°C using 2,2′-Azobis(2-methylpropionitrile) (AIBN) as radical source. With F ions higher conversion and molecular weight than with other halides were obtained as the deactivation step is too slow and the monomer addition is favored. In fact, it is possible to observe greater percentage of monomer conversion at the same reaction time (3h) changing the halide as follow $Conv_{(F)} > Conv_{(Cl)} > Conv_{(Br)} > Conv_{(I)}$. Electrochemical investigation of activation by copper catalysts composed by two different ligand as TPMA and Me_6TREN allowed to understand that it is possible to activate the fluorinated initiator by both complexes, even if more enhanced activation was found when Me_6TREN as ligand was used. At the end two series of experiments by normal ATRP with the fluorinated initiator were carried using MA and Sty as monomers . With MA the best condition that led to an initiation efficiency of 0.73 was reached when CuBr/TPMA was used as ligand at 80°C with a polydispersity as 1.76. But, the best conditions with initiation efficiency of 0.95 was achieved with styrene at 65°C with CuBr/TPMA allowing to think that different reactivity and stability of radicals is fundamental to regulate the kinetics of the reaction; the more nucleophilic styril radical shows the highest affinity for halogen abstraction, whereas the most electrophilic acrylate radical has the lowest, allowing a possible improvement of deactivation reaction and livingness of process when styrene is used.

This study confirms that it is possible to use C-F bond as initiating site for ATRP reaction selecting very well the effective catalyst but the livingness and the control of the final chains strongly depend on the operative conditions as temperature, monomer, ligand and copper salt employed.

References

1. B. Ameduri, *Macromolecules*. **43**, 10163–10184 (2010).
2. J. Xia, K. Matyjaszewski, *Macromolecules*. **32**, 2434 (1999).
3. N. Bortolamei, A. A. Isse, V. B. Di Marco, A. Gennaro, *Macromolecules*. **43**, 9257–9267 (2010).
4. J. Qiu, K. Matyjaszewski, L. Thouin, C. Amatore, *Macromol Chem Phys*. **201**, 1625–1631 (2000).
5. J. S. Wang, K. Matyjaszewski, *Macromolecules*. **28**, 7572–7573 (1995).
6. K. Matyjaszewski, D. A. Shipp, J. L. Wang, T. Grimaud, T. E. Pattern, *Macromolecules*. **31**, 6836–6840 (1998).
7. J. Gromada, K. Matyjaszewski, *Macromolecules*. **35**, 6167–6173 (2002).
8. B. M. Rosen *et al., J. Pol. Sci. Part A Pol. Chem.* **47**, 5606–5628 (2009).

SECTION 2

SUPERCRITICAL CARBON DIOXIDE (SC-CO_2) FOR THE MODIFICATION OF HALOGENATED NANOPARTICLES BY ATRP AND STERILIZATION OF TRIDIMENSIONAL POLYMERIC BIOMATERIAL

CHAPTER 5
SUPERCRITICAL CARBON DIOXIDE AND RADICAL POLYMERIZATIONS

5.1. Supercritical fluids

Darr and Poliakoff (*1*) offer a practical definition of a supercritical fluid (SCF) describing it as a "substance at values of the temperature and pressure higher than their critical values and which has a density close to or higher than its critical density". Most applications involve CO_2 under conditions of temperature and pressure so that the density frequently exceeds the critical density (0.47 g cm^{-3}); indeed, many techniques require densities that are in the range expected for conventional liquid solvents (0.8±1.0 g cm^{-3}). The concept of supercritical fluid was discovered in 1822 by Baron Cagniard de la Tour who defined it as a state of matter where the liquid and vapour phases are indistinguishable (*2*). For example, a SCF may be relatively dense and dissolve certain solids while being miscible with permanent gases and exhibiting high diffusivity and low viscosity. In addition, supercritical fluids are highly compressible and the density (and therefore solvent properties) can be "tuned" over a wide range by varying pressure (*3*)(Fig. 5.1).

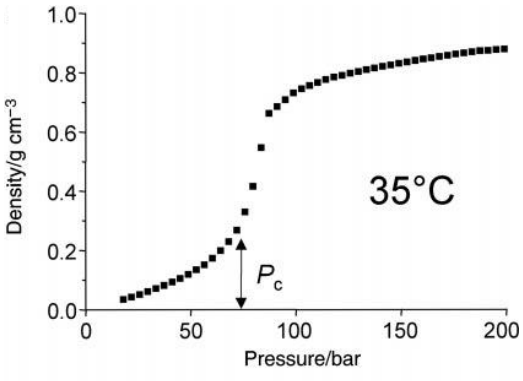

Fig.5.1 Graph showing the variation in density for pure CO_2 at 35 °C as a function of pressure. At this temperature (i.e., close to T_c for CO_2) there is a rapid but continuous increase in density near the critical pressure (Pc) (*4*).

It is possible to observe the transition from liquid to supercritical fluid in a continuous way when a liquid is heated above its critical temperature at nominal density corresponding to the critical one as shown in figure 5.2

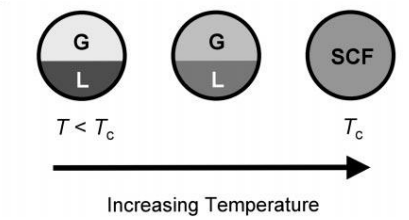

Figure 5.2 Schematic representation of the change from liquid-gas equilibrium (T< Tc) to supercritical fuid (T>Tc) conditions as a substance is heated above its critical temperature at nominal density corresponding to the critical one (*4*)

Figure 5.3 shows the P-T diagram where the coesistence of the two phases liquid and vapour in equilibrium exists and, at the critical point, the densities of the equilibrium liquid phase and the saturated vapour phase become equal, resulting in the formation of a single supercritical phase. SCFs can exhibit changes in solvent density with small changes in temperatures or pressure within the critical region.

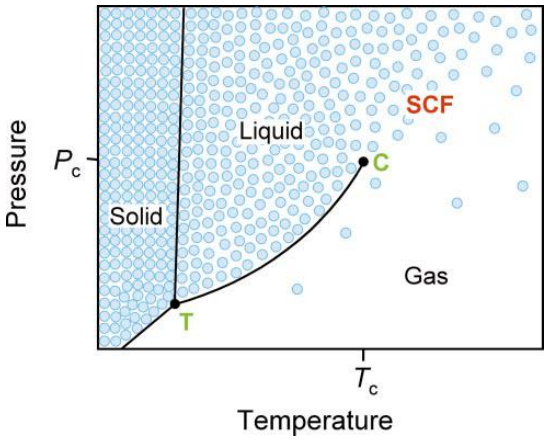

Figure 5.2 Schematic phase diagram for a pure component showing the supercritical fluid (SCF) region. The triple point (T) and critical point (C) are marked. The blue circles represent the variation in density of the substance in the different regions of the phase diagram.(*4*)

Under the appropriate conditions (i.e., slightly below the critical temperature and pressure), liquid CO_2 may be considered as a "near-critical" fluid. This means that, while being a liquid, the substance may exhibit some SCF-like properties such as reduced viscosity and density. A "near critical" fluid displays a limited degree of compressibility and the solvent properties may be fine-tuned with pressure, even if in a much lesser extent than in the supercritical state. A practical advantage of working with liquid CO_2 is that relatively high solvent densities can be achieved at moderate pressures: for example, the density of liquid CO_2 at 20°C is greater than 0.84 g cm^{-3} at pressures above 75 bar. For certain processes that operate near the critical temperature for CO_2 (31.1°C) one may be able to choose between working with CO_2 in the liquid state or under supercritical conditions. In such cases the best choice will be determined by the specific process requirements (*4*).

5.2. CO_2 properties and utilization as reaction medium for polymer synthesis and modification

Carbon dioxide is a clean and versatile solvent used either for polymer synthesis (*5–9*) or for polymer processing (*10–12*), two interrelated research areas. The unique physical properties of this substance make it an excellent alternative to solvents commonly used because it is not flammable, not-toxic, thermally and chemically stable and it presents mild critical temperature (31.1 °C) and pressure (7.38 MPa) (*13*). This properties give rise to a range of interesting possibilities for the materials chemist, not only in polymer science but also in areas such as organic synthesis (*14*), heterogeneous (*15*, *16*) and homogeneous (*17*) catalysis, and inorganic/metal-organic coordination chemistry (*1*).

More interesting for this PhD thesis is the employment of supercritical carbon dioxide in polymer field as solvent where it is used for several reasons:

- ✓ As the critical temperature of CO_2 is very close to room temperature this solvent can be used in applications involving polymers and heat sensitive materials such as enzymes, flavours, pharmaceuticals and highly reactive monomers
- ✓ at supercritical state CO_2 has low viscosity and is able to penetrate complex structures
- ✓ CO_2 is inexpensive and readily available, which makes switching to CO_2-based processes economically feasible
- ✓ it can be easily removed from the reaction environment by simple depressurization (*18*)
- ✓ A further relevant feature of $scCO_2$ is its capability of highly plasticizing polymers thus lowering their glass transition temperature (T_g). The plasticization effect is particularly important in heterogeneous processes where polymer coagulum, with relatively high local viscosity, are formed during the process. The plasticization effect leads to an increase in the free volume of the polymer chains which in turn increases the value of the diffusion coefficient of the species inside the coagulated particle thus allowing the progression of the polymerisation process up to high value of monomer conversion. Also translational and segmental diffusivity of the growing polymer chains are enhanced by this effect and this leads to a shift in the onset of the gel effect at higher value of the conversion or to a practical suppression of it with a consequent advantage for the thermal control of the process in spite of the relatively low heat capacity of dense CO_2. Moreover this properties can be used to perform space diffuce grafting in bulk polymers thanks to the enhancement of diffusion rate of monomer and free radicals inside the macromolecular matrix.

Futhermore, the possibility to tune in a wide range the pressure and temperature lead to change several properties as density, dielectric constant, heat capacity and viscosity. Finally, in radical copolymerization sc-CO_2 do not take part in chain transfer reactions, thus making easier the control of the molecular weight (*19*).
Very interesting is the effect of the pressure on the rate constants of initiation, propagation and termination. At constant temperature, the qualitative effect of pressure on a rate constant is given by equation 5.1:

$$\frac{dlnk}{dP} = \frac{-\Delta V}{RT} \tag{5.1}$$

where : k = reaction constant
ΔV = volume of activation

Variation of ΔV leads to change in the rate constant with pressure: a negative value of ΔV leads to an increase in the reaction rate constant as consequence of an increased pressure. Taking into account that k depends on the variation of the term $k_p(k_d/k_t)^{1/2}$ (see chapter 1) the equation 5.1 become:

$$\frac{dln(k_p(k_d/k_t)^{1/2}}{dP} = \frac{-\Delta V}{RT} \tag{5.2}$$

where it is possible to observe that the effect of the pressure on the polymerization rate will depend from ΔV that is the overall volume of activation due to the sum of initiation, propagation and termination volumes as expressed by equations 5.3.

$$\Delta V = \frac{\Delta V_d}{2} + \Delta V_p - \frac{\Delta V_t}{2} \tag{5.3}$$

When radical decomposition of conventional initiators occurs, the activation volume of the initiation step is positive (due to the unimolecular decomposition), thus the initiation rate decreases as pressure increases. On the other hand, during the polymerization the activation volume related to the propagation is negative (because

the reaction involves two species coming together). For what concern the sign of ΔV_t it can be inferred that, since the termination step is diffusion-controlled, an increase of pressure, leading to an increase in the viscosity of the reaction medium, decreases k_t and so the sign of the activation volume results positive. (*20*, *21*).

As the decomposition and termination contributions are both positive they partially cancel each other and the effect of pressure on the kinetic of the polymerisation can be largely estimated from the propagation term thus leading to an acceleration of the process.

However it must be underlined that the effect of pressure begins to be relevant only at very high value of pressure. For example, in the case of methyl methacrylate, using as a value of the activation volume for bulk polymerisation ΔV= -17 cm^3 mol^{-1} (*22*) and assuming it independent on pressure and solvent, we can estimate an increase of about 20% in the polymerisation rate at 65°C and 340 bar which are the initial conditions often adopted for dispersion processes carried out in $scCO_2$. To get a tenfold increase in the reaction rate a pressure of about 3800 bar should be used (*23*).

5.3 Solubility of polymers in supercritical CO_2

CO_2 is a very poor solvent for most high molecular weight polymers under readily achievable conditions (<100 °C, <1000 bar) while is a good solvent for many non-polar (and some polar) molecules with low molecular weights (*24*). The intermolecular forces between solvent-solvent, solvent-polymer segment, polymer segment-segment pairs in solution and the free volume difference between the polymer and CO_2 strongly influence the values of pressures and temperatures needed to dissolve a polymer in CO_2 (*25*).

Carbon dioxide has a low dielectric constant (relative permittivity) (1.01±1.67, depending on conditions)(*26*) and its polarisability ($27.6*10^{-25}$ cm^3) (*27*) is close to that of gases such as methane, perfuoromethane and fuoroform. The only polymers that show a good solubility in pure CO_2 under mild conditions are certain

amorphous fuoropolymers and silicones, maybe due to weak complexes that these polymers create with CO_2, or by preferential clustering of CO_2 near the fuorine atom of the C-F bonds, which are more polar than C-H bonds. Hence, fluorinated side groups may "shield" the hydrocarbon main chain from interacting with the solvent (*25*).

Many researchers have used spectroscopic methods to elucidate specific CO_2-polymer interactions. FTIR studies by Kazarian et al.(*28*) have shown that CO_2 can participate in Lewis acid-base type interactions with polymers containing electrondonating groups such as carbonyls. Dardin et al. used in situ high-pressure ^{1}H and ^{19}F NMR spectroscopy to show that specific solvent-solute van der Waals interactions exist between CO_2 and certain fuorinated solutes, and that these interactions cause magnetic shielding of the fuorine nuclei (*29*).

Whatever the precise physical basis for the unusual solubility of amorphous fuoropolymers, for practical purposes the materials chemist may consider CO_2 as a non-solvent for the majority of high molecular weight polymeric materials. While this imposes certain restrictions, the poor solvent strength of CO_2 has also been exploited in areas such as polymer fractionation, selective extraction and polymer purification , and the formation of polymer particles by antisolvent precipitation (*25*).

5.4 State of the art on controlled radical polymerization with ATRP carried out in sc-CO_2.

Several studies are reported in literature concerning the graft copolymerization in sc-CO_2 of a backbone with conventional radical grafting techniques (i.e., grafting mediated by conventional initiators (*30*, *31*)) , but controlled free radical graft copolymerization in sc-CO_2 has been much less investigated.

In this paragraph the studies carried out until now in the supercritical medium by ATRP were reported.

An interesting study in 1999 was reported by Matyjaszewski and coworkers (*32*) related to precipitation ATRP of MMA in $scCO_2$ at 80 °C using methyl 2-bromopropionate/CuCl/Cu(0). Cu(0) was added to increase the polymerization rate (Cu(0) reduces Cu(II) to Cu(I)). The ligand used was 4,4'-di(tridecafluoro-1,1,2,2,3,3-hexahydrononyl)-2,2'-bipyridine (dRf_6bpy; Fig. 5.3), which was specifically designed to have enhanced solubility in $scCO_2$.

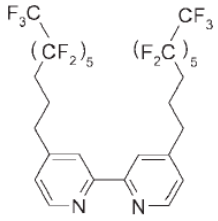

Figure 5.2 . ATRP ligand : dRf_6bpy

Homogeneous ATRP of fluorinated acrylate monomers in $scCO_2$ performed by the same authors (*32*) resulted in higher polymerization rate and better matching between M_n and $M_{n,th}$ when the fluorinated ligand dRf_6bpy was used instead of bpy and dNbpy, which was attributed to higher $scCO_2$ solubility of dRf_6bpy. However, in the precipitation ATRP of MMA, the limiting conversion was 55% (M_n = 12,000 g/mol; M_w/M_n not reported). Precipitation ATRP (*33*) of MMA (34 vol %) in $scCO_2$ at 70 °C and 32 MPa initiated by methyl a-bromophenylacetate/ CuBr using the ligand tetraethyldiethylenetriamine has also been reported as part of a study on dispersion ATRP . Control was very poor, with M_w/M_n = 1.90, although M_n (33,000 g/mol) ~ $M_{n,th}$ (27,000 g/mol), and no distinct particles were formed. The poor control was attributed to insufficient solubility of the ligand in the continuous phase.

Okubo and coworkers (*34*) carried out dispersion ATRP of MMA (20% v/v) in $scCO_2$ at 65°C using CuBr, the ligand HMTETA, and PDMS-Br macroinitiator (M_n = 6500 g/mol; M_w/M_n =1.06; Scheme 5.1) as initiator-stabilizer (inistab).

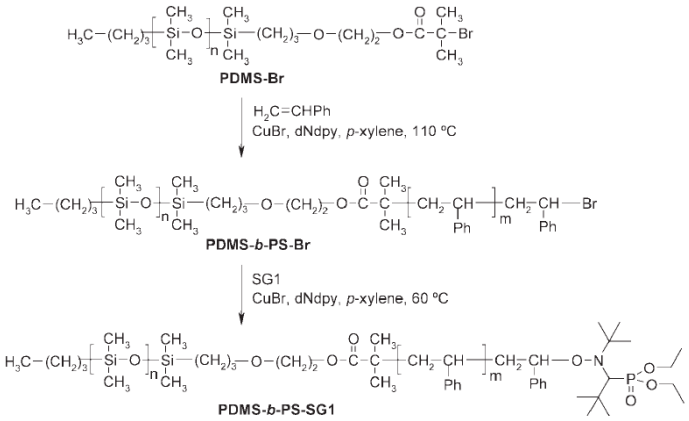

Scheme 5.1 Synthesis of PDMS-b-PS-SG1 (inistab) from PDMS-Br .

The inistab species have both roles of initiator and colloidal stabilizer. The PDMS segment is soluble in $scCO_2$, whereas the in situ formed PMMA segment would become insoluble. The polymer-philic segment of the block copolymer anchors to the forming particles, while the CO_2-philic segment extends into the continuous phase. The polymerizations reached 71 and 91% in 24 h using 5 and 10 wt % inistab related to MMA, respectively, with good control/livingness (M_w/M_n ~ 1.25). In contrast to the conventional dispersion polymerization of MMA in $scCO_2$ using a PDMS macroazoinitiator,109 the particles were non spherical with approximate diameters of 558 and 300 nm for 5 and 10 wt % inistab (Fig. 5.3), respectively, displaying a core-shell structure with PDMS comprising the shell.

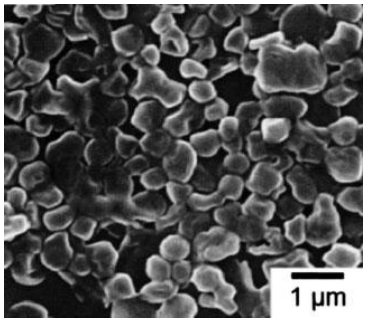

Figure 5.3 SEM micrograph of PDMS-b-PMMA particles prepared by dispersion ATRP of MMA with a PDMS-Br inistab species (5 wt %) in $scCO_2$ at 65 °C.

Recently, Islam et al synthesized poly(vinyl acetate) (PVAc) by atom transfer radical polymerization of vinyl acetate (VAc) in supercritical carbon dioxide using CuBr/2,2′:6′,2″-terpyridine complex as a catalyst and ethyl 2-bromoisobutyrate as an initiator. Polymerization proceeded in a controlled manner, and moderate conversion was achieved as reported in figure 5.4 (a).

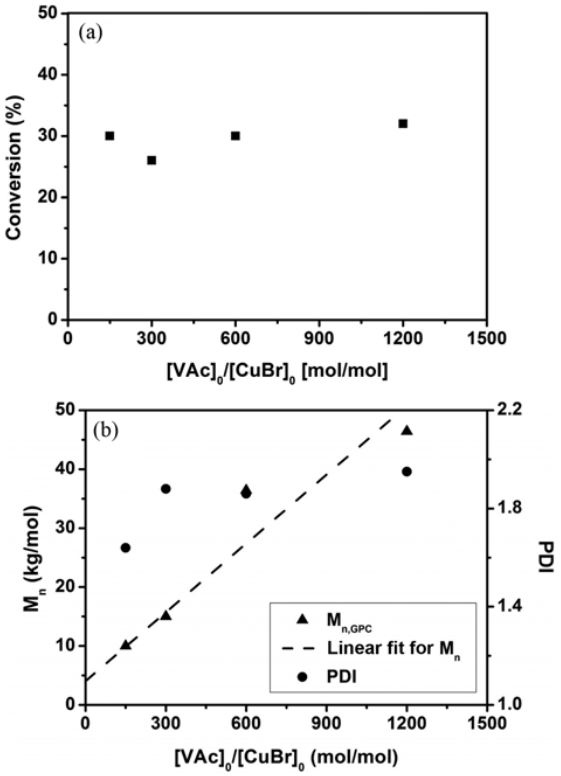

Figure 5.4 Conversion (a) and M_n and PDI (b) as a function of monomer content ($[VPi]_0/[CuBr]_0$) for the ATRP of VAc in $scCO_2$ (Reaction conditions: Molar feed ratio of $[EBiB]_0 : [CuBr]_0 : [tPy_]_0$=1: 1 : 1, temperature=65°C, pressure=310 bar, and time=24 h).

Fig. 5.4(b) shows the number average molecular weight (M_n) and polydispersity index (PDI) obtained and the results suggest that both the M_n and PDI increased with increasing monomer content in the feed. The M_n increased from 10 to 46.4 kg/mol (PDI increased from 1.64 to 1.95) nearly linearly when the

monomer/catalyst mole ratio changed from 150 to 1200. This is possibly because for a higher amount of monomer, the ratio of initiator to monomer decreases, (i.e., the number of radicals formed decreases) resulting in higher molecular weights. Moreover, when the monomer/catalyst mole ratio was higher, the polymerization was not controlled and a broader MWD (PDI 1.95) was observed.

In this context the study carried out in this thesis and presented in Chapter 6 related to the modification of PVDF nanoparticles by ATRP in sc-CO_2 is a interesting study until now not reported in the literature; this study also confirms the possibility of using sc-CO_2 as green solvent for the modification of polymers and not only for the synthesis using a controlled radical technique as ATRP.

5.5. sc-CO_2 as a new potential medium to sterilize biomaterial

Taking into account the employment of sc-CO_2 in biomedical field as a green solvent, in the last part of this work the potentiality of this solvent as sterilization medium on a model matrix was evaluated. This work was born also from an increasing attention of the scientific community on tissue engineering concerning the regeneration of damaged tissue or the creation of artificial organs (*35*) and the model matrix chosen is a biodegradable aliphatic polyester. Synthetic resorbable polyesters such as poly(lactic acid) (PLA), poly(L-lactic acid) (PLLA), poly(D,L-lactic acid) (PDLLA), poly(glycolic acid) (PGA) and poly(L-lactic glycolic acid) (PLGA) were often used to prepare porous polymer matrixes since they are already used in a large number of approved medical implants because they are considered safe, non toxic and biocompatible (*36*). A fundamental requisite before implantation is surely their "total sterilization" refering to both the external and internal surface of these complex porous structures.

Supercritical carbon dioxide ($scCO_2$) is an alternative solvent against the most common adopted methods used until now as ethylene oxide exposure, steam sterilization, γ-irradiation and hydrogen peroxide plasma to sterilize biomedical devices (*18*). All of these techniques exhibits some drawbacks that make them not

suitable for such polymers. For example, the toxic ethylene oxide can remain adsorbed in the material (*37*, *38*); steam sterilization is not adapt for thermo-labile materials (*39*); γ-irradiation induces degradation of the polymeric matrixes by cross-linking or chain scission reactions leading to relevant changes in the molecular architecture of the materials (*40*); finally, free radicals generated during the hydrogen peroxide plasma process may adversely react with the polymer chains of the sterilized materials and degrade them (*41*).

Recently, the sterilization with $scCO_2$ in different application fields such as those related to food (*42–44*) and biomedical products (*45–47*) was carried out. Reverchon et al. have shown that $scCO_2$ technology is very interesting in biomedical field to sterilize medical device like endoscopes which are very difficult to clean with common methods (*46*). Indeed the main problems in the sterilization of these materials are connected with their complex geometry and with the nature of their constituting materials (such as metals, glasses,..) that present in their surface micro or nano spaces more easily accessible by gaseous or supercritical CO_2 (*46*).

Tarafa et al. reported the decontamination of both metallic and polymeric biomaterials removing lubricant oil from titanium surfaces and disinfecting poly(acrylicacid-co-acrylamide) potassium salt powders contaminated with *Staphylococcus aureus* (*S. aureus*)(*48*). This work demonstrated that $scCO_2$ at relatively low temperature and moderate pressure can be used to remove contaminants from metallic surface and from hydrogel polyelectrolyte (*48*).

Figure 5.5 shows that higher or equal oil removal was achieved with $scCO_2$ than with detergent and some fraction of the oil was also removed by centrifugal forces for the negative control. Because stirring is applied on the oil-contaminated disks in the pressure vessel, it is concluded that some oil was mechanically removed by centrifugal force.

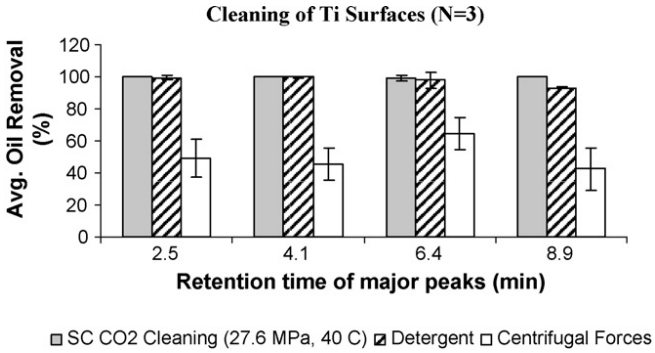

Figure 5.5. Average oil removal (%) for each cleaning process

Figure 5.6 shows that the cell walls of S. aureus, a spherical bacterial cell typically found in clusters, were mostly unaffected by the liquid CO_2 disinfection process. Some cell walls may have been affected by the pulverization process. The disinfection mechanism is apparently not based on cell rupture.

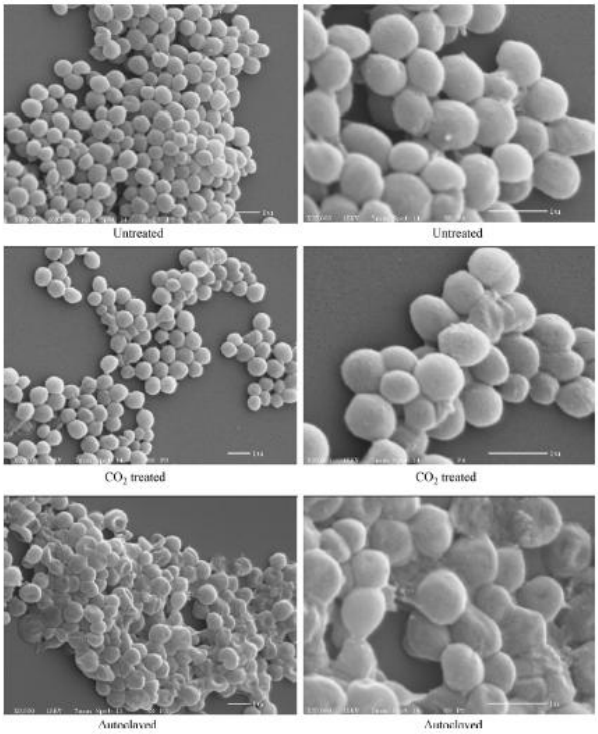

Figure 5.6. SEM micrographs of untreated, CO_2 treated at 25 ◦C and 6.9MPa for 90 min and autoclaved samples.

Furthermore in these study drying curves of the hydrogel were observed and no significant change between treated and untreated samples suggesting no change in hydrogel structure and therefore no apparent change in properties after CO_2 treatment. Also, both treated and untreated samples absorbed very similar amount of water as determined by the average equilibrium swelling ratio (*48*).

Jimenez et al. (*45*) have studied the sterilization of the same hydrogel contaminated with *S. aureus* and *E. coli* used in the latter mentioned work by CO_2 based cold sterilization. Figure 5.7 shows the efficacy of the sterilization process on both microorganisms with and without H_2O_2 while no significant changes in the hydrogel structure after exposure to CO_2 pure or modified by addition of H_2O_2 were observed (*45*) as shown by frying curves in figure 5.8.

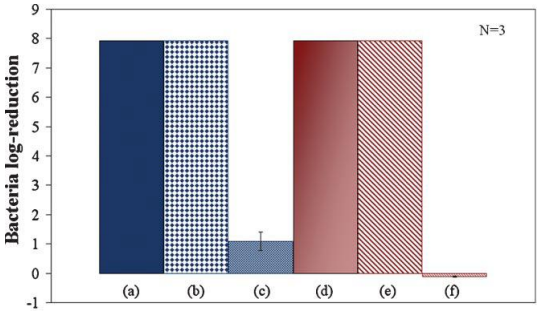

Figure 5.7 Log-reduction of S. aureus and E. coli in the model hydrogel poly- (acrylic acid-co-acrylamide) after pure sc-CO_2 and sc-CO_2/H_2O_2 treatments. All treatment times are 4 h at 40°C and 27.6 MPa. (a): S. aureus pure sc-CO_2 treatment. (b): S. aureus sc-CO_2/H_2O_2 treatment. (c): S. aureus thermal control (40°C for 4 h). (d): E. coli pure sc-CO_2 treatment. (e): E. coli sc-CO_2/H_2O_2 treatment. (f): E. coli thermal control (40°C for 4 h).

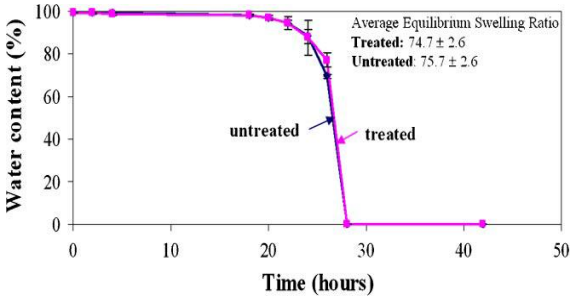

Figure 5.8. Drying curve of crosslinked poly(acrylic acid-co-acrylamide) potassium salt treated with pure CO_2 at 40°C and 27.6 MPa for 4 h, hydrated with deionized water and dried in a vacuum oven (50°C, 20 in Hg).

It is important to report that a particular class of microorganism has been treated in this work. They were bacterial spores characterized by very resistant protective structures that make very difficult the sterilization of contaminated samples without damaging them. For this reason, it is very important to find out a sterilization method that does not alter the morphology and the chemico-physical properties of the polymeric materials. Worth mentioning, it was previously shown that, usually, bacterial spores are drastically more resistant to treatment with pure CO_2 than vegetative bacteria unless high temperatures (80–100 °C) or extended treatment times (days) are used (*13*, *49–55*).

References

1. J. A. Darr, M. Poliakoff, *Chem. Rev.* **99**, 495 (1999).
2. C. Cagniard de la Tour, *Ann. Chim. Phys.* **22**, 127 (1822).
3. O. Kajimoto, *Chem. Rev.* **99**, 355 (1999).
4. A. I. Cooper, *J. Mater. Chem.* **10**, 207–234 (2000).
5. J. L. Kendall, D. A. Canelas, J. L. Young, J. M. DeSimone, *Chem. Rev.*, 99, 543 (1999).
6. D. A. Canelas, J. M. DeSimone, *Adv. Polym. Sci.,*. **133**, 103 (1997).
7. D. A. Canelas, A. L. C. Burke, J. M. DeSimone, *Plast. Eng.* **53**, 37 (1997).
8. A. I. Cooper, J. M. DeSimone, *Curr. Opin. Solid State Mater. Sci.* **1**, 761 (1996).
9. K. A. Shaffer, J. M. DeSimone, *Trends Polym. Sci.* **3**, 146 (1995).
10. M. Aresta, *Quim. Nov.* **22**, 269.
11. B. Bungert, G. Sadowski, W. Arlt, *Ind. Eng. Chem. Res.* **37**, 3208 (1998).
12. S. G. Kazarian, *Appl. Spectrosc. Rev.,*. **32**, 301 (1997).
13. M. Perrut, *J. Supercrit. Fluids*. **66**, 359–371 (2012).
14. P. G. Jessop, W. Leitner, (1999).
15. A. Baiker, A. J. Mesiano, *Chem. Rev.* **99**, 453.
16. E. J. Beckman, A. J. Russell, *Chem. Rev.* **99**, 623.
17. P. G. Jessop, T. Ikariya, R. Noyori, *Chem. Rev.* **99**, 475 (1999).
18. A. K. Dillow, F. Dehghani, J. S. Hrkach, N. R. Foster, R. Langer, *Proc. Natl. Acad. Sci. U. S. A.* **96**, 10344–10348 (1999).
19. Y. Ogo, *Macromol. Sci. Rev. Macromol. Chem Phys.* **C24,1** (1984).
20. K. F. O'Driscoll, *Makromol. Chem.l. Chem.* **178**, 899 (1977).
21. K. F. O'Driscoll, *Makromol. Chem.* **180**, 2053 (1979).
22. S. Beuermann, M. Buback, G. T. Russell, *Macromol. Rapid Comm.* **15**, 351–355 (1994).
23. P. W. Moore, F. W. Ayscough, J. G. Clouston, *J.Polym. Sci. Pol. Chem.* **15**, 1291 (1977).
24. J. A. Hyatt, *J. Org. Chem.* **49**, 5097 (1984).

25. C. F. Kirby, M. A. McHugh, *Chem. Rev.* **99**, 565.
26. F. G. Keyes, J. G. Kirkwood, *Phys. Rev.* **36**, 754 (1930).
27. R. C. Reid, J. M. Prausnitz, B. E. Poling, *McGraw-Hill, New York, 4th edn.,* (1987).
28. S. G. Kazarian, M. F. Vincent, F. V. Bright, C. L. Liotta, C. A. Eckert, *J. Am. Chem. Soc.* **118**, 1729 (1996).
29. A. Dardin, J. B. Cain, J. M. DeSimone, C. S. Johnson, E. T. Samulski, *Macromolecules*. **30**, 3593 (1997).
30. K. Clark, S. Lee, *Polym. Eng. Sci.*, 631–639 (2005).
31. A. M. Van Herk *et al.*, *Macromolecules*. **29**, 1027–1030 (1996).
32. J. Xia, T. Johnson, S. G. Gaynor, K. Matyjaszewski, J. M. DeSimone, *Macromolecules*. **32**, 4802–4805 (1999).
33. B. Grignard *et al.*, *Chem Commun*, 314–316 (2008).
34. H. Minami *et al.*, *Des Monom Polym*. **7**, 553–562.
35. C. Liu, Z. Xia, T. J. Czernuszka, *Chem. Eng. Res. Des. (Trans IChemE)*. **85**, 1051–1064 (2007).
36. Y. S. Nam, T. G. Park, *Biomaterials*. **20**, 1783–1790 (1999).
37. J. L. Clayton, *Minim. Invasive Surg. Nurs.* **10**, 13–20 (1996).
38. R. Guidoin *et al.*, *Biomaterials*. **6**, 122–128 (1985).
39. D. J. Dempsey, R. R. Thirucote, *J. Biomater. Appl.* **3**, 454–523 (1989).
40. Y. Z. Zhang, L. M. Bjursten, C. Freij-Larsson, M. Kober, B. Wesslen, *Biomaterials*. **17**, 2265–2272 (1996).
41. R. E. Duffy *et al.*, *Arch. Ophthalmol.* **118**, 1167–1176 (2000).
42. G. Ferrentino, S. Spilimbergo, *Food Sci. Technol.* **22**, 427–441 (2011).
43. G. Ferrentino, S. Balzan, A. Dorigato, A. Pegoretti, S. Spilimbergo, *J. Food Sci.* **77**, E137–E143 (2012).
44. L. Garcia-gonzalez *et al.*, *Int. J. Food Microbiol.* **117**, 1–28 (2007).
45. A. Jimenez, J. Zhang, M. A. Matthews, *Biotechnol. Bioeng.* **101**, 1344–1352 (2008).
46. E. Reverchon, G. Della Porta, R. Adami, *Recent Patents Chem. Eng.* **3**, 142–148 (2010).

47. S. Spilimbergo, N. Elvassore, A. Bertucco, *J. Supercrit. Fluids*. **22**, 55–63 (2002).
48. P. J. Tarafa, A. Jiménez, J. Zhang, M. A. Matthews, *J. Supercrit. Fluids*. **53**, 192–199 (2010).
49. M. Kamihira, M. Taniguchi, T. Kobayashi, *Agric. Biol. Chem.* **51**, 407–412 (1987).
50. S. Spilimbergo, A. Bertucco, *Biotechnol. Bioeng.* **84**, 627–638 (2003).
51. J. D. Hemmer, M. J. Drews, M. Laberge, M. A. Matthews, *J. Biomed. Mater. Res. Part B Appl. Biomater.* **80B**, 511–518 (2006).
52. J. Zhang *et al.*, *J. Microbiol. Methods*. **70**, 442–451 (2007).
53. A. White, D. Burns, T. W. Christensen, *J. Biotechnol.* **123**, 504–515 (2006).
54. S. Spilimbergo, A. Bertucco, F. . M. Lauro, G. Bertoloni, *Innov. Food Sci. Emerg. Technol.* **4**, 161–165 (2003).
55. J. Zhang *et al.*, *J. Microbiol. Methods*. **66**, 479–485 (2006).

CHAPTER 6
ATRP OF HALOGENATED NANOPARTICLES IN sc-CO_2

6.1 Introduction

In the work presented in this chapter , the modification of PVDF nanoparticles by grafting of HEMA was realized. The specific monomer was selected in order to create pH-sensitive matrixes improving also the hydrophilicity of the pristine PVDF. This study was carried out using ATRP based controlled radical polymerization techniques with the aim of obtaining a better control of the molecular weight of the grafted chains. The graft copolymerizations were carried out using supercritical carbon dioxide as solvent to take benefit of its peculiar properties as biocompatibility, easy recovery from the processed polymer by depressurization and good swelling of the polymer particles.

The experimental work was opportunely planned in order to study the influence of some operative parameters such as different initiation systems (with or without reducing agent), ligands, oxidation state of salt precursors, ternary catalytic complexes, reaction temperature, density of scCO_2.

Moreover, it was investigated the presence of grafting by FT-IR, while eventual variation of the cristallinity and of the morphology of the nanoparticles were analyzed by DSC and SEM analyses, respectively.

6.2. Experimental

6.2.1. Materials

Cu(I)Br (98%), Cu(II)Br_2 (99%), Cu(I)Cl (98%) and Cu(II)Cl_2 (99%) (Sigma Aldrich) were stored under nitrogen atmosphere. Bpy, DMBP, TPMA (Tris(2-

pyridylmethyl)amine, 98%, and Me_6TREN(Tris[2(dimethylamino)ethyl]amine, 97%,) were used as ligands and ascorbic acid (AscA) or benzoyl peroxide (BPO) as reducing agent. All these chemicals were supplied from Aldrich and used as received. PVDF used in this study is Hylar 461, obtained in powdery form (250 nm average particle size) from Solvay Specialty Polymers. Anhydrous 2-hydroxyethyl methacrylate (HEMA) (97%, stabilized with 250 ppm of monomethylether hydroquinone as inhibitor, reagent grade), ethanol (ACS, 99.8%) and KBr for FTIR analyses (Potassium bromide 99+%, FT-IR grade) were purchased from Aldrich and used without further purification.

6.2.2. Grafting procedure

The reactions were carried in an AISI 316 stainless steel reactor having a free volume of about 27 mL, consisting of a cylindrical body and a threaded cap and showed in Figure 6.1.

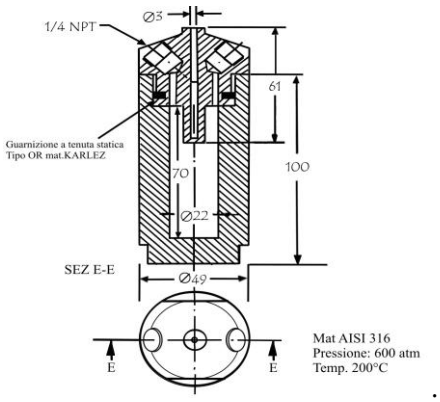

Figure 6.1 Schematic representation of the batch reactor.

In the central position of the reactor closure was settled a thermo well for the Pt 100 temperature sensor. In the cap two threaded ports (¼ inch NPT) used to mount the pressure sensor and a valve for the loading and the venting of gaseous substances

were also present. The pressure sensor was a Barksdale type UPA 3 transducer, calibrated against a precision manometer, the gas valve was of the needle type supplied by Parker. The reactor was heated to reaction temperature using an electric heating mantle controlled by a PID electronic controller (Eurotherm).

The loading of the reactor before each grafting reaction was carried using the following sequence: about 1±0.1 g of the PVDF powder previously dried in an oven at 80 °C for 3 h under vacuum was initially loaded followed by the weighed amount of monomer, copper salt, ligand and reducing agent when used. All these components were added under a stream of inert gas to limit the contact with the atmospheric air. The reactor was then closed and, before of the solvent loading , purged at least five times with low pressure CO_2 to remove residual atmospheric oxygen. After purging the oxygen, liquid CO_2 was loaded at room temperature using an ISCO syringe pump, up to reach the desired nominal density. The total amount of CO_2 introduced was measured by weighing the vessel with an electronic scale (Sartorius LP 8200S, precision 0.01 g). After loading the heating mantle was mounted and the autoclave was heated up to desired temperature. Heating time lasted less than 15 minutes and the reaction time was counted from the instant at which the reaction temperature was reached. The temperature and the pressure in the reactor were monitored during the whole test. At the end of the desired reaction time, the system was cooled down in ice water and slowly depressurized by bubbling the gaseous effluent in water.

After venting, the reactor was opened and the product was recovered and washed at room temperature with ethanol (25 mL) for two hours to remove unreacted monomer and catalytic complex. The polymer powder was separated by centrifugation (3500 rpm for 5 min) and extracted six times with hot ethanol at 90°C in the sealed reactor to recover any residual components and ungrafted poly(HEMA) chain (extraction time for each batch 1 hour, cumulative volume of alcohol used 150 mL).The treated PVDF was again recovered by centrifugation, and then it was dried in an oven at 70°C overnight, to eliminate residual traces of ethanol.

6.2.3. Characterization of grafted PVDF

An estimation of the amount of grafted HEMA in the PVDF powder was made by infrared (IR) spectra recorded on a Perkin-Elmer Spectrum 2000 Explorer FTIR with an averaging of 16 scans at a resolution of 1 cm^{-1} using a near-IR fast recovery deuterated tryglicinesulfate detector using a procedure described in the literature (*1*, *2*). Weighed amounts of grafted samples were mixed with KBr in a mortar and pressed into discs with a 10 tonn pressure to obtain a film. The determination was made by calculating the ratio of the absorbance of the 1716 cm^{-1} band (A_{CO}) corresponding to the stretching of the carbonyl group in poly(HEMA) chain to the absorbance of the CF_2 stretching band at 877 cm^{-1}(A_{CF2}) which was used as the internal reference in the normalization of the different spectra. Assuming validity of the Lambert-Beer law, the absorbance of aforementioned characteristic peaks can be expressed by equations:

$$A_{CO} = K_{CO}\, C_{HEMA}\, L \qquad (6.1)$$

$$A_{CF2} = K_{CF2}\, C_{VDF} L \qquad (6.2)$$

where, K_{CO} and K_{CF2} are the molar absorption coefficients at the specific wavenumbers, C stands for the molar concentration of repeat units in the KBr disc and L is its thickness.

By dividing member to member eq. 6.1 and 6.2 and by introducing the cumulative mass of repeat units in the analyzed sample we obtain the equation 6.3

$$\frac{A_{CO}}{A_{CF2}} = \frac{K_{CO}}{K_{CF2}} \frac{C_{HEMA}}{C_{VDF}} = F \frac{M_{HEMA}}{M_{VDF}} \qquad (6.3)$$

where $F = (K_{CO}/K_{CF2})(PM_{VDF}/PM_{HEMA})$.

The grafting level DG in the modified polymer was given by the following equation

$$DG = 100 \frac{M_{HEMA}}{M_{VDF}} = 100 \frac{1}{F} \frac{A_{CO}}{A_{CF2}} \qquad (6.4)$$

According to eq. 6.3, a plot of A_{CO}/A_{VDF} versus M_{HEMA}/M_{VDF} should yield a straight line, and its slope would represent the ratio F.

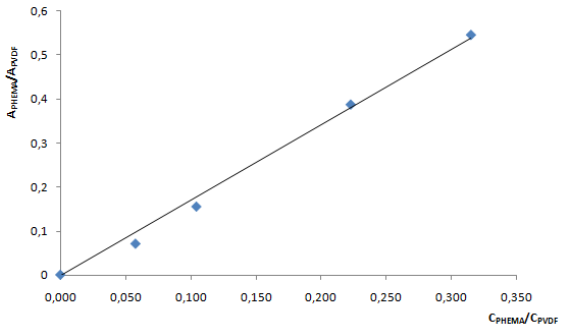

Figure 6.2. Calibration curve for FT-IR quantitative analysis of the grafting degree

Calorimetric analyses of the copolymers were performed with a Perkin Elmer Jade differential scanning calorimeter (DSC). A pre-weighed amount M_{POL} of the copolymer (3–5 mg) was loaded into an aluminium pan sealed with an aluminium lid pressed slightly using a metal plunger and placed into the calorimeter holder under a N_2 flow of 20 $mLmin^{-1}$. The sample was heated twice from 18 ºC up to 220 ºC with a heating rate of 10 $ºCmin^{-1}$. The cooling rate between the two scans was 10 $ºC\ min^{-1}$ too. The melting enthalpies, ΔH_m, were determined from the peak areas, whereas the melting temperatures, T_m, where measured at the maximum of the peaks. The percentage of crystallinity of the grafted and pristine powders, χ_c, was then calculated from the measured melting enthalpies values by using the equation 6.5:

$$\chi_c = 100 \frac{\Delta H_m * \left(1 - \frac{DG}{100}\right)}{M_{POL}\, \Delta H_{100\%} crystalline} \qquad (6.5)$$

where $\Delta H_{100\%crystalline}$ is the specific heat of fusion of pure crystalline PVDF, which is reported to be 104.6 J g^{-1}(*3*).

The particle morphologies were analysed and imaged with a Philips scanning electron microscope. Samples were sputter-coated with gold to a thickness of 200 Å.

6.2.4.Investigation of the phase behaviour of the reaction system

The phase behaviour of the CO_2/HEMA mixture was investigated under conditions adopted to perform grafting reactions, by visual observation in a constant volume stainless steel high pressure vessel equipped with two sapphire windows with 180° orientation (1.24 inch diameter). The vessel reported in Figure 6.3 had three port equipped with Swagelock male connectors; one of them was closed by a screw cap and used for loading of the liquid component, a second port was connected to a valve and a pressure transducer, the third male connector was used to insert a Pt100 thermal sensor. The temperature control was ensured by inserting the cell in the electronically controlled heating tape, whereas the pressure was recorded by means of the pressure transducer. After the loading of a proper amount of HEMA, the cell was purged from air with a small flow rate of carbon dioxide inserted from the valve, maintaining the cap open. After venting, the cell was closed and a weighted amount of CO_2 was loaded up to reach the desired fluid phase density.

Figure 6.3. View cell adopted for phase behaviour study

The phase behavior of the CO_2/HEMA system was investigated by coupling visual observation of the physical state of the mixture to the recording of the values of pressure and temperature measured by the transducer and the PID controller, respectively. The reactor was charged with an amount of HEMA as 4.8 % v/v and , after the loading of carbon dioxide, an average density (defined as the sum of the masses of CO_2 and of HEMA divided by the free volume of the view cell) as 0.86 g/mL was reached, that correspond to a density of CO_2 (defined as the ratio between mass of CO_2 and the free volume of the view cell) as 0.81 g/mL. At room temperature, the investigated system was composed of two phases; the temperature was increased gradually and the two phases merged into a single phase during the heating. Once reached the value of 65°C at a pressure of 18 MPa it was observed a not homogeneous system , but a further addition of carbon dioxide until a pressure of 20 MPa led to homogenous conditions. Figure 6.4 shows the phase behaviour of the mixture varying the temperature at the higher pressure before reported (20 MPa); at a temperature below 60°C (fig. 6.4a) the presence of liquid monomer on the bottom and a clear interface that separates it from solvent was observed, at 63°C (fig.6.4b) the system is not yet homogenous but the interface is disappeared and (c) at 65°C (c) the system is homogeneous, thus indicating that these operative conditions allow to solubilize the amount of monomer charged.

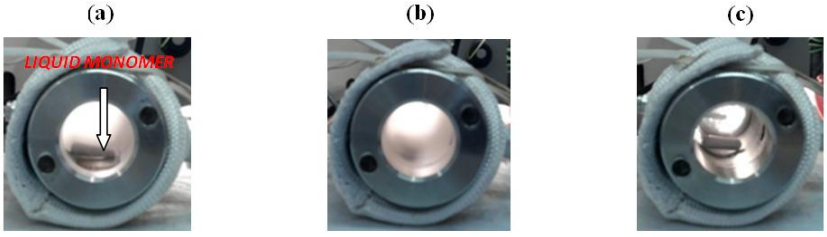

Figure 6.4 Phase behaviour of HEMA in sc-CO_2

6.3 Results and discussions.

6.3.1.Effect of different initiation systems

Three different ATRP techniques (normal ATRP, AGET ATRP and SR&NI ATRP) were firstly analyzed. These techniques are characterized by different initiation systems; in particular AGET and SR&NI differ from normal ATRP because of the presence of a reducing agent such as ascorbic acid (AGET) or benzoyl peroxide (SR&NI) that reduce in situ the catalytic complex charged in its higher oxidation state (Cu^{II} and not Cu^{I} as in a normal ATRP). In this way it is possible to avoid oxidation of copper catalyst during the loading and to employ lower amount of catalyst that it will be reduced continuously in situ (*4*). Typical descriptions of these reactions are reported in Scheme 6.1 that shows homopolymer formation when a conventional radical initiator as AIBN for SR&NI (a) or AscA for AGET ATRP (b) is used (SR&NI).

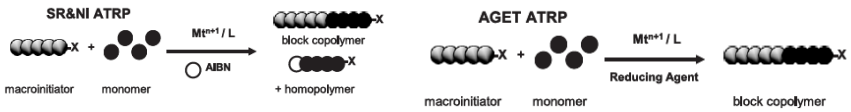

(a) (b)

Scheme 6.1. Schematic illustrations of (a) AGET and (b) SR&NI ATRP reaction.

Graft copolymerizations of HEMA and PVDF nanoparticles with normal ATRP were carried using Cu(I)Cl/DMBP as catalyst at a temperature of 65°C and a CO_2 density of 0.81 g/mL and $Cu(II)Cl_2$/DMBP in AGET or SR&NI conditions. Obtained DG is reported in Table 6.1 where it is possible to observe that the highest degree of grafting was reached when SR&NI technique was employed (46.1%), followed by AGET but at considerably less values (2.9%). Table 6.1 shows that the nanoparticles were not modified using normal ATRP, but very high degree of grafting was reached in the presence of BPO; this result could be also attributed to the extraction of the H atoms and not of the F from the backbone of PVDF. Further,

in this case, a lot amount of homopolymer was observed (PHEMA) most probably created by free radical polymerization initiated by benzoyl peroxide.

Table 6.1. Graft copolymerization of PVDF-g-PHEMA samples with different initiation systems. Operative conditions : PVDF = 1g, HEMA = 0.4 M, CuCl/DMBP (1:1) = 1.33 mM, T = 65°C, t= 16 h , ρCO_2 = 0.81 g/mL.

entry	AscA (mM)	BPO (mM)	DG (%)
nATRP			0
AGET	0.44		2.9
SR&NI		1.33	46.1

In order to confirm the presence of grafting on PVDF powders EDX analyses of three samples with different DGs were conducted. These analyses showed that in the absence of DG (figure 6.5 a) the amount of C and F atoms is similar but when the grafting occurs (figure 6.5b and 6.5c) the relative level of the peaks corresponding to C and F atoms change maybe due the extraction of fluorine by copper catalyst; the presence of the grafting was also confirmed by the comparison of the oxygen peak when AGET and SR&NI techniques are used (Figure 6.5 (b) and (c)) .

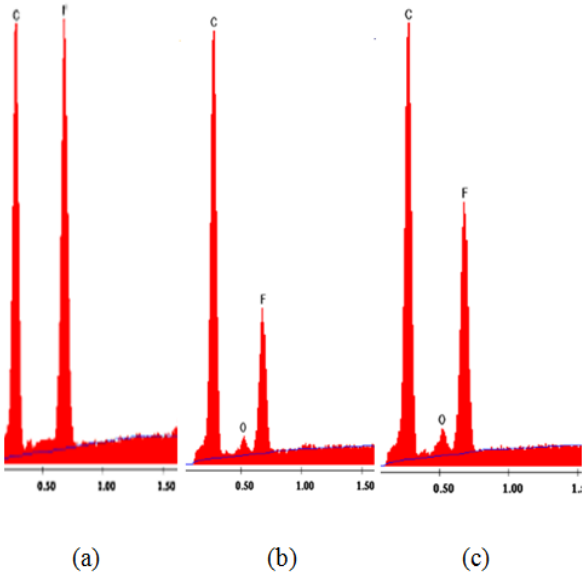

Figure 6.5 EDX of PVDF-g-PHEMA samples obtained by Normal (a), AGET (b) and SR&NI ATRP (c) .

As a confirmation of the modification realized, FT-IR analyses have shown the comparison of the peak of carbonyl of HEMA when grafting occurs ,while by DSC measurements (Table 6.2) a decrease of the crystallinity (χ) from 44 to 28 in the first heating and from 53 to 37 in the second one, was observed at high level of grafting. Concerning the decrease of χ, more pronounced when BPO is used, it could be attributed to an higher hydrogen extraction also in the amorphous portion that are located close to the interface of crystalline portions, that can be distorted by the local variation in the polymer composition and microstructure induced by grafting.

Table 6.2. Melting temperature and cristallinity values recorded during first and second heating of graft copolymers obtained at the following operative conditions : PVDF = 1g, HEMA = 0.4 M, CuCl/DMBP (1:1) = 1.33 mM, T = 65°C, t= 16 h , ρCO_2 = 0.81 g/mL.

Sample	$T_{Imelting}$ *[°C]*	$\chi_{Imelting}$ *(%)*	$T_{II\ melting}$ *[°C]*	$\chi_{\ II\ melting}$ *(%)*
PVDF	165	44	159	53

nATRP	*159*	*41*	*159*	*50*
AGET	*158*	*38*	*159*	*48*
SR&NI	*157*	*28*	*159*	*37*

SEM micrographs (Figure 6.6) showed that PVDF nanoparticles in the presence of high level of grafting (46.1%) are coated with a sticky layer and glued in agglomerates probably as a consequence of the higher surface concentration of grafted poly(HEMA) chains but, the spherical morphology of nanoparticles can be anyway recognized in the micrographs.

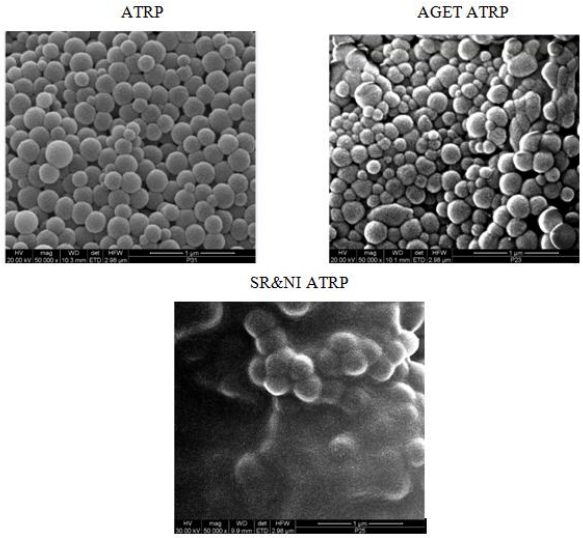

Figure 6.6. SEM micrographs of PVDF-g-PHEMA obtained by different initiation systems.

6.3.2. Effect of the oxidation state of copper ions

Once defined that normal ATRP do not allow to modify the nanoparticles , grafting reactions with AGET and SR&NI techniques were carried out. Grafting experiments with catalyst in different oxidation state were carried out. As reported in Table 6.3 data in good agreement with the specific technique were obtained in the presence of Ascorbic Acid taking into account, as before reported, that the technique is based on the utilization of copper in its higher state of oxidation. In fact, higher level of

grafting was obtained in the presence of Cu(II) complex, but when BPO is used as reducing agent (SR&NI) the opposite behaviour was detected.

Table 6.3. Graft copolymerization of PVDF-g-PHEMA samples with different copper salt precursor . Operative conditions : PVDF = 1g, HEMA = 0.4 M, CuCl/ligand (1:1) = 1.33 mM, T = 65°C, t= 16 h , ρCO_2 = 0.81 g/mL.

entry	AscA (mM)	BPO (mM)	Catalyst	DG (%)
1	0.44		Cu(II)Cl_2/TPMA	10.6
2	0,44		Cu(I)Cl/TPMA	1.3
3		1,33	Cu(II)Cl_2/DMBP	0
4		1.33	Cu(I)Cl/DMBP	46.1

It seems as ATRP reaction works better with Cu(II) when AGET technique is used, as it is reported by literature (*5*), reaching a DG as 10.3% but, surprisingly, in SR&NI the DG becomes zero when Cu^{II} is employed . A possible explanation is related to scheme 6.2 that shows a set of reactions involving BPO with the formation of a new initiator more active than PVDF.

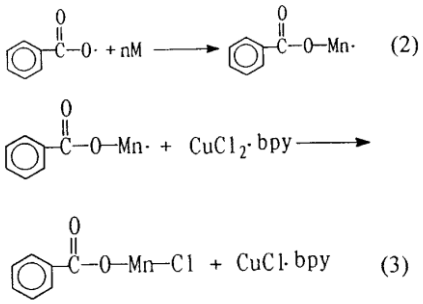

Scheme 6.2 . Possible mechanism involved in the presence of copper catalyst composed by $Cu^{II}X_2L$ (where L=ligand and X = halogen atom) and BPO.

Scheme 6.2 shows that the radical formed by decomposition at 65°C could react with the monomer leading to the formation of oligoradical (step 2) that it is able to react with the Cu(II) species to form a new alkyl halide with a different halogen atom (step 3) and Cu(I). At this point nATRP can begin due to the presence of the

activator Cu(I) but a new alkyl halide which presents a C-Cl bond easier to activate than the C-F of PVDF was created in the reaction medium. Most probably the degree of grafting is zero because the reaction has been totally shifted in the bulk of the reaction medium and not at the interface with the macroinitiator. Coherently with this hypothesis significant amount of homopolymer was found when BPO was employed as probable combination of FRP initiated by BPO and of the mechanism reported in scheme 6.2.

6.3.3 Effect of Reaction Temperature and CO_2 density on AGET and SR&NI Grafting

To investigate the effect of the temperature on the degree of grafting a series of experiments were carried out at 50, 65, 75 and 90°C with a molar feed ratio of $[HEMA]_0$:$[CuCl_2]_0$:$[TPMA]_0$ = 300:1:1 with AGET ATRP and at 65 and 90°C with SR&NI. The effect of the temperature in the presence of AscA was reported in figure 6.8 (a) that shows an increase of the DG until the temperature of 75°C and a decrease at very high temperature as 90°C. High value of temperature seems to influence equally the degree of grafting with SR&NI technique; in particular, as regard SR&NI technique, increasing the temperature from 65°C to 90°C a reduction of DG was observed (Table 6.4).

Table 6.4 Effect of temperature on the grafting of PVDF nanoparticles by SR&NI technique. Operative conditions: PVDF = 1g, HEMA = 0.4 M, DMBP = 1.33 mM, CuCl = 1.33 mM, t = 16h.

entry	Temperature (°C)	DG (%)	P (MPa)	Melting point (°C)	Cistallinity(%)
PVDF				159	53
1	65	46.1	26	159	37
2	90	23	48	159	46

This can also be explained by the effect of this parameter on the catalytic complex; initially, the increases of the temperature leads to an improvement of the solubility of the catalytic complex until 75°C (Figure 6.7a). At higher temperature (90°C) the degree of grafting decreases maybe due to a less stable catalytic complex. Also in this cases, calorimetric measurements have shown a decrease of cristallinity increasing the degree of grafting (Table 6.4).

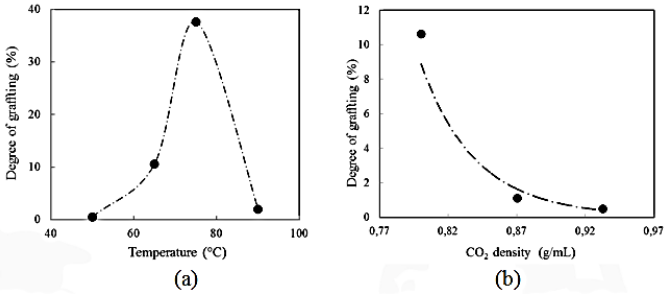

Figure 6.7. (a) Effect of reaction temperature on grafting at ρ=0.81 g/mL and (b) effect of density of CO_2 on grafting degree at 65°C. Operative conditions : PVDF = 1g, HEMA = 0.4 M, Cu(II)Cl_2/TPMA (1:1) = 1.33 mM, t= 16 h , [AscA]=0.44 mM.

Figure 6.7 (b) shows the dependence of DG on carbon dioxide density at 65°C. Graft copolymerizations were carried out with a catalytic complex composed by $Cu^{II}Cl_2$/TPMA at 65°C for a reaction time of 16 h . It can be seen that there is a significant rise as the pressure drops. The DG decreases from 10.6 to 0.5% as carbon dioxide density is increased from 0.80 g/mL to 0.93 g/mL. This can be explained by the remarkable change of solvency of sc-CO_2 with the density. At higher density, scCO_2 has stronger solvent power, and thus monomer partitioning is biased in the CO_2 phase.

In other words, more monomer is extracted from the PVDF membrane by scCO_2 when density increases. As a result, the local concentration of ads/absorbed monomer is reduced with consequent depression of the grafting level. This indicates that the DG can also be controlled by tuning the density of supercritical medium.

FT-IR spectra of samples obtained by AGET and SR&NI techniques show less enhanced peak of the carbonyl group when high temperature is used (90°C) while

SEM micrographs (Figure 6.10) show that PVDF nanoparticles in the presence of high level of grafting (in SR&NI condition) are glued in agglomerates.

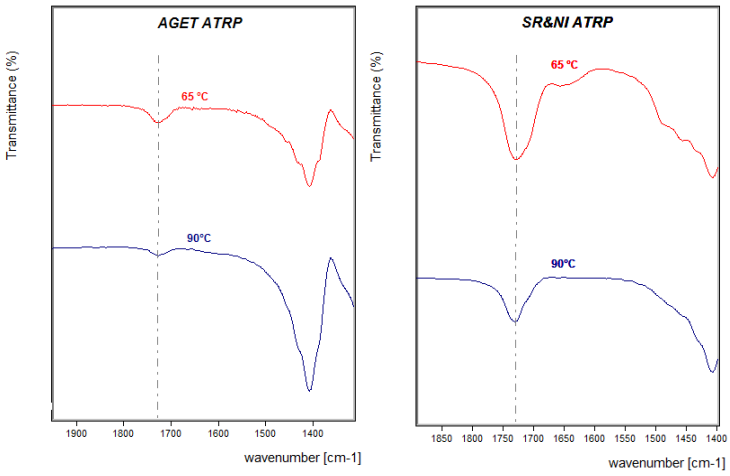

Figure 6.9. FT-IR spectra of samples obtained at different temperatures .

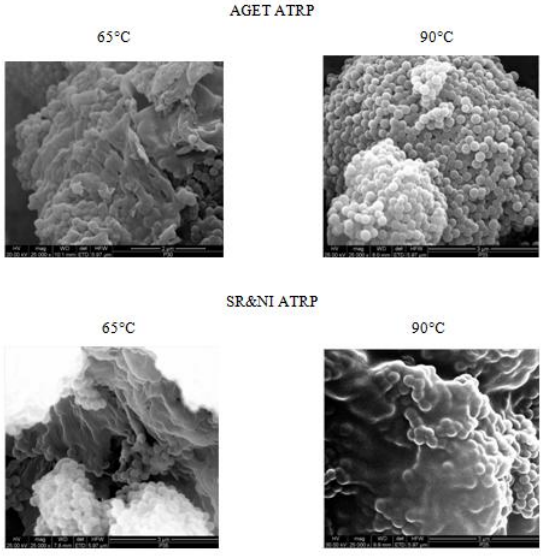

Figure 6.10. SEM micrographs of PVDF-g-PHEMA obtained at different temperatures.

6.3.4 Effect of ligand

In ATRP processes the nature of the ligand affects the stability and the activity of the catalytic complex. The ligand also allows to increase the solubility of the transition metal in the reaction medium and adjust the redox potential and the halogenophilicity of the metal. In this study, it is therefore essential to ensure an high enough solubility of the ligands in supercritical carbon dioxide, since an higher solubility certainly accelerates the kinetics of the processes. In this regard, please note that Bai et al. (*6*) analyzed the solubility of ligands such as Bpy (bipyridine) and DMBP (4-4dimetil-2-2-bipyridine) in supercritical CO_2 at different values of pressure, temperature and mole fraction of the component. Through this study, it was possible to verify that under the operating conditions used in this work, the catalytic system is completely dissolved. On the other hand Zetterlund et al. (*7*) studied the solubility of Cu-based complexes typically used in ATRP in supercritical CO_2, pointing out that it is not necessary to create specific ligands to carry out the process in the supercritical fluid.

In this work the influence of the ligands was investigated by performing tests with different types characterized by different structures in order to identify the most active catalytic complex . Some experiments were carried out under the same operative conditions (0.4 M of HEMA, 1.33 mM of Cu(II)Cl_2, 1.33 mM of ligand, 0.44 mM of ascorbic acid for AGET or 1.33 mM of BPO for SR&NI, carbon dioxide density of 0.81 g/mL) for a reaction time of 16 hour and at temperature of 65°C.

Table 6.5 Effect of ligands on the grafting of PVDF nanoparticles by AGET and SR&NI technique. Operative conditions: PVDF = 1g, HEMA = 0.4 M, [Ligand] = 1.33 mM, $CuCl_2$ = 1.33 mM, [AscA]=0.44 mM (AGET) or [BPO]=1.33 mM (SR&NI) ρCO_2 = 0.81 g/mol, t = 16h.

entry	ATRP technique	Ligand	DG (%)	Melting point (°C)	Cistallinity(%)
				159	53
1	AGET	Bpy	0	158	48

2	AGET	DMBP	2.9	158	48
3	AGET	Me_6TREN	2.3	159	52
4	AGET	TPMA	10.6	159	48
5	SR&NI	DMBP	46.1	157	37
6	SR&NI	TPMA	20.2	158	45

It is well known that the ligand changes the redox potential and the activity of the catalyst. As regard reactions carried out with AGET technique, results which confirm studies realized in organic medium and information obtained about the activity of complexes with ligand were obtained. The less active catalytic complexes employed composed by Bpy and DMBP as ligands led to the lowest DGs (entries 1 and 2 Tab. 6.5). When more active catalytic complexes composed by TPMA and Me_6TREN (entries 3 and 4 Tab. 6.5) were used different results were obtained; in particular, with TPMA, the most active and stable ligand, higher degree of grafting was achieved, while lower DG was obtained with Me_6TREN due to its involving , as explained in the literature (*8*), in the disproportionation reaction.

Different results were achieved when BPO is employed as reported in Table 6.5 (entries 5 and 6). In this case DMBP is the ligand that allows to the higher DG (46.1%) while the utilization of the more stable and active TPMA led to lower DG. This result, very difficult to analyze, could be due to a more enhanced involvement of TPMA in the reactions showed in scheme 6.2 that shift the reaction in the bulk favoring the homopolymerization.

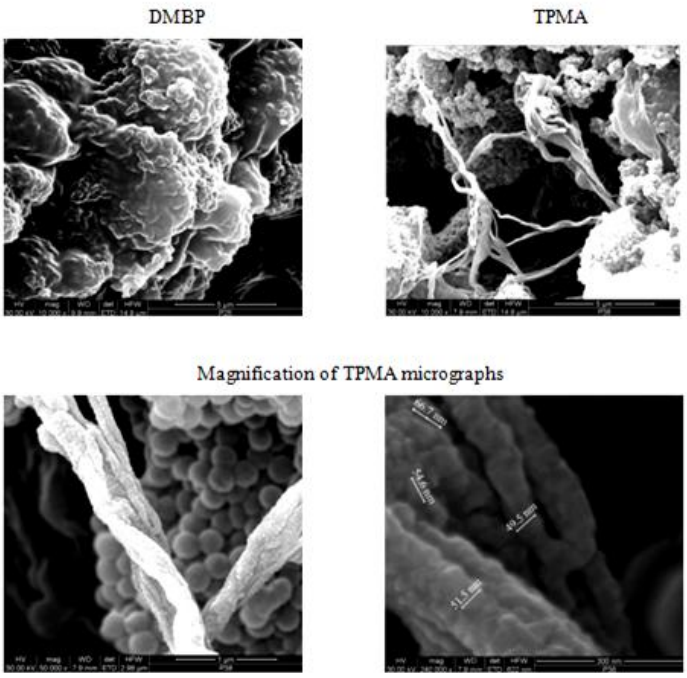

Figure 6.11. SEM micrographs of PVDF-g-PHEMA in the presence of different ligands.

The morphologies of the grafted powders (figure 6.11) were investigated and the magnification reported in figure 6.11 shows the comparison of new chains with dimensions very different from these one of the nanoparticles of PVDF, most probably attributed to the new chains of PHEMA. The average diameter of the PVDF nanoparticles is about 250 nm , whereas these new chains are composed by particles with diameters as about 50 nm.

6.3.5. Effect of copper salts precursor

Finally, the effect of different ternary complexes composed by different Cu-halogen bond was analyzed (Cu(II)LX, where X = Cl or Br) (Figure 6.12).

To investigate the effect of different halide ion in the reaction medium on the grafting a set of experiments was carried out at 65°C , with a molar feed ratio of $[HEMA]_0:[CuCl_2]_0:[TPMA]_0$ = 300:1:1, [AscA=0.44 mM , reaction time 16h and CO_2 density of 0.81 g/mL.

Higher degree of grafting was obtained when $Cu^{II}Cl_2$ was used (Figure 6.12) than $Cu^{II}Br_2$. A possible explanation is in the different kinetic of the deactivation reaction in the presence of chlorine or bromine ions: the slower the kinetic, the higher the amount of radicals in the reaction medium with increasing possibility to add monomer molecules. The presence of different halides ions as reported in chapter 4 could strongly influences the deactivation rate; studies carried out in DMF and reported before have shown that higher reaction times are necessary to deactivate ternary complexes composed by halides as chlorine or fluorine atoms. This slow kinetic lead to have more radicals in the reaction medium and the equilibrium of the ATRP reaction is not shifted to the left as is crucial to achieve a good control of the final products avoiding side reactions between radicals.

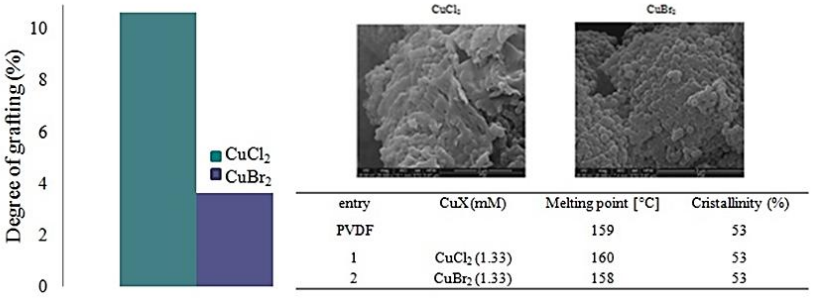

entry	CuX (mM)	Melting point [°C]	Cristallinity (%)
PVDF		159	53
1	$CuCl_2$ (1.33)	160	53
2	$CuBr_2$ (1.33)	158	53

Figure 6.12. Effect of different ternary complexes on the grafting of HEMA on PVDF nanoparticles.

Figure 6.12 reports also the cristallinity of the two samples analyzed showing that no variation of the χ was obtained changing the ternary complex that begin the reactions.

6.3.6. Conclusions

Grafting of HEMA on PVDF nanoparticles with ATRP techniques in supercritical carbon dioxide was carried out; the study was conducted in order to identify the best metal-ligand complex and the best operating conditions. The ATRP reactions were carried out with three different initiation systems: normal ATRP, AGET ATRP and SR&NI ATRP. Furthermore, the effect of temperature, the oxidation state of the metal, the type of ligand and metal salt were analyzed.

At the same operating conditions, the system SR&NI (which involves the use of BPO) allowed to obtain the highest level of grafting, followed by the system AGET. The normal ATRP was substantially ineffective. It is correct to emphasize that the presence of the radical initiator may lead to the extraction of the H atom from PVDF and not of the halogen.

As regards the oxidation state of the metal it is noticed that in AGET ATRP it is better to use Cu^{II} but, quite surprisingly, in SR&NI Cu^{I} allows to reach very high DG (46.1%), most probably due the extraction of H atoms from the polymer backbone of the PVDF nanoparticles by BPO).

The reaction temperature is another fundamental operating parameter. Low DG were obtained at the highest investigated T of 90°C. This could be tentatively explained considering that too high temperature can make the catalyst more subjected to disproportionation reaction.

The effect of the type of ligands and salt were studied in AGET or in SR&NI; four ligands were tested in the presence of AscA and TPMA was the more active , while DMBP led to best DG in SR&NI. The effect of the salt, the precursor of the metal, has been tested in AGET mode and it was noted that the chloride allows to obtain grafting more pronounced than bromide most probably due to slow kinetic od the deactivation reaction involving copper(II) complexes composed by chlorine atoms,

This study demonstrated that the modification of PVDF powders with a controlled technique as ATRP was succesfully carried out. Further investigations and especially NMR analyses have to be made to have more information on the structure of the grafted copolymer.

References

1. L. Mascia, K. Hashim, *J. Appl. Polym. Sci.* **66**, 1911 (1997).
2. Z. Xuejuan, C. Jing, C. Shuangjun, Z. Jun, W. Xiaolin, *Colloid Polym. Sci.* **288**, 1327 (2010).
3. U. Gaur, E. Wunderlich, B. B. Wunderlich, *J. Phys. Chem. Ref. Data*. **12**, 29 (1983).
4. W. A. Braunecker, K. Matyjaszewski, *Prog. Polym. Sci.* **32**, 93–146 (2007).
5. S. Zhu, W. Wang, W. Tu, D. Yan, *Acta Polym.* **50**, 267–269 (1999).
6. Y. Bai, H.-J. Yang, H.-J. Yang, C. Quan, C.-Y. Guo, *J. Chem. Eng. Data*. **52**, 2074–2076 (2007).
7. B. Zetterlund, F. Aldabbagh, M. Okubo, *J. Polym. Sci. Part A Polym. Chem.* **47**, 3711–3728 (2009).
8. B. M. Rosen *et al.*, *J. Pol. Sci. Part A Pol. Chem.* **47**, 5606–5628 (2009).

CHAPTER 7
STERILIZATION OF POLYMERIC BIOMATERIAL BY sc-CO_2

7.1. Introduction

In order to assess the potentiality of sc-CO_2 as a green solvent in the biomedical field not only the modification of halogenated polymers was carried out, but also the sterilization of a complex porous membrane composed by PLLA, which is widely used in tissue engineering. The study reported in this chapter was born from the increasing attention paid by the scientific community to the utilization of supercritical fluids as an alternative method to the conventional techniques (*1*).

In this work, it has been studied the utilization of scCO_2 to sterilize 3-D porous poly(L-lactic acid) (PLLA) scaffolds suitable for tissue engineering applications.

and the model matrix chosen is a complex 3D porous membrane in PLLA with the aim to understand the effect of the supercritical fluid on a tridimensional matrix.

In this study the PLLA scaffolds were contaminated, both in surface and in the bulk, by the gram-negative bacterium *E. coli* and by spores of *S. coelicolor*.

The effect of the supercritical medium on the morphology and properties of the porous matrix was also studied. For this purpose scaffolds sterilized at different operative conditions such as treatment time and pressure were analysed by DSC to observe possible changes in the crystallinity, while their morphology was observed by SEM micrographs. Finally, the effect of the treatment on the cell adhesion and growth was studied throughout cell cultures on scCO_2 sterilized devices.

7.2 Experimental

7.2.1 Materials

PLLA (RESOMER^{TN} L 209 S) supplied by Boehringer Ingelheim Pharma KG, 1,4 dioxane (Sigma) and double distilled water were utilized to prepare the ternary solution for scaffold preparation. CO_2 used to perform sterilization experiments was supplied from Air Liquide (purity 99.998% vol/vol, water content ≤ 3 vpm). Ethanol (70% vol/vol) adopted in control sterilization tests and hydrogen peroxide (30% v/v in water) were both purchased from Aldrich.

7.2.2 Scaffold preparation and characterization

Scaffold were made by the group of prof. Valerio Brucato of the Department of Civil, Environmental, Materials Engineering (DICAM) of the University of Palermo and the methodology is reported below.

A homogeneous ternary solution composed by PLLA, 1,4 dioxane and water was prepared, with a polymer concentration of 4% w/w and a constant dioxane to water weight ratio of 87/13 w/w. The solution, initially kept at 60 °C, was poured into a cylindrical polypropylene sample holder (diameter 14 mm, height 30 mm). The temperature was then suddenly lowered to 30 °C (demixing temperature) for a well-defined demixing time (30 minutes), by pool immersion of the sample holder into a thermostatic water (*2*). Then a quench by pool immersion in an ethyl alcohol bath at a temperature of -20 °C for 15 minutes was carried out in order to freeze the as-obtained structure. Finally, a freeze-drying step under vacuum at -28 °C for 72 hours was performed for solvents removal from the sample by sublimation, in order to reduce the risk of damaging sample structure. By this methodology porous disk-shaped scaffolds with a diameter of 14 mm and a thickness of 2 mm were obtained.

7.2.3 SCF-Sterilization apparatus

The experiments in $scCO_2$ were carried out using the system shown in Fig. 7.1.

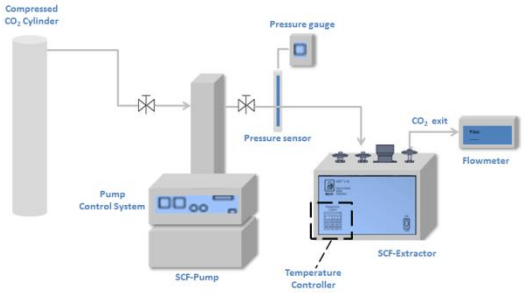

Figure 7.1 Experimental setup for CO_2 sterilization.

This sterilization unit was constituted by a SFX 2-10 (ISCO) fluid extractor equipped with temperature controller and connected with a D260 syringe pump (ISCO). The pressure of the pump was controlled by a control system and the pressure in the zone near the supply valve of the extractor was monitored by a pressure transducer type UPA 3 (Barksdale), calibrated against a precision manometer and connected with a digital read-out.

The apparatus lines consist of 1/8 and 1/16 in OD AISI 316 stainless steel tubes. At the exit of the extractor the flow-rate of CO_2 was measured at room conditions by an electronic flowmeter Bronkhurst mod. F-11C-GD-00-V equipped with a totalizer Seneca mod. S164. Inside the extractor, the scaffolds were placed in stainless steel cartridges with internal volume 10 mL (length 5.83 cm, section s = 1.73 cm^2).

7.2.4 Preparation of bacteria suspensions

Cultures of *E. coli* bacteria and *S. coelicolor* spores *used* for the contamination of PLLA scaffolds to investigate the sterilization effect of $scCO_2$ were prepared by the group of prof. Giulio Ghersi of the Department of Sciences and Biological

Technologies (STEBICEF) of the University of Palermo. *E. coli* is a gram-negative bacterium and represents one of the most common bacteria of the gut of warm-blooded animal. Its presence is related with fecal contamination, together with enterococci and it was chosen as model to test the sterilization of scaffold for tissue engineering applications (*3*). In order to investigate the spore sterilization, *S. coelicolor* was selected because it has an optimal growth temperature close to the human physiological interval so, in principle, it can proliferate in scaffolds used for biomedical applications (*4*). Moreover, these spores can be easily manipulated in laboratory and their growth becomes visible in culture plate after 48-72h.

E. coli was stored in Lysogeny broth (LB) (Usb Corporation) Agar plate at 4°C just for one week long. For each experiment, a fresh colony was incubated in LB broth at 37°C for 24h in order to obtain diluted bacteria suspension used for the contamination of PLLA scaffolds.

S. coelicolor A(3)2 were grown at 30°C on Mannitol Soya flour (SFM) agar. Spores were harvested from the Petri dish with sterile water, filtrated through glass funnels containing cotton wool, washed by centrifugation at 3000 rpm for 11 minutes and re-suspended in water or in a solution of 20% glycerol in order to be stored at -20°C.

7.2.5 Scaffolds Contamination and SCF-Sterilization experiments

Before the contamination with bacteria or spores suspensions, PLLA scaffolds were disinfected by Ethanol 70% treatment under vacuum-seal and washed with sterile phosphate buffer solution (BPS).

The contaminations of the samples were performed together with the group of prof. Giulio Ghersi before mentioned by immersion in *E.coli* or *S. coelicolor* suspension (in agitation for 15 minutes) or by direct inoculation of spore suspension

For each experiment, two samples were used: one of them was sterilized by $scCO_2$ and the other one, used as positive control, was maintained in sterile conditions at

37°C for *E. coli* or at 30°C for *S. coelicolor* for the same time adopted to perform the sterilization.

Sterilization was performed soaking contaminated scaffolds with $scCO_2$ at different densities and temperature for different processing times (Table 7.1 and 7.2).

Prior to each experiment, the lines of the sterilization apparatus were cleaned by two or more pressurization/depressurization cycles at 40 MPa, each one lasting for 5 minutes. The cartridge used as sterilization chamber was cleaned after each experiments by washing with sodium hypochlorite and bi-distilled water. Furthermore, before each experiment it was sterilized under UV light in the laminar flow hood to remove environmental contamination. The contaminated scaffold was placed in the cartridge in a laminar flow hood and sealed by two caps in PTFE; these caps were prior sterilized by flame in order to avoid environmental contamination of the cartridge. It must be pointed out that the total mass of water soluble in the mass of carbon dioxide loaded in the high pressure cell at operative conditions adopted in this study is lower than 35 mg (*5*). From the mass variation of control samples of the scaffold treated in pure water by the same procedure adopted to perform contamination a residual amount of water in the matrix of 100-180 mg was estimated. Then it can be concluded that the sterilization experiments were carried out with $scCO_2$ saturated with water. The cartridge containing the contaminated scaffold was mounted in the extractor, whose chamber was already heated to the desired temperature, and carbon dioxide was charged in less than 2 minutes using the ISCO pump under constant pressure mode. When the proper value of pressure was reached, the supply valve was closed and the temperature of the cartridge was maintained at the selected value by the control unit. At the end of the selected processing time the extractor chamber was vented to room pressure (depressurization time was generally 15 min) and opened to recover the treated scaffold. All sterilization experiments were carried out at least in duplicates.

7.2.6 Bacteria and spores inactivation (plate counting)

After the $scCO_2$ treatment, the samples were washed with 7 mL of *Dioctyl sodium sulfosuccinate* (AOT) solutions at 1% w/w concentration for 7 minutes and washed tree times (3 minutes) with sterile water under vacuum-seal in order to allow the release of residual contaminant agent (bacteria or spores) from scaffolds.
This work was conducted together with the group of prof. Giulio Ghersi before mentioned Then, 100 µL of this solution and of its serial dilutions, were plated on Petri dishes with LB agar for *E. coli* colonies or MS agar for *S. coelicolor* spores and grown under their optimal condition (37°C or 30°C respectively). The untreated scaffold used as control, was subjected to the same treatment with AOT 1% and sterile water and the same serial dilution were plated in appropriate media. The amount of living bacteria cells on each sample (treated and not) was counted by the standard method (CFU: Colony-Forming Unit). The survival ratio was expressed as the log reduction of *E. coli* or spores from *S. coelicolor* calculated with Eq. (7.1)

$$\text{Log reduction} = \log N_0/N \qquad (7.1)$$

where N_0 is the initial microbial count (on untreated contaminated scaffold) and N is the microbial count after treatment with $scCO_2$.
As control, scaffolds contaminated with *E. coli* were contacted with LB medium and incubated at 37°C for 72h and the absorbance at 600 nm was evaluated by spectrophotometer analysis.

7.2.7 Biocompatibility of PLLA scaffolds after $scCO_2$ treatment

Biocompatibility of the scaffold was evaluayted by the group of prof. Giulio Ghersi before mentioned SK-HEP1 cells (Human Hepatic Adenocarcinoma Cell Line)

were prepared to investigate the biocompatibility of PLLA scaffolds contaminated by *E. coli* or *S. coelicolor* and sterilized by $scCO_2$ treatment.

After sterilization process, the scaffolds were soaked with 20 mL of AOT solutions at 1% w/w concentration under vacuum-seal for 7 minutes and washed with sterile PBS and water. PLLA supports disinfected by ethanol 70% v/v were used as control. All the samples were coated with 1 mg/mL collagen in D-MEM (Dulbecco's Modified Eagle Medium) and incubated at 37°C for 1 hour. After washing with culture medium, SK-HEP1 cells, re-suspended in D-MEM with 600µg/mL collagen, were seeded on the scaffolds at a density of $2x10^3$ cells/scaffold. They were maintained using suitable culture medium supplemented with 10% v/v Fetal Bovine Serum (FBS) 1% 2 mM L-glutamine, 100 units/mL penicillin G, 100 µg/mL streptomycin in a 37 °C humidified incubator in an atmosphere of 5% CO_2 in air.

After 3, 6, 9 and 13 days, cell viability was evaluated using Cell Counting Kit-8 (CCK-8) (Sigma-Aldrich). The water-soluble tetrazolium salt (WST-8) was added to each well (1:10 dilution in complete medium) followed by incubation for 2 h at 37 °C. Only the living cells present a functional mitochondrial dehydrogenases that can reduce the WST-8 into soluble formazan dye: therefore, the amount of formazan is directly proportional to the number of living cells. The absorbance at 460 nm was read with a microplate reader DU-730 Life Science spectrophotometer (Beckman Coulter). Scaffold without cells were used as negative control.

7.2.8 Scaffold characterization after CO_2 treatment

The scaffold were cut in two identical parts. One of them was subjected to $scCO_2$ treatment, whilst the other one (not treated) was utilized as blank control. The morphology of the untreated and $scCO_2$ treated samples was analyzed by Scanning Electron Microscopy (SEM) using a SEM-FEI QUANTA 200F on sample cross section fractured in liquid nitrogen and gold sputtered (Sputtering Scancoat Six,

Edwards) for 40 seconds under Argon atmosphere before imaging. SEM images were exported as 24-bit image files using the tagged image file format (tiff). The melting temperatures and melting enthalpies of $scCO_2$ treated samples were determined with a Setaram 131 evo Differential Scanning Calorimeter. The samples were heated at a rate of 10 °C/min, under a nitrogen gas flow of 1 ml/min. The X_c values were evaluated according to the following equation (*6*).

$$X_c\ (\%) = 100(\Delta H_m)/135$$

where ΔH_m is the calorimetric melting enthalpy of exposed samples and 135 J/g is the melting enthalpy of a PLLA crystal of infinite size, as reported by Miyata and Masuko (*7*).

7.3 Results and discussions

7.3.1 Study of bacteria inactivation from PLLA scaffolds

PLLA scaffolds independently contaminated with either Gram-negative bacteria *E. Coli* or spores of *S. coelicolor*, both throughout the surface and in the scaffold bulk, were treated by $scCO_2$ under different operating conditions, and the results obtained are summarized in Tables 7.1 and 7.2 for each contaminant. In order to minimize the risk of significant morphological modification of the porous scaffold, the working temperature was never higher than 40 ºC since it has been observed that glass transition temperature of PLLA can decrease up to 50 °C when the value of CO_2 pressure approaches 7 MPa (*8*).

First, the sterilization treatment of macroscopic PLLA scaffolds contaminated with *E. coli* using $scCO_2$ was studied. A set of experiments was carried out at 40°C, with different pressures (5 – 20 MPa) and time periods (5 – 360 min). Worth highlighting, as shown in Table 7.1, even at such low temperature, a complete three dimensional sterilization of the matrix was achieved regardless of the processing

time, provided that pressure values higher than the critical pressure of CO_2 (7.4 MPa) were used.

For example, total sterilization was reached after only 5 min using a pressure of 10 MPa (i.e., 100 bar), which corresponds to a fluid phase density of 0.63 g/mL as estimated by the Span & Wagner EOS (*9*) (Table 7.1). The large effectiveness of the process was only limited when reducing the pressure up to a subcritical value of 5 MPa (5 min at 40°C). In that case, it was impossible to determine the amount of bacteria at the end because they were well distributed throughout all the Petri dish, and may probably be explained by the rather low density of $scCO_2$ reached under these conditions (see trial at 5 MPa in Table 7.1).

It is worth mentioning that, aiming to gain further confirmation of these data, contaminated treated scaffolds were placed in liquid medium at 37 °C under stirring to allow the bacterial growth. The spectrofluorometric analysis at 600 nm showed no bacteria growth in the sterilized scaffold.

Table 7.1 Sterilization of *Escherichia coli* upon treatment with $scCO_2$ at 40 °C.

Contaminating organism	**P (MPa)**	**ρ CO_2 (g/mL)**	**Time (min)**	**CFU[(a)] (initial)**	**CFU[(a)] (final)**
E. coli	20	0.84	360	10^8	0
	15	0.78	360	10^9	0
	15	0.78	120	10^8	0
	15	0.78	15	10^8	0
	10	0.63	5	10^9	0
	5	0.11	5	10^9	confluence

[a] Colony-Forming Unit.

Since the PLLA scaffolds would find their potential application in tissue engineering and regenerative medicine applications, it is mandatory that the $scCO_2$ treatment does not alter their biocompatibility. In order to demonstrate this, a viability assay of SK-HEP-1 tumor cells (Hepatocarcinoma) grown on the surface and internal pores of the scaffolds was carried out. As can be observed in Fig. 7.2,

after 3 days of seeding, the cells started to grow and kept dividing for next days (6 and 9 days in that figure). The cells reached the plateau of the growth curve (e.g., the number of the new cells is the same of dying ones) after 9 days. Cell growth on scaffolds sterilized with ethanol 70% were used as positive control (light grey bars). These results reveal that the cells can be seeded into the scaffold and they keep growing similarly to the cells seeded on PLLA scaffolds sterilized with ethanol. Therefore, it would be adequate to use a sterilization protocol based on $scCO_2$ for these kinds of scaffolds, since treated matrices are viable for medicine and biological purposes.

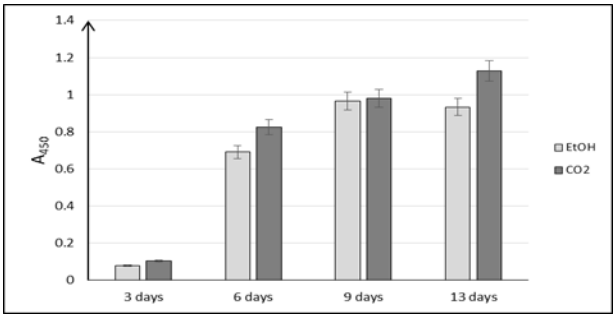

Figure 7.2 MTS assay on Sk-HEP1 cells seeded on PLLA scaffolds sterilized with ethanol 70% (light grey) and $scCO_2$ (dark grey).

7.3.2 Study of spore reduction from PLLA scaffolds

Similarly to previous experiments with *E. coli*, the feasibility of the treatment with $scCO_2$ for scaffolds contaminated with spores was investigated upon contamination of the PLLA samples with spores from *S. coelicolor*. The effect of various parameters was studied, including the pressure value (20 and 30 MPa), the temperature (30 and 40 °C), the treatment time (2, 4 and 6 h), and the addition of H_2O_2. At 30 °C, a complete sterilization was not obtained but, as shown in Table 7.2, increasing the CO_2 density caused a considerable reduction of the amount of spores. Thus, when the contaminated scaffold was exposed to dense CO_2 at 20

MPa and 30 °C for 2 h, the estimated log reduction was 0.85, which accounts for a 10-fold reduction of the number of spores. When the pressure was increased to 30 MPa, log reductions increased to 4.24 and 4.87 after 4 and 6 h of treatment, respectively. They account for a 10000-fold reduction at such pressure, which suggests that the utilization of high value of CO_2 density is of paramount relevance to impair the resistance of the selected spores (see comparison in Fig. 7.3).

The experiments performed at 30 MPa and 30 °C for 6 h were repeated in the presence of 200 ppm H_2O_2. In contrast to trials without H_2O_2, a complete sterilization was obtained. The same result was obtained when the sterilization tests were performed for 6 h at a higher temperature of 40 °C without changing the pressure. This means that both the addition of H_2O_2 and the increase of temperature could enhance the effectiveness of the sterilization process.

Table 7.2 Sterilization of spores of *Streptomyces coelicolor* upon treatment with scCO_2.

Contamination	**T (°C)**	**P (MPa)**	**ρ CO_2 (g/mL)**	**Time (min)**	**H_2O_2 (ppm)**	**CFU[(a)] (initial)**	**CFU[(a)] (final)**	**Log red.**
Spores of S. coelicolor	30	20	0.89	120	-	$1.03*10^{10}$	$1.46*10^{9}$	0.85
	30	30	0.95	240	-	$3.70*10^{8}$	$2.13*10^{4}$	4.24
	30	30	0.95	360	-	$2.64*10^{9}$	$3.60*10^{4}$	4.87
	30	30	0.95	360	200	$1.16*10^{11}$	0	-
	40	30	0.91	360	-	$2.38*10^{10}$	0	-

[a] Colony-Forming Unit.

Images obtained by SEM analysis showed a change in the structure of the spores after the treatment with dense CO_2 (Fig.7.4). It is clear that treated spores become damaged, in particular on the protective coverings. Therefore, it can be concluded that the high pressure induces an alteration of the spore structure that, once the

H_2O_2 is present or at a higher temperature is employed, ends in the deactivation of the whole population.

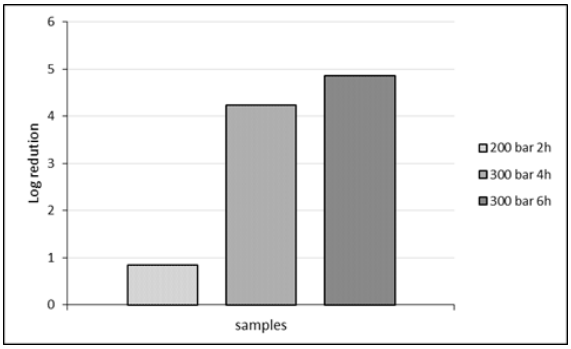

Figure 7.3 Spore reduction on PLLA scaffolds treated at different pressure values for different time periods. The temperature in each experiment was maintained at 30 °C. The spore reduction is expressed as log reduction.

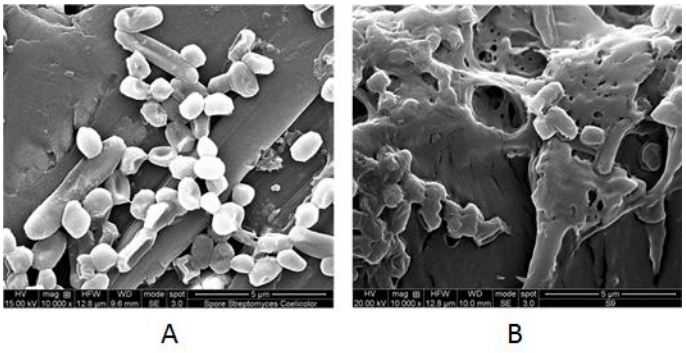

Figure 7.4 SEM analysis of *S. coelicolor*'s spores before (A) and after (B) $scCO_2$ treatment (30 MPa, 6 h, 40 °C).

7.3.3 Scaffold characterization after CO_2 treatment

Once confirmed that $scCO_2$ was able to sterilize the PLLA scaffolds, another important goal was to assess if the PLLA scaffolds had undergone some kind of

modification during the treatment in terms of morphological and thermal properties. For this reason , DSC and SEM analysis were carried out both on treated and raw PLLA samples. The data reported in Table 7.3 suggest that none of the treatments performed under the aforementioned operative conditions (Tables 7.1 and 7.2) induce a variation of calorimetric properties (i.e., crystallinity and melting temperature). As a matter of fact, a slight reduction of sample crystallinity is observed only when the treatment time was dramatically increased (20 h). Conversely, at 20 h, no changes in melting temperature were observed. On the other hand, the SEM analyses confirmed that also from a morphological point of view the sterilization treatment did not affect the porous scaffold in terms of pore size compared to the control sample (Fig. 7.5). These results are quite important since, a priori, differential swelling of the matrix during CO_2 venting could plausibly induce deformation of the channel networks with consequent adverse effects on the growth of cells during the scaffold colonization.

Table 7.3. Effect of exposure of polymeric scaffolds to dense CO_2 at different pressures. CO_2 soaking experiments were performed at 40 °C. Calorimetric data reported in the table were obtained during the first heating scan.

Pressure (MPa)	**Time**	**Melting Enthalpy (J/g)**		**Crystallinity (%)**		**Melting Temperature (°C)**	
		raw	**treated**	**raw**	**treated**	**raw**	**treated**
10	15 min	51	50	38	37	179	180
	20 h	53	50	39	37	181	181
20	2 h	55	54	40	40	180	181
	20 h	55	49	41	36	181	181
30	4 h	53	53	39	39	180	180
	20 h	54	49	40	36	181	181

However, it has been demonstrated that the adopted depressurization rate is slow enough in comparison with the diffusion rate of CO_2 in the amorphous domains of the polymer matrix. Consequently, this prevents the appearance of a significant concentration gradient of CO_2 inside the polymer matrix and then, the onset of differential tensions in the matrix is avoided.

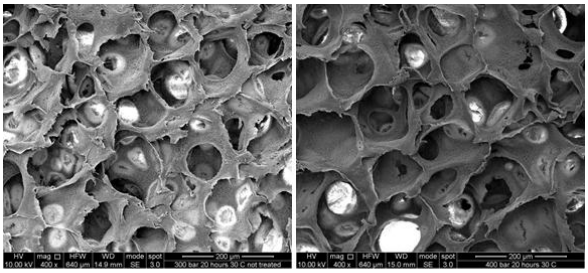

Figure 7.5 SEM images of cross sections of raw (A) and scCO_2-treated (B) PLLA scaffolds. (40 MPa, 40 °C, 20 h).

7.4. Conclusions

In this part of the research, the effectiveness of a scCO_2-based sterilization protocol for PLLA scaffolds contaminated with *E. coli* bacteria or with *S. coelicolor* spores has been discussed. As shown, the treatment did not alter the biocompatibility, the morphology and the crystallinity of the processed matrixes. By varying the pressure and treatment time, it has been possible to achieve a total sterilization of matrices with *E. coli* after only 5 min at 10 MPa and 40 °C without affecting the scaffold biocompatibility and physical properties, as demonstrated upon viability assays and DSC and SEM analysis. Conversely, the spores are more refractory to sterilization, probably because of their excellent adaptation capacity. A drastic enhancement of log reduction from 0.85 to 4.24 at 4 h was obtained when the pressure was increased from 20 to 30 MPa. The total sterilization of spores was achieved at after

6 h of treatment at 30 °C and 30 MPa only in the presence of 200 ppm H_2O_2, or after 6 h at 40 °C and 30 MPa in the absence of peroxide.

SEM micrographs showed a clear effect of supercritical fluid on the shell structure of spores. According to collected experimental results, it is feasible to sterilize a complex 3D macroscopic structure in a final form already suitable for implantation without affecting its biocompatibility, morphology and crystallinity, which represents a promising alternative to existing methods.

References

1. C. Liu, Z. Xia, T. J. Czernuszka, *Chem. Eng. Res. Des. (Trans IChemE)*. **85**, 1051–1064 (2007).
2. F. . Carfì Pavia, V. La Carrubba, S. Piccarolo, V. Brucato, *J. Biomed. Mater. Res. Part A*. **86A**, 459–466 (2008).
3. C. Carlos *et al.*, *BMC Microbiol.* **10**, 161 (2010).
4. S. Sigle, N. Ladwig, W. Wohlleben, G. Muth, *Int. J. Med. Microbiol.* **305**, 183–189 (2015).
5. R. Wiebe, *Chem. Rev.* **29**, 475–481 (1941).
6. H. Tsuji, Y. Tezuka, K. Yamada, *J. Polym. Sci. B Polym. Phys.* **43**, 1064–1075 (2005).
7. T. Miyata, T. Masuko, *Polymer (Guildf).* **39**, 5515–5521 (1998).
8. T. Fujiwara, T. Yamaoka, Y. Kimura, K. J. Wynne, *Biomacromolecules*. **6**, 2370–2373 (2005).
9. R. Span, W. Wagner, *J. Phys. Chem. Ref. Data*. **25**, 1509–1596 (1996).

General conclusions

As presented in this thesis, new interesting insights into the modification and the sterilization of macromolecular materials used in biomedical field have been presented. In particular, the mechanism of atom transfer radical polymerization carried out using fluorinated compounds as halogenated initiators have been revealed, mainly by exploiting the potentialities of electrochemistry. The results obtained during this project, with particular regard to those pertaining to the analyses of the activation and the deactivation reactions of a reaction involving fluorine ions, gave a significant contribution towards the understanding of the livingness of this controlled polymerization. The study carried out in NMP has shown that the grafting of HEMA on PVC and PVDF by copper catalysts was realized. Cyclic voltammetries of catalysts composed by Cu(II)/X_2/L (where X= Cl or Br and L=TPMA or ME_6TREN) have shown that the activity and the stability of copper complexes strongly depend on the nature of the ligand employed, on the temperature and on the presence of the monomer. TPMA allows the formation of the more stable complex , while the addition of the monomer, the increase of temperature or the utilization of Me_6TREN ligand led to a decrease of the stability of the catalytic complex. These catalysts were also used to analyze the effectiveness of PVC and PVDF as ATRP macroinitiators by cyclic voltammetric and chronoamperometric measurements, leading to find that Cu(I)Br/TPMA complex is able to activate PVC, while the more active catalyst composed by CuBr and ME_6TREN has to be used to activate PVDF. Grafting experiments confirmed the indication of electroanalytical experiments showing that the modification of PVC was achieved with short reaction times in a wide range of temperatures using Cu(I)/TPMA as catalyst, whereas, in the case of PVDF, Cu/Me_6TREN and high temperature have to be used to reach DG of 5%. The results obtained in this first part shows that the activation of the C-F bond is very difficult to realize due to its strong energy and in this direction it was carried out the study on the model fluorinated initiator (DFM), designed and performed to collect information on the

evolution of an ATRP reaction activated after cleavage of a C-fluorine bond. This study started by the analyses of the redox potentials of complexes composed by $Cu^{II}(OTf)_3$/TPMA/X (where X = I^-, Br^-, Cl^- and F^-) carried out in DMF allowing to observe that all ternary catalytic complexes show potentials more negative than that of the binary, but the complex composed by iodine. The redox potentials become more negative varying the nature of the halogen in the following order $E^0_F > E^0_{Cl} > E^0_{Br}$ (> is for more negative). Furthermore, higher temperature displayed the $E_{1/2}$ towards more positive potentials, thus giving rise to a less reducing complex. Cyclic voltammetric analyses were also conducted to analyze the activation of the fluorinated initiator by observing the comparison of the ternary complex composed by $Cu^{II}(OTf)_3$LF when fluorine atoms have beeen exctracted by the initiator. The effect of two catalysts composed by different ligands (TPMA or Me_6TREN) on the activation was analyzed, showing that in both cases the activation occurs, even if, as expected, more enhanced peak current of the ternary complex was found when Me_6TREN is used. The main goal of this study was the investigation of the crucial effect of the deactivation reaction on the livingness of an ATRP activated by C-F bond breaking; to this purpose, the deactivation studies carried out by reverse ATRP of MMA and MA in the presence of copper complexes composed by $Cu^{II}(OTf)_3$/TPMA/X (where X = I^-, Br^-, Cl^- and F^-) have shown that the longest deactivation time of the ternary complexes occurs when Cu/L/F catalysts are used leading to a loss of the control of the homopolymerization. With F ions conversion and molecular weight higher than with other halides were obtained due to the slow kinetic characterizing this case. At the end, normal ATRP of MA and Sty with DFM as initiator have demonstrated that C-F bond could be used to begin the reaction, thus confirming the results obtained by activation studies, but the control of the final molecular weight and polydisperisity of the polymer strongly depend on the adopted operative conditions. Different reactivity and stability of radicals is fundamental to regulate the kinetics of the reaction : the more nucleophilic styril radical shows the highest affinity for halogen abstraction, whereas the most electrophilic acrylate radical has the lowest, allowing to a possible improvement of deactivation reaction and livingness of process when styrene is used.

In the second section of this Ph.D. project, the grafting of HEMA on PVDF nanoparticles with ATRP techniques in supercritical carbon dioxide was carried out, in order to identify the best metal-ligand complex and the best operating conditions. The ATRP reactions were carried out with three different initiation systems (normal ATRP, AGET ATRP and SR&NI ATRP) and the effect of temperature, CO_2 density, oxidation state of the metal, nature of ligand and metal salts were analyzed. Alternative initiation systems characterized by low concentration of copper catalyst (AGET and SR&NI ATRP) were analyzed in order to perform the modification process in a best way suitable for biomedical applications. Preliminary investigations have shown that normal ATRP does not lead to grafting, whereas alternative methods (AGET and SR&NI) allowed to realize the modification of the halogenated nanoparticles. In particular, very high degree of grafting (46.1%) was achieved when BPO as reducing agent and CuCl/TPMA are used, even if the presence of the conventional radical initiator may lead to the extraction of the H atom from PVDF and not of the halogen. The utilization of the AscA in the presence of CuCl/DMBP complex leads to moderate DG (10.6%) at 65°C, while low DG were obtained at the highest investigated temperature (90°C) with both alternative methods (AGET and SR%NI). This could be tentatively explained considering that too high temperature can make the catalyst more subjected to the disproportionation reaction, thus damaging its performance. Different ligands and state of the oxidation of the metal were analyzed with both low concentration methods, leading to find that the best performances are obtained when TPMA and DMBP are used in AGET and SR&NI techniques, respectively. Even if, as largely reported in the literature, copper in its higher oxidation state has to be used in the presence of reducing agents, when BPO was used the best results were obtained with Cu(I),. This result could be attributed to the effect of this thermal initiator that initiates in the reaction medium a reverse ATRP leading to the formation in the bulk of an alternative alkyl halide more reactive than PVDF. From these studies it seems that AGET is the most promising technique due the fact that when BPO is used a possible extraction of hydrogen atoms occurs. Prompted by this observation, at the end, the effect of CO_2 density and the nature of coppers salts were analyzed only using AGET method. The dependence of DG on

carbon dioxide density at 65°C was analyzed showing that there is a significant fall in DG (from 10.6 to 0.5%) as the pressure drops and this cuold be explained by the remarkable change of solvency of sc-CO_2 with the change of density. Finally, as regard the effect of different copper salts, and then different ternary complexes, higher DG was obtained when chlorine atoms are present in the reaction medium, thus confirming the results obtained by the deactivation studies carried out in DMF, by which higher conversion were observed with halogen atoms as chlorine or fluorine that are more difficult to deactivate. This study demonstrated that the modification of PVDF powders with a controlled technique as ATRP can be successfully carried out, but further investigations and especially NMR analyses have to be made to have more information on the structure of the grafted copolymer. Finally, in order to make the utilization of sc-CO_2 more suitable for biomedical application, the effectiveness of a scCO_2-based sterilization of PLLA scaffolds contaminated with *E. coli* bacteria or with *S. coelicolor* spores has been discussed. A 3-D complex structure was chose to evaluate the potentiality of the solvent also in the presence of porous membranes, contaminated in the inner parts and not only on their surface. Total sterilization of *E. coli* and *S. coelicolor* was achieved, even if with different operative conditions that strongly depend on the nature of the microorganism. In particular, *E. coli* was totally sterilized in only 5 min at 10 MPa and 40 °C without affecting the scaffold biocompatibility and physical properties, while more severe conditions (6 h of treatment at 30 °C and 30 MPa in the presence of 200 ppm H_2O_2 as additive) have to be used to sterilize *S. coelicolor* . SEM micrographs showed a clear effect of supercritical fluid on the shell structure of spores.

This thesis aims to be a useful work not only for the application of electrochemical methods in the study of mechanistic aspects of ATRP activated by the cleavage of very strong C-halogen bond as C-Cl and C-F, but also, and even more incisively, for opening new ways to perform successfully the modification of fluorinated macromolecules as PVDF in organic and in supercritical media; in particular , this project has clearly confirmed that the modification is activated by the cleavage of the C-halogen bond and that the control of the structure of the formed co-polymers

becomes very difficult to achieve when fluorine atoms are involved. The kinetics of activation and deactivation are very slow and proper conditions governing the equilibrium of the ATRP reaction must be ensured. Further, it has been demonstrated that the supercritical medium also sterilize microorganisms without damaging the structure of very thermolabile polymers of interest in the biomedical field making these processes very interesting from an applicative point of view.

Dissemination of Results

Publications in ISI Journals

6. S. Lanzalaco, O. Scialdone, A.Galia. *Modification of PVDF nanoparticles by controlled free radical graft copolymerization in supercritical carbon dioxide*.In preparation.

5 . S. Lanzalaco, M. Fantin, O. Scialdone, A.Galia and K. Matyjaszewski. *Understanding the mechanism of Atom Transfer Radical Polymerization activated by a fluorinated initiator: is it "living"or not?* In preparation.

4. A. Galia, S. Lanzalaco, M.A. Sabatino, C. Dispenza, O. Scialdone, I. Sirés. *Crosslinking of poly(vinylpyrrolidone) activated by electrogenerated hydroxyl radicals: A first step towards a simple and cheap synthetic route of nanogel vectors.* Electrochemistry Communications 62 (2016) 64–68

3. S. Lanzalaco, S. Campora, F.Carfì Pavia, E.R. Di Leonardo, G. Ghersi, O. Scialdone, A. Galia. *Sterilization of three-dimensional tissue engineering scaffolds by supercritical carbon dioxide.* The Journal of Supercritical Fluids (2015) (Under Review).

2. S. Lanzalaco, A. Galia, F. Lazzano, R.R. Mauro, O. Scialdone. *Utilization of poly(vinylchloride) and poly(vinylidenefluoride) as macroinitiators for ATRP polymerization of hydroxyethylmethacrylate. Electroanalytical and graft-copolymerization studies.* Journal of Polymer Science Part A: Polymer Chemistry (2015)

1. S. Lanzalaco, O. Scialdone, A. Galia. *Effect of interfacial area on heterogeneous free radical grafting of vinyl monomers in supercritical carbon dioxide: Grafting of acrylic acid on poly(vinylidenefluoride) nanoparticles*. Journal of Applied Polymer Science, 132 (2015).

Participation in National Conferences

S. Campora, S. Lanzalaco, F. Carfì Pavia, E.R. Di Leonardo, G. Ghersi, O. Scialdone, A. Galia. *Supercritical carbon dioxide induces sterilization of PLLA*

scaffolds contaminated by E. coli. Ricerca di base, interdisciplinare e traslazionale in ambito Biologico e Biotecnologico (II Ed.).Palermo (Italy). Giugno 2014.

S. Lanzalaco, A. Galia, O. Scialdone. *Grafting of vinyl monomers on PVC and PVDF by ATRP*. Italian Electrochemistry Days (GEI 2013). Pavia (Italy). Settembre 2013.

S. Lanzalaco, A. Galia, O. Scialdone. *Electrochemically assisted Atom Transfer Radical graft copolymerization. Preliminary Studies*. Italian Electrochemistry Days & Electrochemistry for Environmental Remediation (GEI-ERA 2012). Santa Marina Salina (Aeolian Islands, Messina, Italy). Giugno 2012

Participation in International Conferences

Galia, S. Lanzalaco, M.A. Sabatino, O. Scialdone, I. Sirés. *Crosslinking of polymers activated by electrogenerated hydroxyl radicals.* 10th European Congress of Chemical Engineering (ECCE 10). Nice (France). Settembre 2015

S. Lanzalaco, S. Campora, F. Carfì Pavia, E.R. Di Leonardo, G. Ghersi, O.Scialdone, A. Galia. 2nd International Conference on Bioinspired and Biobased Chemistry and Materials. Nice (France). Ottobre 2014

S. Lanzalaco, O. Scialdone, A. Galia. *Modification of PVDF nanoparticles by controlled free radical graft copolymerization in supercritical carbon dioxide.* 2nd International Conference on Bioinspired and Biobased Chemistry and Materials. Nice (France). Ottobre 2014

S. Lanzalaco, A. Galia, F. Lazzano, R.R. Mauro, O. Scialdone. *Study of ATRP process for the grafting of vinyl monomers on PVC and PVDF*. 65th Annual

Meeting of the International Society of Electrochemistry (65th ISE). Lausanne (Switzerland). Settembre 2014

Other scientific experiences

S.Lanzalaco. Invited lecture at a Seminar of Prof. Morbidelli's group at "Institute for Chemical and Bioengineering (ICB)", ETH Hönggerberg. *Grafting of vinyl monomer onto halogenated polymers by Atom Transfer Radical Polymerization assisted by supercritical carbon dioxide or by electric field.* Zurich (Switzerland). Settembre 2013

4-Month PhD stay as visiting researcher at the Chemistry Department of *Carnegie Mellon University* (CMU, Pittsburgh, USA). Research topic: *Carbon-fluorine (C-F) bond activation by copper-based catalyst*
Head: Professor Krystof Matyjaszewski

Aknowledgements

Prof. Alessandro Galia
Prof. Onofrio Scialdone
Prof. K. Matyjaszewki
Prof. Ignacio Sirés Sadornil
Prof. A.Gennaro
Prof. A.A.Isse
Dott.ssa Adriana D'Angelo
Ing. Simona Sabatino
Dott. Ing. Benedetto Schiavo
Ing. Leonardo Interrante
Ing. Fabrizio Vicari
Ing. Rosalia Rita Mauro
Ing. Flavia Lazzano
Dott. Paolo Guerra

And finally I would like to thank my lovely family for the assistance and the love of every day.